LONG-RANGE ELECTRON TRANSFER IN RUTHENIUM-LABELLED MYOGLOBIN

Thesis by
Jennifer Lynn Karas

In Partial Fulfillment of the Requirements
for the Degree of
Doctor of Philosophy

California Institute of Technology
Pasadena, California

1989
(Submitted September 9, 1988)

Acknowledgements

I would like to thank all the members of the Gray group (both past and present) whose support made this work possible and enjoyable. In particular, I would like to acknowledge Mike Albin and Brad, and Tom and Adrienne who read and reread my props and thesis offering much needed advice and encouragement. Thanks to Miriam for all the dinners, talk and movies. I would also like to thank Dave Wheeler who cheerfully answered all my questions about the NMR machine and Jay Winkler for measurements performed at Brookhaven National Labs. My undergraduate advisor, Dave "the Doo" Dooley encouraged me to broaden my horizons and attend Caltech; thank you, Dave.

I have greatly enjoyed working with Harry Gray. He has given me invaluable insight into the field of Chemistry and other aspects of life--remember the Winnebago trip!

Finally, I'd like to thank Charlie for assistance in lab, encouragement in and out of lab and all his love.

To my Mom and Dad, Mark, Melissa

and Charlie

Abstract

The driving force dependence of electron-transfer (ET) reactions has been investigated in protein derivatives of the type *trans*-$Ru(NH_3)_4L$-myoglobin (L=NH_3, pyridine, isonicotinamide). In these species, the labelling sites of the ruthenium moiety were determined by proton NMR spectroscopy. ET rates have been measured from the iron(II)-heme in myoglobin to both a_5Ru (a=NH_3) and a_4pyRu (py=pyridine) acceptors bound to histidine 48 (k_{ET}=0.04 and 2.5 s^{-1}; ΔE^o=0.02 and 0.275, respectively). These kinetic results demonstrate for the ruthenium-labelled Mb system that long-range ET is reversible and that the dependence of the ET rates on reaction free energy closely follows Marcus theory. ET rates were also determined for high driving-force systems that were prepared by substitution of palladium and zinc(mesoporphyrin IX), (PdP, ZnP) into the a_4LRu(His-48) derivatives of Mb. ET from the excited state MbMP* (M=Pd or Zn) to the ruthenium acceptor was measured by transient spectroscopy. Reverse ET rates from the surface Ru^{II} to the ZnP radical cation, ($Ru^{II}\rightarrow ZnP^+$) were also determined. The ET rates range from 0.04 s^{-1} for $Fe^{II}\rightarrow Ru^{III}$ ET in a_5Ru(His-48)MbFe (ΔE^o=0.02 V), to $3x10^5$ s^{-1} for $ZnP^*\rightarrow Ru^{III}$ ET in a_4isnRu(His-48)MbZn (ΔE^o=1.2 V). The driving force dependence of the ET rates in the ruthenium-labelled Fe, Zn and Pd(His-48)Mb derivatives has provided information on the reorganization energy. Using Marcus theory, a reorganization energy of 1.5(2) eV has been estimated.

Table of Contents

List of Figures

List of Tables

Chapter I.

Introduction

Long-range electron transfer (ET) is an important step in many biological processes[1-13] including respiration[1,2] and photosynthesis.[3,4] In these processes a series of ET steps between oxidation/reduction (redox) centers is coupled to the production of ATP for biosynthesis. The redox active groups in the electron transport chains, such as metal ions, hemes, iron-sulfur clusters, flavins and quinones, are usually enclosed in proteins and are often greater than 10 Å apart. The electron transport chains for bacterial photosynthesis and mitochondrial respiration are shown in Figure 1.[14] In both systems the reduction potentials decrease gradually along the chain in order to use energy efficiently. To understand these processes it is important to know what controls the electron transfer steps.

Many ET reactions in biological systems are not yet fully understood. Recently, however, attention has focused on the photosynthetic reaction center, because the crystal structures have been solved for the reaction centers from *Rhodopseudomonas viridis* and *Rhodobacter sphaeroides*.[15,16] From these structures the spatial organization of the chromophores was determined (Figure 2). The redox centers involved in the initial ET step include; two bacteriochlorophylls (BChl) that make up the special pair (P), a bacteriopheophytin (BPh) and an accessory bacteriochlorophyll that lies in the pathway between the special pair and BPh. When the special pair is excited with light an electron is transferred to a BPh: $P^{*}+BPh \rightarrow P^{+}+BPh^{-}$. This initial photochemical act is very fast, occurring in less than 3 ps;[3] (the ET distance is ~10 Å). The nature

Figure 1. Electron transport chains of a) mitochondrial respiration and b) photosynthesis. From reference 14.

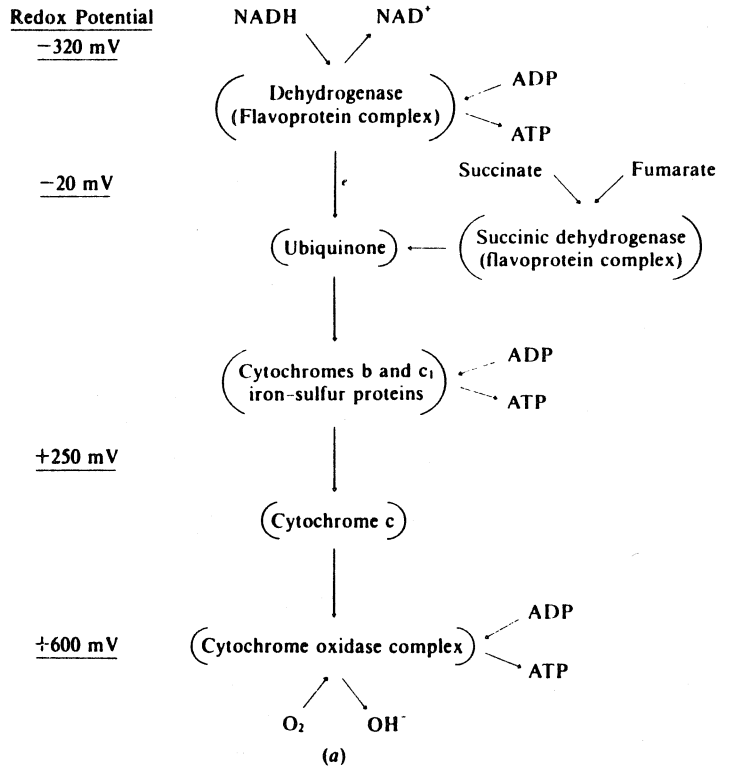
Redox Potential
−320 mV
−20 mV
+250 mV
+600 mV
NADH
NAD+
Dehydrogenase (Flavoprotein complex)
ADP
ATP
e
Succinate
Fumarate
Ubiquinone
Succinic dehydrogenase (flavoprotein complex)
Cytochromes b and c1 iron-sulfur proteins
ADP
ATP
Cytochrome c
Cytochrome oxidase complex
ADP
ATP
O2
OH−
(a)

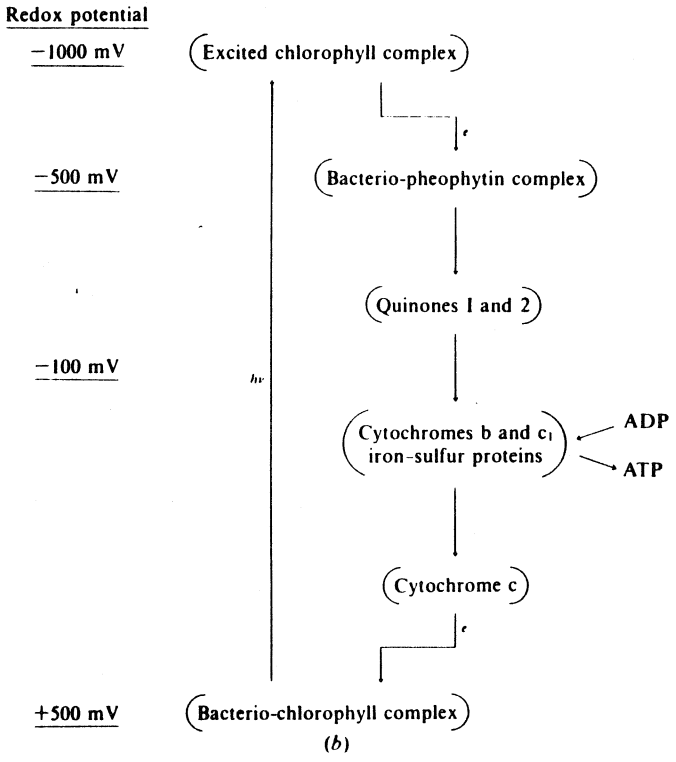
Redox potential
−1000 mV
−500 mV
−100 mV
+500 mV
Excited chlorophyll complex
e
Bacterio-pheophytin complex
Quinones 1 and 2
Cytochromes b and c1 iron-sulfur proteins
ADP
ATP
Cytochrome c
e
hν
Bacterio-chlorophyll complex
(b)

Figure 2. Spatial organization of the chromophores in the bacterial photosynthetic reaction center.[4,15,16]

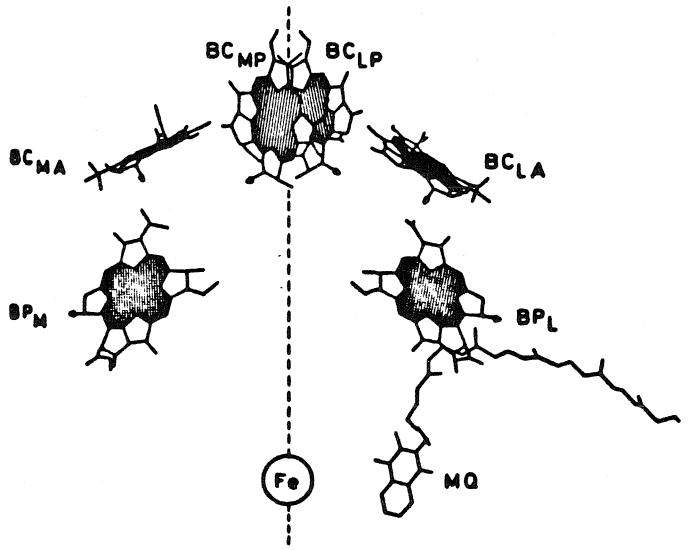
BC_MP
BC_LP
BC_MA
BC_LA
BP_M
BP_L
Fe
MQ

of this ET step and the role of the accessory BChl ($BChl_A$) are not well understood. It has been suggested that the $BChl_A$ is an intermediate in the initial ET process and that a two-step reaction occurs.[17,18] However, the $BChl_A$ intermediate has never been detected. A single-step superexchange mechanism, in which the $BChl_A$ is strongly coupled to the special pair and the BPh, has also been proposed.[19] Systems of this type raise fundamental questions about the role of the intervening medium in controlling ET reactions. A number of other factors are also important. These will be discussed below.

In biological systems electron transfer occurs between fixed redox sites (a donor and an acceptor) at distances ≥ 10 Å.[1-13] These donor/acceptor (D/A) systems can be represented by a model (Figure 3). In this two-site model the D and A are fixed in a rigid matrix (such as a protein) and are separated by a through-space distance, d. Theory and experiment suggest that there are several factors that play an important role in controlling ET rates, including:

1) The distance between the donor and the acceptor;

2) The nature of the intervening medium between the donor and the acceptor;

3) The reaction free energy or driving force, i.e., the difference in reduction potential between the donor and the acceptor; and

4) The nuclear reorganization at the redox centers that accompanies ET.

Figure 3. Model of a donor/acceptor system.

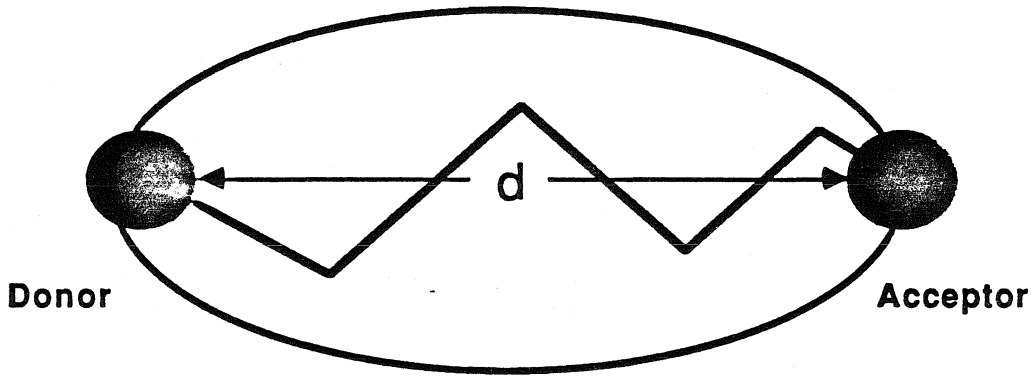
d
Donor
Acceptor

There are several theoretical treatments that have been used to treat biological ET reactions.[5,20-22] One of the earliest and most successful theories was developed by Marcus.[5,23] He derived a classical description for the ET rate that can be used to describe intramolecular ET in D/A systems:

1) $k_{ET}=\nu_n\kappa_e\kappa_n$.

This expression is composed of three parts; a nuclear frequency factor, ν_n, an electronic term, κ_e and a free energy term, κ_n. In equation 1, ν_n is typically assumed to be 10^{13} s^{-1}. The electronic term is unity when the donor and acceptor are strongly coupled (i.e., an adiabatic reaction), and $\kappa_e<1$ for weakly coupled (nonadiabatic) systems. In the nonadiabatic regime, κ_e is expected to fall off exponentially with distance;

2) $\kappa_e=\kappa_e^o \exp[-\beta(d-d_o)]$.

In this equation, d_o is the van der Waals contact distance, usually assumed to be 3 Å, and κ_e^o is the electronic coupling term when $d=d_o$. (If the reaction is adiabatic at $d=d_o$, then κ_e^o is1.) Equation 2 reflects the decrease in D/A electronic coupling with increasing distance. The rate of this decay is given by β, which is believed to depend on the nature of the medium. The parameter β can be determined experimentally from investigations of k_{ET} versus distance.

The free energy term, κ_n, is dependent on two parameters; the total reaction free energy or driving force, ΔG^o and the reorganization energy, λ:

3) $\kappa_n = \exp[-(\Delta G^o + \lambda)^2/4\lambda RT]$.

For a barrierless reaction ($-\Delta G^o = \lambda$) $\kappa_n = 1$. The reorganization energy, λ, can be determined from a plot of $\ln k_{ET}$ versus $-\Delta G^o$. A number of studies have been performed to experimentally investigate both the electronic and free energy contributions.[7,11-13]

The approaches used to investigate long-range ET include protein D/A systems[7,11,12] as well as synthetic organic model systems.[13] The necessary requirements for a successful D/A system include; 1) a rigid framework and 2) a known ET distance, driving force and medium. One method that has been used by several groups is synthesis of organic D/A molecules that are separated by a rigid spacer. The rigid molecules (rather than the semi-rigid or flexible systems) help to mimic biological ET in that the D and A are held at a fixed and well-defined distance. In flexible systems the uncertainties in the distance and conformation complicate interpretations of the resulting kinetics.

There are many examples of rigid organic models[24-28] including the biphenyl-steroid-naphthyl molecules (Closs et al.[13,24]), and the porphyrin-spacer-quinone systems (Wasielewski et al.[25] and Joran et al.[26]) that mimic the photosynthetic reaction center (Figure 4). Organic systems in which the donors, acceptors

Figure 4. Organic donor/acceptor molecules. a) Biphenylyl-steroid-acceptor.[13] b) Porphyrin-spacer-quinone.[25] c) Porphyrin-spacer-quinone.[26] d) Dimethoxynapthalene-spacer-dicyanoethylene.[27] e) Dimethylaniline-aromatic spacer-anthracene.[28]

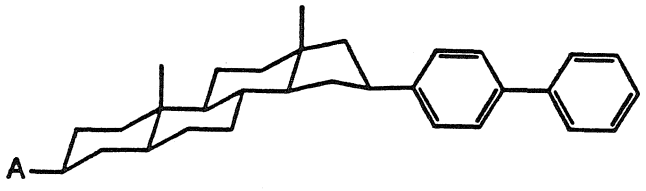

a

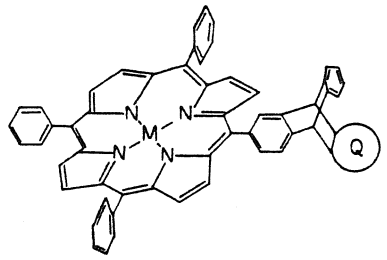

b

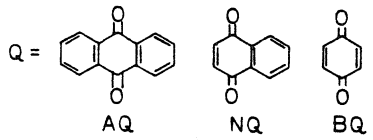

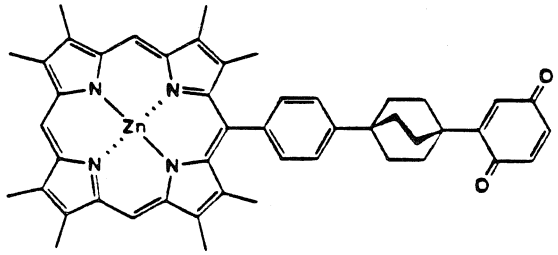

c

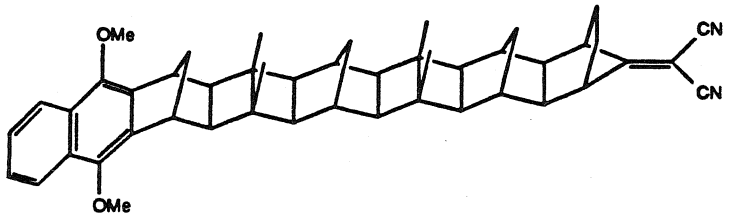

d

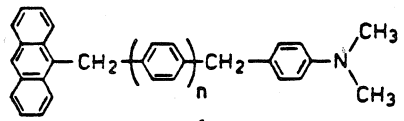

n = 1

n = 2

e

and spacers can be systematically varied have been used to study the effects of distance, reaction free energy and medium on ET rates.

Another approach that has been used to investigate long-range ET utilizes physiological protein partners.[7,8] A well-defined noncovalent complex stabilized by hydrophobic and electrostatic interactions can often be formed from two reacting proteins.[7] In most cases the structures of the individual proteins have been characterized by x-ray crystallography and a model of the complex has been generated by computer modeling studies. Protein-protein complexes in which ET has been studied include: cytochrome c (cyt c)/cytochrome b_5 (cyt b_5),[29] cyt b_5/hemoglobin (Hb),[30] cyt c/cytochrome c peroxidase (ccp)[31] and the α and β subunits of Hb.[32] The binding between partners in these systems has been studied. The donor to acceptor distances range from 8 to 25 Å. To observe the electron transfer in some of these systems, metal-substituted derivatives have been prepared. The various porphyrin derivatives in the protein-protein complexes allow investigation of ET rate versus reaction free energy at a fixed distance.

The strategy that has been employed in our laboratory involves covalently attaching a redox-active ruthenium complex to a surface histidine of a crystallographically characterized metalloprotein.[10,11] Using this method it is possible to prepare D/A systems in which the ET distance and the intervening medium are known. In addition, the reaction free energy can be tuned through systematic changes in the ruthenium complex. ET rates have been measured in $(NH_3)_5$Ru-labelled myoglobin,[33-37] cyt c[38-41] and

azurin.[42,43] The results from several ET studies are summarized below, including distance dependence and reaction free energy dependence of ET rates.

Distance Dependence of Electron Transfer Rates

One question that has been addressed both in organic model systems and in protein systems is: How does the ET rate depend on the distance between the donor and acceptor? Several theories predict that k_{ET} will drop off exponentially with distance according to equation 4,[5,20-22]

4) $$k_{ET} = k_o \exp[-\beta(d-d_o)],$$

where d is the D-A distance and d_o is the van der Waals contact distance, generally taken to be 3 Å. k_o is the ET rate at $d=d_o$. β can be determined from a logarithmic plot of ET rate versus distance; the slope will be equal to $-\beta$. To investigate the distance dependence of k_{ET}, it is desirable to keep the reaction free energy, the reorganization energy, the intervening medium and the orientation of the D and A constant.

Closs et al. have synthesized several D/A complexes in which the intervening spacer was varied.[13,24] To keep the free energy constant the donor (4-biphenylyl) and the acceptor (2-naphthyl) remained unchanged as the spacer was varied from cyclohexane, to decalin to androstane (Figure 4a). The ET rates (measured by pulse radiolysis) varied from 4.2×10^9 to 1.5×10^6 s^{-1} for distances 10-17.4 Å. Since several types of isomers were being compared (equatorial

versus axial donors and acceptors) it was found that the results did not correlate well with distance. It was suggested based on molecular orbital considerations that the electronic coupling was different in the equatorial versus axial isomers. Using only the molecules with equatorial donors and acceptors, β was determined to be 0.95 $Å^{-1}$.

Results in other systems give similar values for β. Oevering et al. have used polycyclic D/A complexes (Figure 4d) that have 4, 6, 8, 10, or 12 sigma bonds between the dimethoxynaphthalene donor and the dicyanoethylene acceptor.[27] ET from the photoexcited naphthalene to the cyanoethylene fragment was measured by fluorescence quenching. A three point distance/rate correlation was obtained with $\beta=0.85$ $Å^{-1}$.

Although there is an abundance of ET rate data for porphyrin-quinone models at fixed distances, only recently has there been a study of a homologous series of rigid porphyrin-quinone models with the same driving force, solvent, orientation and spacer unit. Leland et al.[44] have recently reported ET results on zinc-meso-phenyloctaalkylporphyrins coupled to a quinone by one and two bicyclooctyl spacers (Figure 4c). The electron transfer rates were calculated from the picosecond fluorescence lifetimes of the D/A molecules. As the distance is increased from 14.8 to 18.8 Å (from one to two spacers) the ET rate decreases by at least a factor of 500-1600, depending on solvent. The value for β was estimated to be ≥ 1.4 $Å^{-1}$.

Heitele et al. have created two homologous linked D/A systems (Figure 4e).[28] In these systems (compared to previous organic D/A molecules), the spacer was an aromatic group rather than an aliphatic spacer. The ET rates were measured from the dimethylaniline (D) to the anthracene (A) by fluorescence quenching. The rate decreased by a factor of 22 to 27 when the distance was increased by 4 Å (phenyl to biphenyl spacer). This is in contrast to the results mentioned before of Leland et al. and Closs et al. in which a 4 Å change resulted in a much greater decrease in ET rate. These results suggest that the nature of the spacer may be an important factor in controlling ET rates. A more efficient coupling to aromatic groups by a superexchange mechanism has been suggested by Heitele et al. to explain the difference in behavior.

Electron transfer rates have been measured in various protein systems in which the D/A distances range from ~8 to 20 Å. The first controlled distance dependence in a single protein based system was performed with $(NH_3)_5Ru$-labelled Zn-myoglobin (ZnMb) derivatives.[35] The advantages of the Mb system include: 1) the protein has four surface histidines (at distances 13 to 22 Å from the heme) that can be labelled with the ruthenium reagent, 2) Mb has been crystallographically characterized, and therefore the ET distances and protein medium between the donor and acceptors are known and 3) the heme center can be easily replaced with a highly reducing photoactive Zn porphyrin so that ET rates can be measured at the longer distances.

The ET rates in these systems were measured by transient absorption as outlined in Scheme I.

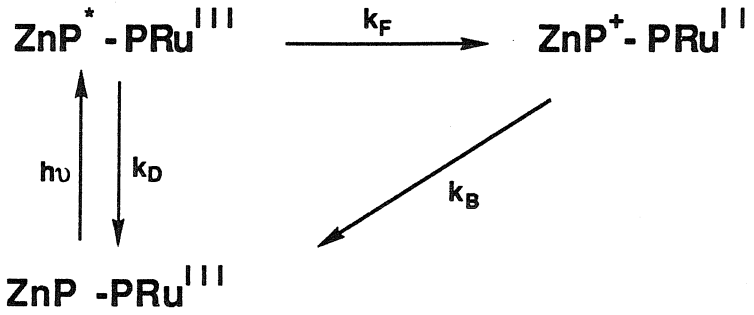

Scheme I

Pulsed laser excitation generates ZnP^* which subsequently returns to the ground state via nonradiative and ET pathways.

The range of distances and ET rates are given in Table I. The through-space distance was determined from computer-modeling studies.[35] The distances correspond to that measured from the edge of the porphyrin ring to the edge of the histidine imidazole to which the ruthenium is bound. The uncertainty in distance was the variation found at 6.5 kcal above the calculated potential minimum. The $\ln k_{ET}$ versus distance plot using the experimental data for ZnMb and the results for $(NH_3)_5Ru$-modified Zn-substituted cytochrome c are shown in Figure 5. The value of β calculated using the minimum distances was equal to 0.91 $Å^{-1}$.

The distance dependence results obtained for the organic-spacer systems and the protein systems yield β values that are very similar. The calculated values of β range from 0.85 to 1.4 $Å^{-1}$. It is interesting that β is similar for both protein and organic systems.

Table I. Electron-transfer distances for ruthenium-labelled heme proteins.[35]

Derivative	Distance (Å)
a_5Ru(His-33)cyt c	10.8-11.7 [11.6]
a_5Ru(His-48)Mb	11.8-16.6 [12.7]
a_5Ru(His-81)Mb	18.8-19.3 [19.3]
a_5Ru(His-116)Mb	19.8-20.4 [20.1]
a_5Ru(His-12)Mb	21.5-22.3 [22.0]

a. The distances were measured from the heme edge to the imidazole edge. The distances are lower and upper values at 6.5 kcal above the potential minimum. The value at the minimum is in brackets.

Figure 5. Logarithmic plot of ET rate versus distance for Ru-labelled ZnMb and Zn-cyt c derivatives.[35]

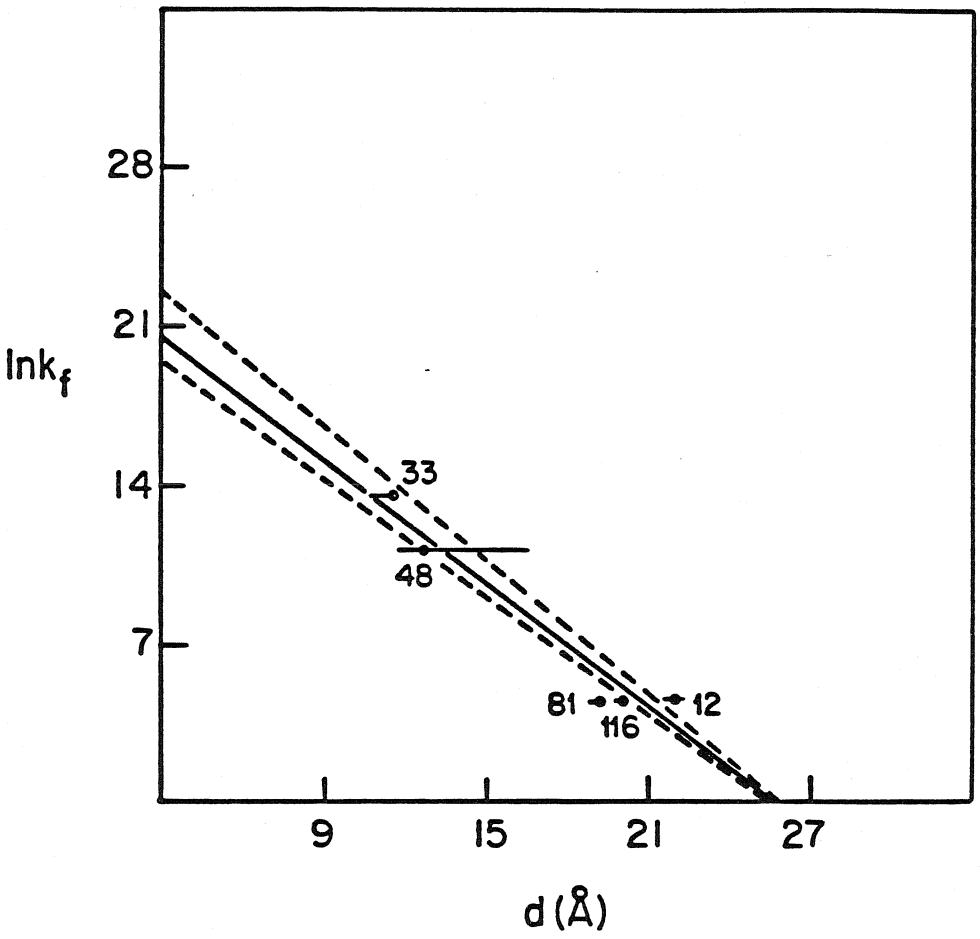
28
21
14
7
lnk$_f$
33
48
81
116
12
9
15
21
27
d (Å)

It might be expected that β would be larger for proteins since viable through-bond pathways are not always available. The maximum ET rates that have been observed in organic D/A systems are significantly faster than the maximum rates observed in protein-protein and Ru-labelled protein systems at similar distances. Since this difference could arise from differences in the free energy term, the next section describes work that has explored the dependence of the ET rate on the reaction free energy.

Free Energy Dependence of the ET Rate: Determination of the Reorganization Energy

Another area that has received much attention is the free energy dependence of the ET rate. The free energy expression from Marcus theory is shown below:[5]

5) $k_{ET}=A\exp-[(\Delta G^{o}+\lambda)^{2}/4RT\lambda]$.

The reorganizaton energy can be determined from an examination of the ET rate. As the reaction free energy is increased, the ET rate is predicted to increase, reach a maximum when $-\Delta G^{o}=\lambda$, and then fall off. The highly exoergic region where the ET rate decreases is often called the "inverted region." A typical Marcus reaction free energy curve is shown in Figure 6.

One of the first demonstrations of the inverted region was reported by Closs et al. using rigid organic D/A compounds. The D/A compounds used were rigid organic spacer systems of the type described before; biphenylyl-donor, androstane spacer and various

Figure 6. A theoretical Marcus free energy curve, λ=1.5 eV.[5]

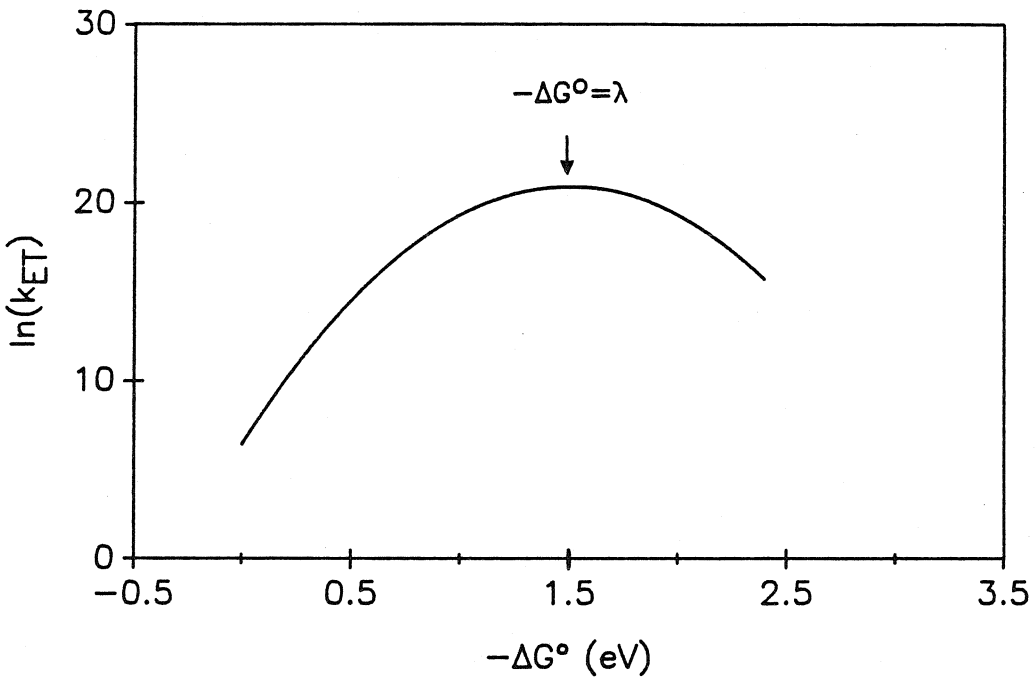
30
20
10
0
−0.5
0.5
1.5
2.5
3.5
−ΔG°=λ
ln(kET)
−ΔG° (eV)

electron acceptors (Figure 4a).[13,24] The advantages of these systems is that the steroids are rigid in structure and have a well-known geometry, and the acceptors can be varied to cover a range of reaction free energies (almost 2.4 eV). The ET results plotted against the reaction free energy are shown in Figure 7. As indicated in the plot; the ET rates increase, go through a maximum and then drop off. The data were fit[45] with the parameters listed in the figure to yield a total reorganization energy, λ=1.2 eV. Further confirmation of Marcus theory was obtained from the solvent dependence in the same series of molecules. As predicted by the dielectric continuum model,[5] as the solvent became less polar the maximum rates occurred at lower free energy and the value for λ decreased. The reorganizaton energies for the same D/A compounds in methyltetrahydrofuran, butylether and isooctane were calculated to be 1.2, 0.9 and 0.6 eV, respectively.

There have been other reports of the inverted region in which rigid porphyrin-quinone systems have been used.[25] The molecules synthesized were of the type shown in Figure 4b. The porphyrin (P) was either a zinc or free base porphyrin and the quinones (Q) were anthraquinone, naphthaquinone or benzoquinone. The formation and decay of the porphyrin-quinone radical pair state was monitored by transient absorption spectroscopy. Rate constants were determined for both the radical ion pair formation from the excited state of the porphyrin (^{1*}P-Q$\rightarrow$P^{+}-Q^{-}) and for radical ion pair recombination to the donor and acceptor ground states (P^{+}-Q$^{-}\rightarrow$P-Q). A plot of the rate constant versus reaction free energy is shown in Figure 8. Once

Figure 7. Logarithmic plot of experimental rate constants for biphenylyl-steroid-acceptor molecules in methyltetralhydrofuran. From reference 13.

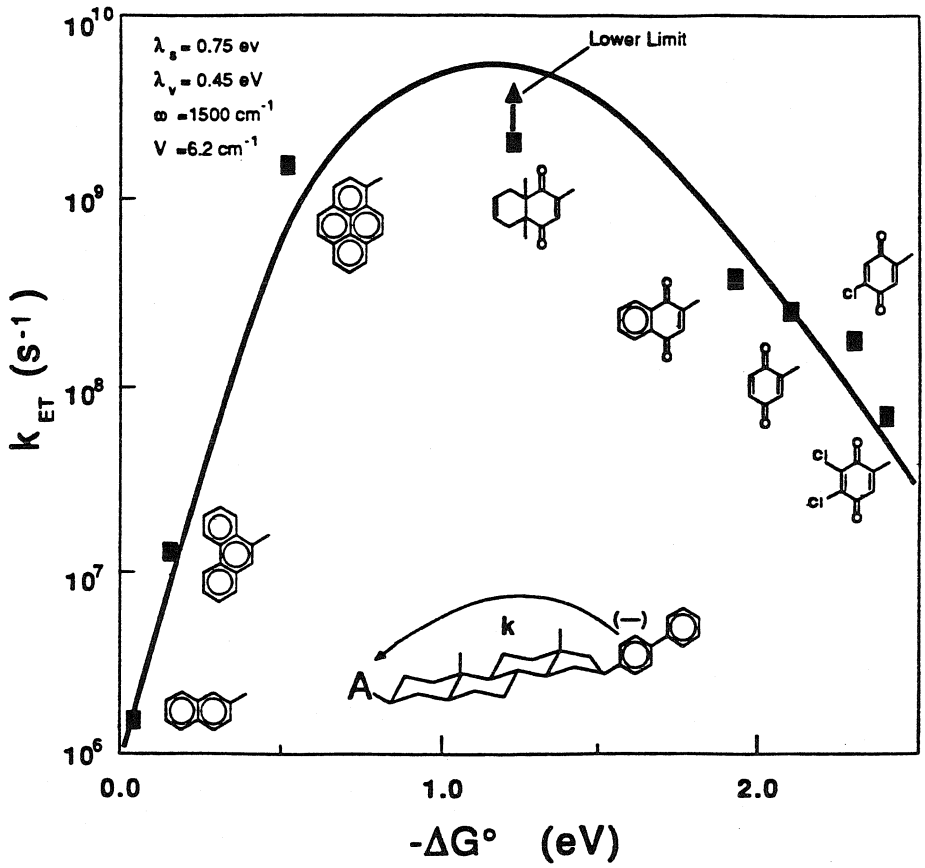
10^{10}
10^{9}
10^{8}
10^{7}
10^{6}
k_{ET} (s^{-1})
λ_s = 0.75 ev
λ_v = 0.45 eV
ω =1500 cm^{-1}
V =6.2 cm^{-1}
Lower Limit
Cl
Cl
Cl
k
(—)
A
0.0
1.0
2.0
-ΔG° (eV)

Figure 8. Plot of rate constant vs. exothermicity for the reaction ^{1*}P-Q$\rightarrow$P^{+}-Q^{-} and for P^{+}-Q$^{-}\rightarrow$P-Q, where P=porphyrin and Q=quinone. The B and T after the name of the compounds indicate data obtained in butyronitrile or in toluene, respectively.[25]

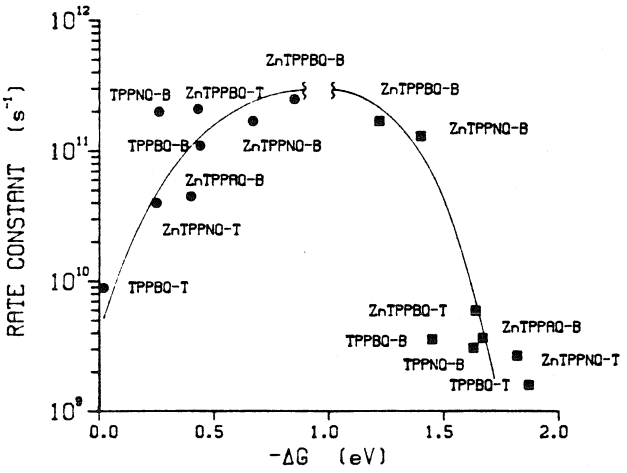
RATE CONSTANT (s⁻¹)
10¹²
10¹¹
10¹⁰
10⁹
0.0
0.5
1.0
1.5
2.0
-ΔG (eV)
ZnTPPBQ-B
TPPNQ-B
ZnTPPBQ-T
ZnTPPBQ-B
ZnTPPNQ-B
TPPBQ-B
ZnTPPNQ-B
ZnTPPAQ-B
ZnTPPNQ-T
TPPBQ-T
ZnTPPBQ-T
ZnTPPAQ-B
TPPBQ-B
TPPNQ-B
ZnTPPNQ-T
TPPBQ-T

again the rates have decreased at high exothermicity. The maximum of the curve is reached at $-\Delta G^o$=0.9 eV, and this was taken as the approximate total reorganization energy for both the charge separation and the recombination reactions.

The reorganization energy has also been determined by the free energy dependence in the rigid porphyrin-quinone systems synthesized by Joran et al.[26] The rates level off at ~1-1.2 eV and at 1.4 eV the ET rate decreases moderately (Figure 9). Using classical Marcus theory, the λ was calculated to be 1-1.3 eV for a variety of solvents. If a single vibrational mode is allowed for, the total reorganization energy is much smaller, ~0.60 eV.[46]

The method used in protein-protein systems to study the free energy dependence of ET is to vary ΔG^o between the donor and acceptor by metal substitution at the porphyrin. Several studies have suggested that protein-protein complexes (cyt c/cyt b_5) do not undergo significant structural changes upon metal removal or replacement.[7] McLendon et al. have used cytochrome c derivatives containing Fe, Zn or the free base-H_2 porphyrin at the heme site to study the free energy effects in both the cyt c/cyt b_5 complex[29] and the cyt c/ccp complex.[31] The metal-substituted cyt c/cyt b_5 complexes yield a range of reaction free energies from 0.2 to 1.1 eV. A plot of the ET rate ($\ln k_{ET}$) versus $-\Delta G^o$ (Figure 10a) can be fit with Marcus theory to yield λ=0.8 eV. One disadvantage of this study is that the nature of the donor and acceptor does not remain constant. From a similar study using the cyt c/ccp couple, the ET rate as a function of free energy yields λ=1.5 eV (Figure 10b). It has been

Figure 9. Plot of log(ET rate constant) against -ΔG(eV). Molecules of type shown in Figure 4c. a) benzene, λ=1.01 eV. b) 2-methyltetrahydrofuran, λ=1.19. c) butyronitrile, λ=1.25. d) acetonitrile, λ=1.31. The dashed line in (a) is semiclassical theory,[46] λ=0.6.[26]

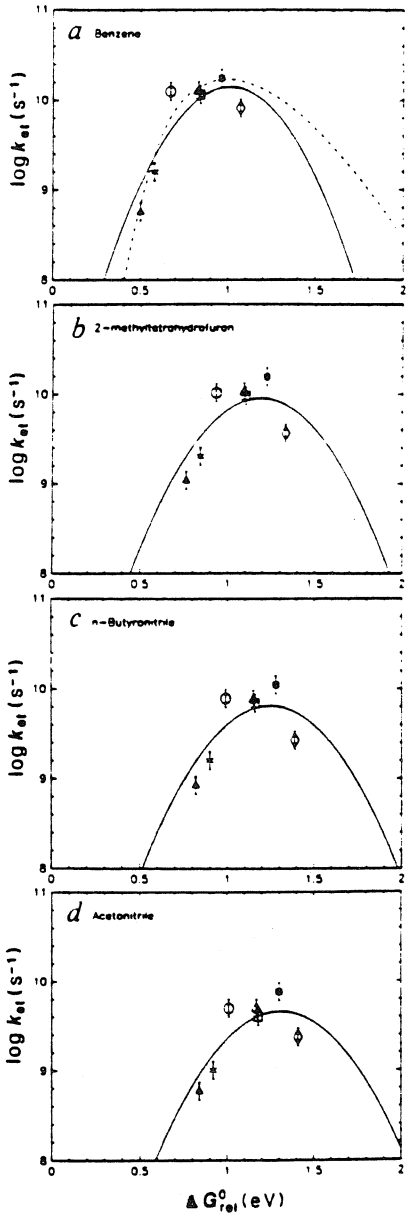
a Benzene
b 2-methyltetrahydrofuran
c n-Butyronitrile
d Acetonitrile
log k_{et} (s^{-1})
ΔG^0_{rel} (eV)

Figure 10. Plot of ET rate as a function of free energy, a) cyt c/cyt b_5, λ=0.8 eV. b) cyt c/ccp, λ=1.5 eV.[7]

a

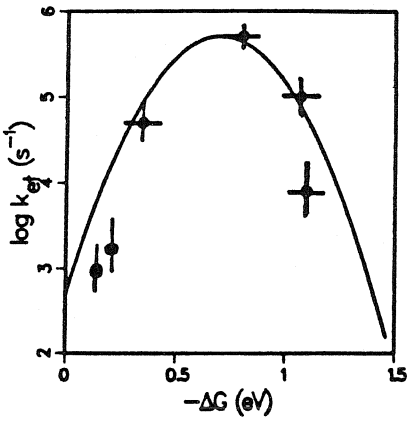
log k_{et} (s^{-1})
2
3
4
5
6
0
0.5
1
1.5
$-\Delta G$ (eV)

b

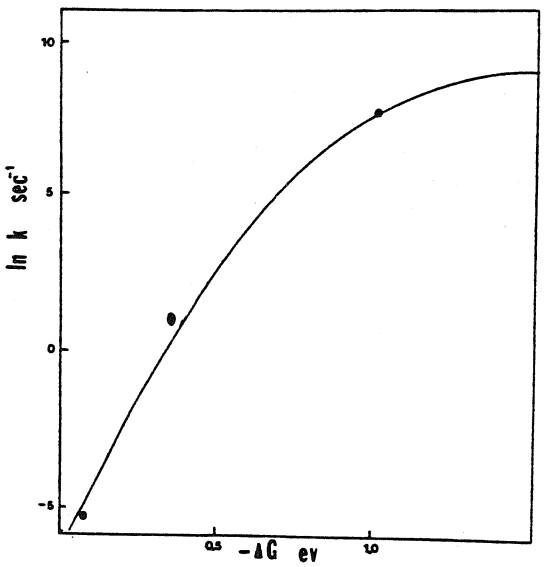
ln k sec^{-1}
10
5
0
-5
0.5
$-\Delta G$ ev
1.0

suggested that structural changes at the protein-protein interface may account for a large fraction of the reorganization energy. A larger reorganization energy (λ=2.0 eV) was obtained for Zn,Fe hybrid Hb by analyzing the temperature dependence of the rate.[32]

In contrast to the previous two protein systems, there is no change in ET rate with increasing free energy in the cyt c/cyt b_2 complex.[47] McLendon et al. have proposed that a conformational change controls the reaction rate in this system.

The investigations of organic-spacer and protein D/A systems have yielded a variety of reorganization energies from 0.6 to 2.0 eV. In general, it appears that λ is larger in proteins, but further investigations are warranted in order to assess the importance of free energy in ET reactions. A study of ET rates in a homologous series of protein based D/A systems is needed.

This thesis contains an investigation of the free energy dependence of ET rates in Ru-labelled myoglobin. In Chapter II, the preparation and characterization of the Ru-labelled myoglobin donor/acceptor systems are described. In Chapter III, the ET results are presented and analyzed in terms of Marcus theory. Conclusions and suggestions for further work are included in Chapter III.

Chapter II.

Preparation and Characterization of Ruthenium-Labelled Myoglobin

Introduction

The first goal of our work is to prepare appropriate donor-acceptor (D/A) systems so that intramolecular electron transfer (ET) can be studied in a systematic fashion. The systems need to have a known medium between the two redox sites, a fixed and known distance between the two sites and a donor and acceptor in which the potentials can be measured. The approach we have employed to prepare our D/A systems involves covalently attaching a redox-active ruthenium complex to a surface histidine of a crystallographically characterized metalloprotein.[10,11] Using this strategy it is possible to prepare D/A molecules in which the ET distance and intervening medium are known. In addition, the reaction free energy can be fine tuned through systematic changes in the ruthenium complex. ET rates have been measured previously in several proteins that have been labelled with ruthenium reagents; these proteins include azurin,[42,43] cytochrome c[38-41] and myoglobin.[33-37]

A particularly attractive metalloprotein system for ET studies is sperm whale myoglobin (Mb), see Figure 11.[48] The prosthetic group at the active site is Fe(Protoporphyrin-IX) Figure 12. This heme is noncovalently bound to the protein and has one axial ligand; histidine 93. Water is bound in the Fe^{III}(metMb) form and it dissociates upon reduction. This structurally characterized heme protein has four surface histidine residues that lie between 13 and 22 Å from the heme center.[11,35] These are histidine 48 at 13 Å and

Figure 11. The α-carbon backbone of sperm whale myoglobin. The protoporphyrin IX center with its proximal histidine ligand is shown.

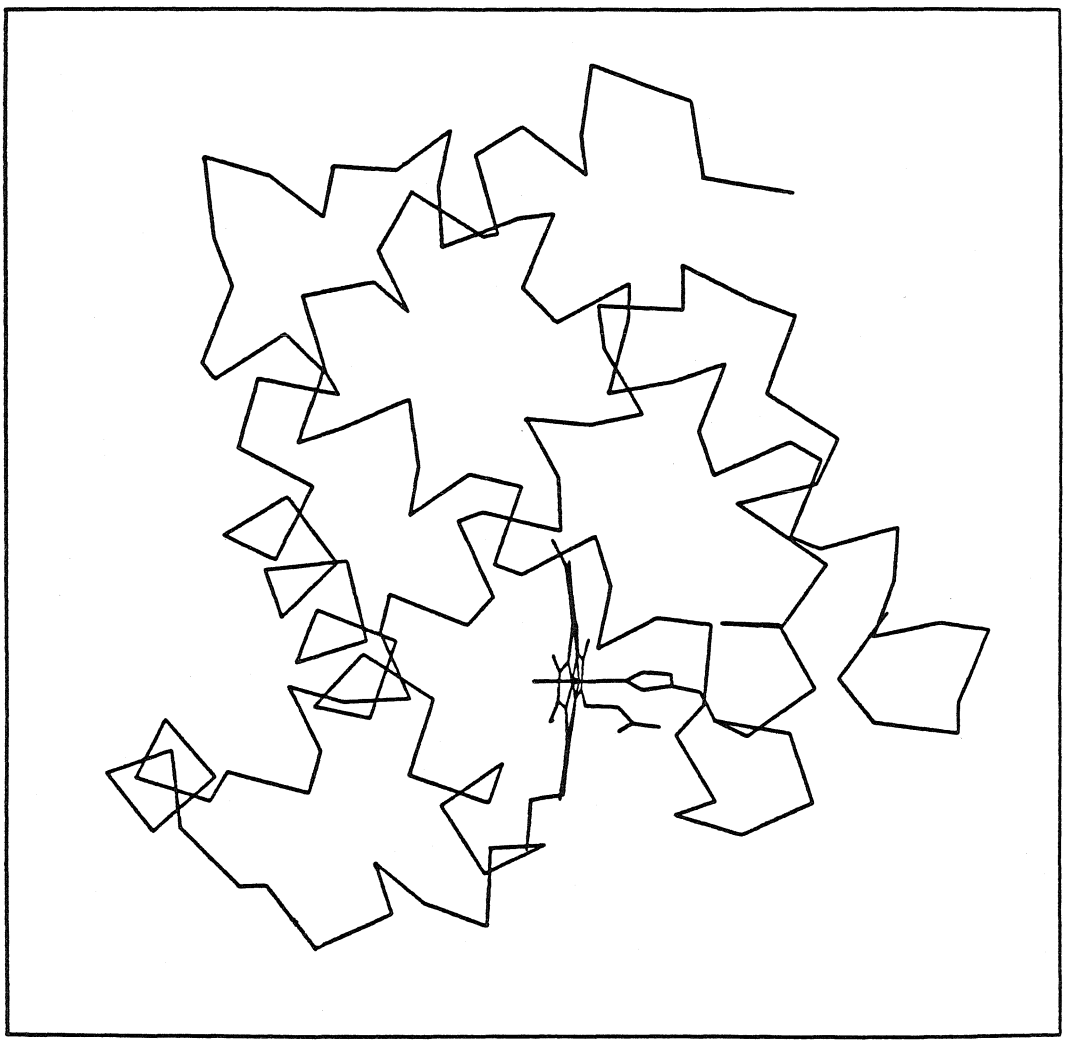

Figure 12. Structure of porphyrin IX. The alkyl groups for the proto and meso forms are indicated.

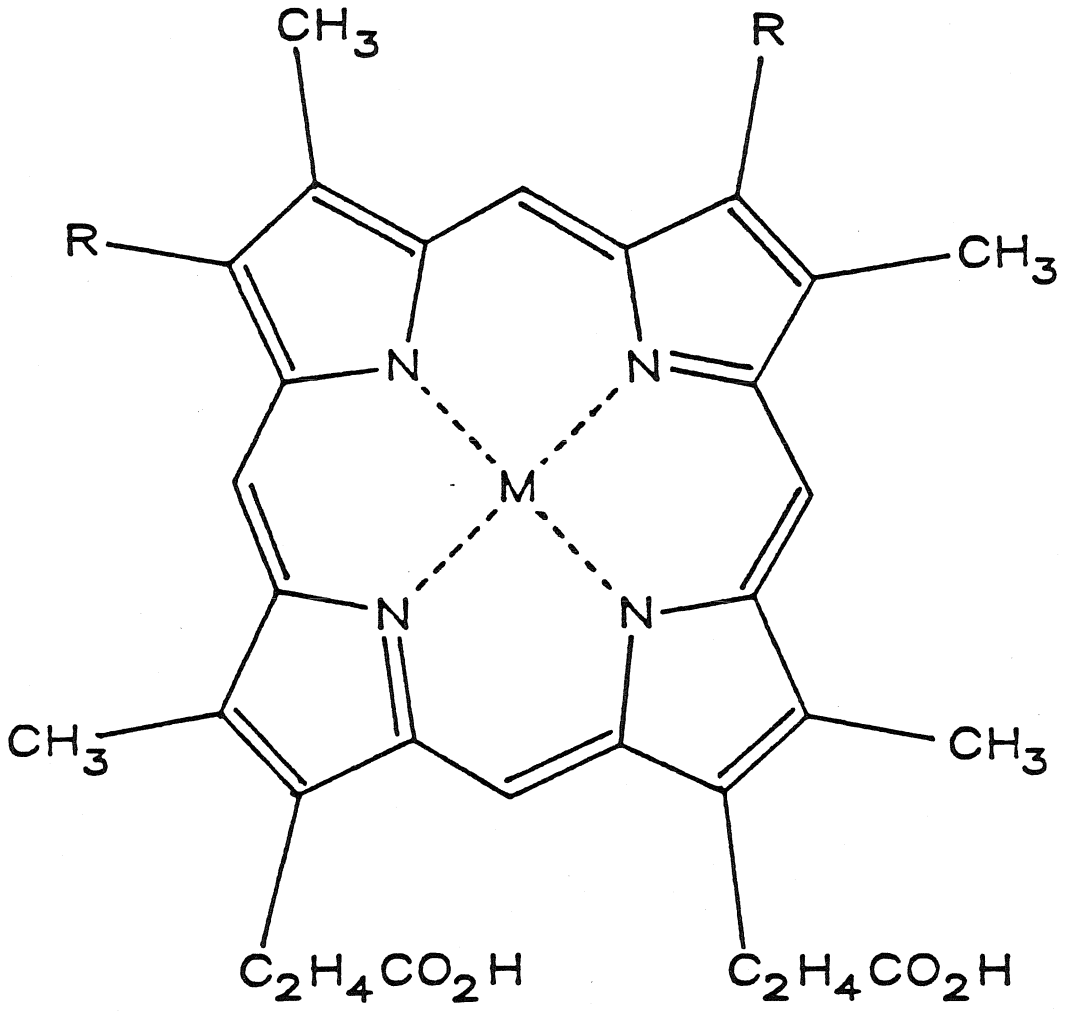

Proto: R = C_2H_3

Meso: R = C_2H_5

M (metal): Fe, Zn, Pd

histidines 12, 116 and 81 at ~20 Å from the edge of the heme, see Figure 13. These four histidine residues have been modified previously with pentaammineruthenium (a_5Ru) using procedures developed in our laboratory (Figure 14).[35-37]

An important assumption in the analysis of our data is that the ruthenium group does not perturb the native structure. Spectroscopic evidence has been used to support this contention. The UV-visible, CD and EPR spectra for the labelled derivatives versus the native Mb are unchanged. The reduction potential of the heme site in Mb is also almost identical to that of the a_5Ru-labelled Mb. In addition, the crystal structure of a_5Ru(His-48)Mb has recently been determined,[49] demonstrating that the native and ruthenium-modified structures are virtually the same (Figure 15). Therefore, we can prepare ruthenium-modified Mb with one Ru per molecule attached to a specific histidine residue at a known distance from the heme.

The preparation and characterization of a_5Ru-labelled Mb was the basis for the further work to prepare D/A systems in which the ET reaction free energy is varied. Our experimental approach involves changing the redox potential of the Ru acceptor using substituted ruthenium complexes of the general form a_4LRu-, L = ammine (a), pyridine (py) etc. By changing the group *trans* to the imidazole, the reduction potential of the ruthenium complex will be varied without any major structural perturbations. The range of potentials achieved for some related complexes ($(NH_3)_5Ru^{III/II}L$) is shown in Table II.

Figure 13. Computer graphics projection of the four surface histidines in Mb that bind ruthenium in the form a_4LRu- (L=ammine (a), pyridine, etc.) The edge-edge donor/acceptor distances for these residues range from 13 Å for the His-48 system to 22 Å for the His-12 system.

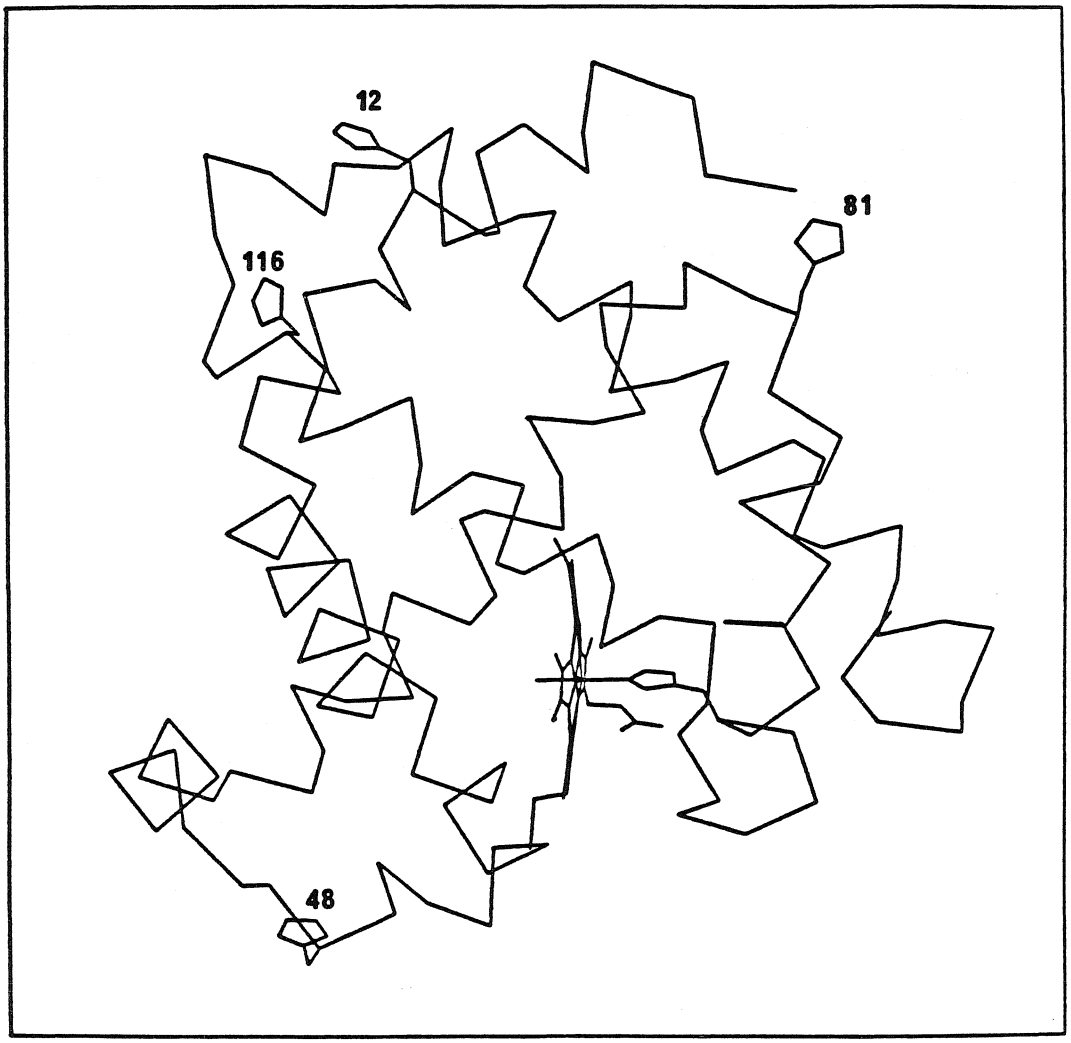
12
81
116
48

Figure 14. View of the heme and four $a_5Ru(His\text{-}X)Mb$ derivatives.[11,35]

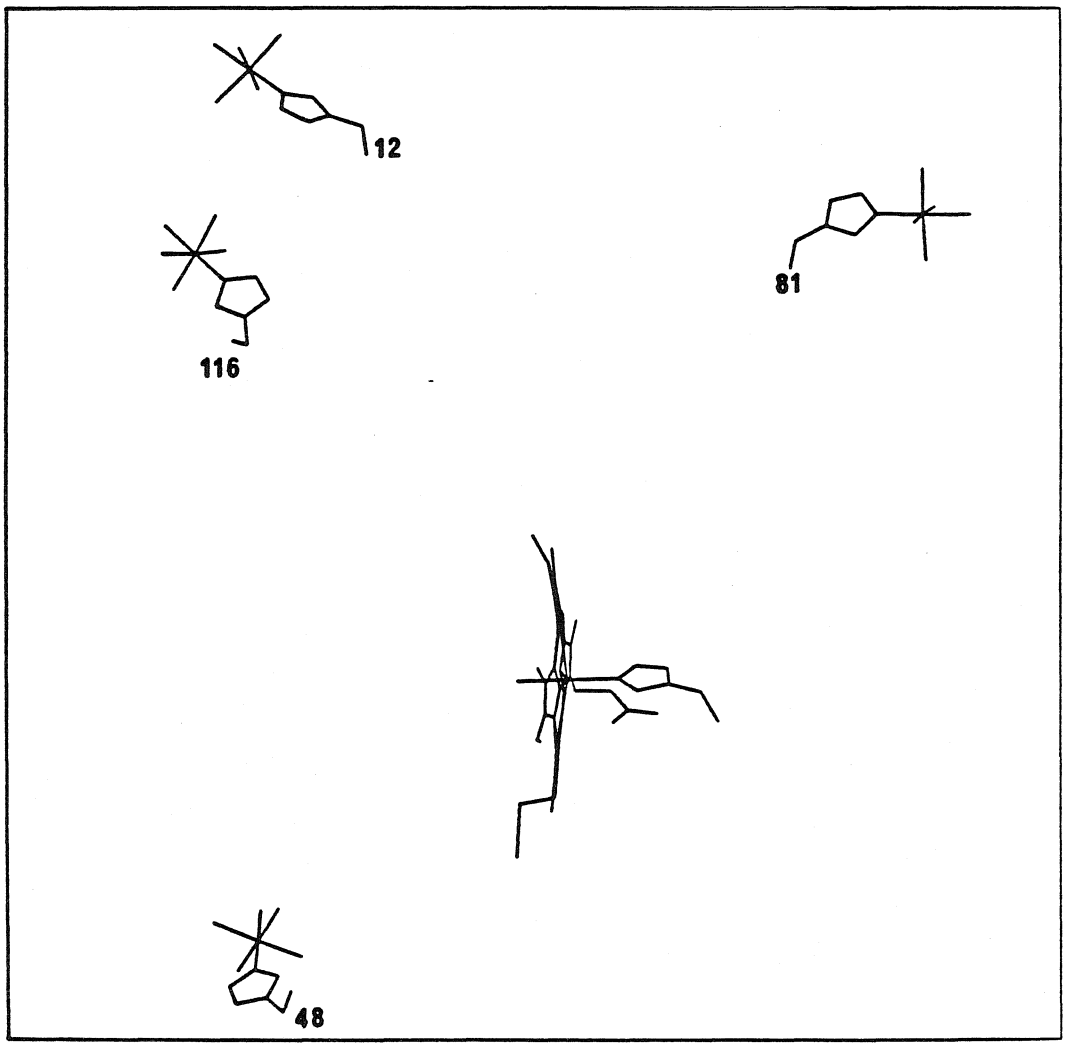
12
116
81
48

Figure 15. Computer graphics projections comparing the native Mb and the a_5Ru(His-48)Mb structure.[11,49] a) Comparison of the α-carbon chain and the native redox centers. b) Zoom on the region of His-48 showing both the native and modified conformations of the histidine.

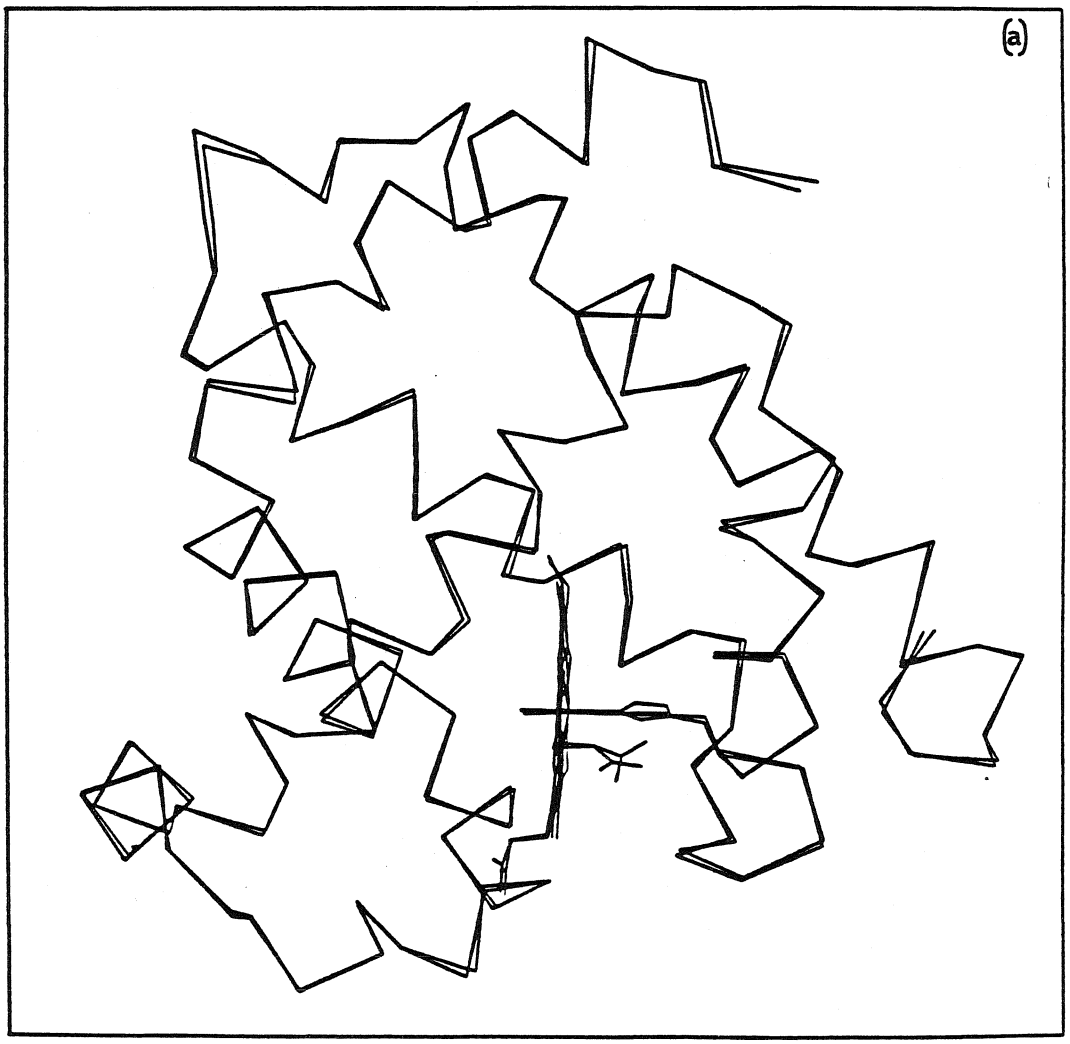
(a)

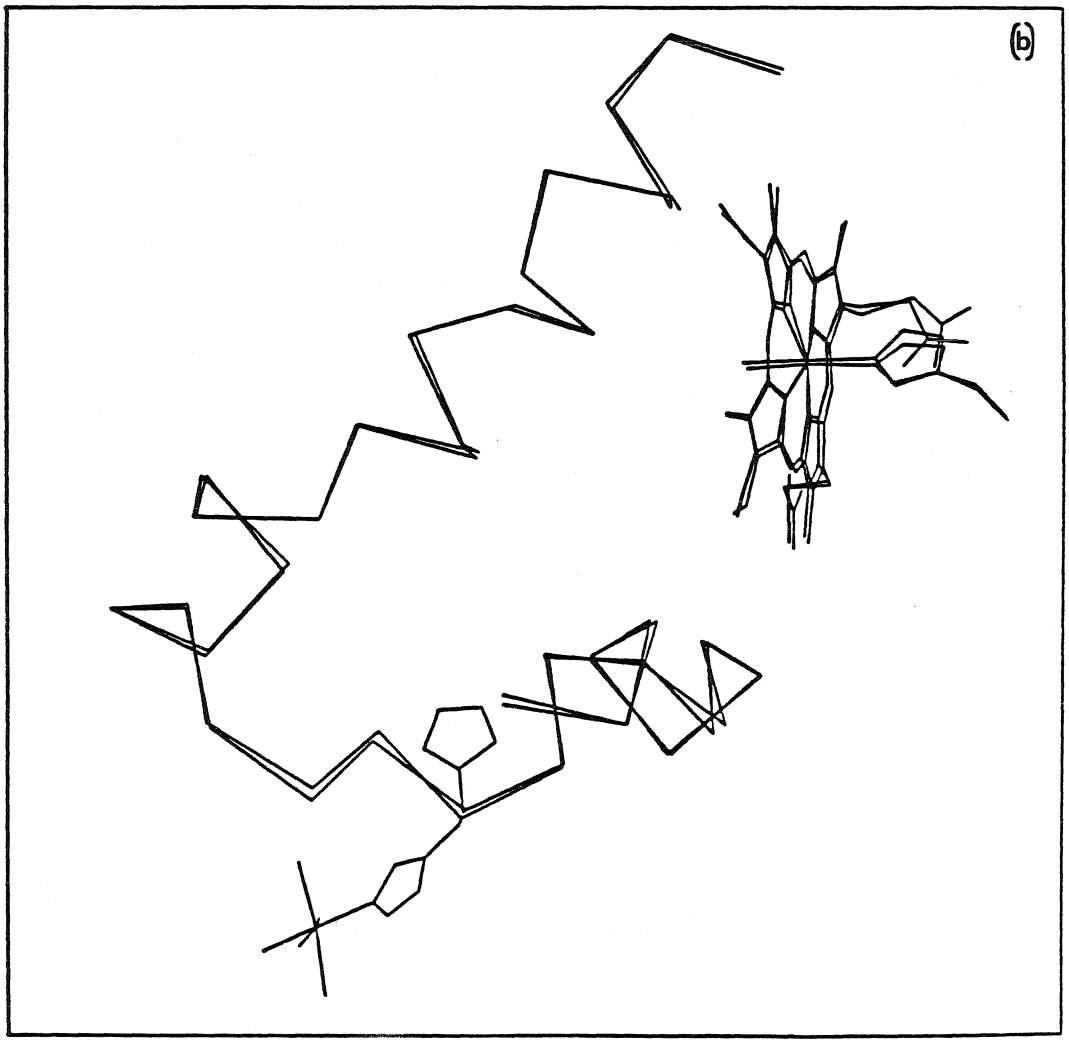
(b)

Table II. Reduction potentials for the model complexes; $(NH_3)_5Ru^{III/II}L$.

L	E^o (V vs. NHE)	Reference
NH_3	0.050	50
4-NH_2pyridine	0.15	51
pyridine	0.30	50
isonicotinamide	0.44	52
pyrazine	0.49	53

With the model complexes in mind, Ru complexes of the type $a_4LRu^{II}(OH_2)$, where L=pyridine, isonicotinamide and pyrazine, have been used to label histidines in Mb. The singly-labelled Mb species have been isolated and characterized to give new ET systems with a range of reaction free energies. The reaction free energy can be further varied by substituting different metal-porphyrin centers for the heme site. We have chosen to replace the heme center with photoactive palladium and zinc(mesoporphyrin IX). This allows for a large increase in driving force. Previous work on Mb substituted with Zn(protoporphyrin IX) indicated that the excited state of the Zn porphyrin in Mb (ZnP^*Mb) was not stable, and therefore ET rates could not be measured in these derivatives.[54] Use of the Zn(mesoporphyrin IX) alleviated these problems with stability. The meso and proto forms of the the porphyrin are similar (Figure 12).

Experimental

Materials and Reagents

The $[Ru(NH_3)_5Cl]Cl_2$ used in the synthesis of *trans*-$[Ru(NH_3)_4SO_2Cl]Cl$ was obtained from Strem Chemicals and was used without further purification.

Distilled water in all buffer and protein preparations had previously been passed through a Barnstead NANOpure system (Model 2794).

All buffer salts and other materials were of reagent grade quality and used without further purification.

Column materials (SP Sephadex C-25-120 and Sephadex G-25-150) used in the purification of the ruthenium complexes and proteins were supplied by Sigma or Pharmacia. CM52 was purchased from Whatman. They were equilibrated according to manufacturer's instructions.

Isonicotinamide and pyrazine were obtained from Aldrich and used without further purification.

Protein solutions were concentrated in ultrafiltration devices from Amicon Corporation using Amicon Diaflo YM5 membranes.

$Co(phen)_3Cl_3$ was prepared using a procedure for $Co(phen)_3(ClO_4)_3$ that had been slightly modified.[55] In a typical preparation, 2.4 g $CoCl_2 \cdot 6H_2O$ and 6 g 1,10 phenanthroline monohydrate (Aldrich) was dissolved in ~600 mL H_2O in a 1 L beaker and heated until boiling. While boiling, Cl_2 gas was bubbled through the solution for 1-2 h. The solution was then heated until the remaining volume was 100-150 mL. The pH was adjusted to pH 5 or 6 and then the $Co(phen)_3Cl_3$ was used with protein solutions as is. Na_2IrCl_6 was obtained from Aldrich.

4,4' bipyridine used for the differential pulse polarography experiments was obtained from Aldrich and recrystallized once from H_2O.

Butanone used for the Mb extraction was stored over aluminum oxide (Woelm neutral, Waters association).

Dialysis tubing (Spectrapor 1, m.w. cutoff 6000-8000) was supplied by Spectrum Medical Industries, Inc.

Zn(mesoporphyrin IX) was either prepared according to previously published procedures[54,56] or purchased from Porphyrin Products. The Pd(mesoporphyrin IX) was obtained from Porphyrin products.

Instrumentation

All absorption measurements were made using a Shimadzu model UV-260 spectrophotometer.

Protein separations and purification were achieved using a Pharmacia FPLC apparatus. This included a 1 or 2 mL injection loop, a MV7 motor valve to control the injection, a column, a UV-M monitor with a 280 nm filter and an LCC-500 controller. The cation-exchange columns used to separate the singly-labelled Mb derivatives were prepacked 1 mL, 8 mL and 20 mL Mono S columns from Pharmacia. All protein samples and buffer were filtered through 0.22 μm (Millipore) filters prior to use.

Proton NMR spectra were acquired using either a Jeol GX-400 or Bruker WM500 spectrometer. Approximately 256 scans were needed for most samples that contained protein concentration between 1 and 4 mM. NMR samples were prepared by exchanging the native and Ru-labelled protein into D_2O (Aldrich) using a 10 mL ultrafiltration device. The protein was contentrated and diluted (6 mL to < 0.5 mL) 7-9 times. The final concentrations of the protein

samples were 1-4 mM. The pH was adjusted with 0.1 M solutions of DCl (Aldrich) or NaOD (Sigma). The pH readings were uncorrected for deuterium isotope effects. All protein samples were referenced versus sodium 2,2-dimethyl-2-silapentane-5-sulfonate, DSS (Merck).

Differential pulse measurements were performed using a Princeton Applied Research Model 174A polarographic analyzer at a scan rate of 2 mV $s^{-1}$and a drop time of 0.5 s. The electrode system consisted of a gold button (2 mm diameter) working electrode (Bioanalytical Inc.), a Pt wire auxillary electrode and a saturated potassium chloride calomel (SCE) reference. The measurements were obtained using 1-3mM protein solutions in μ=0.1, NaPi, pH 7 plus 10mM 4,4' bipyridine.

Preparation of Ruthenium Complexes

trans-$[Ru(NH_3)_4SO_2Cl]Cl$ was prepared according to literature procedures[57] and was used as the starting material for the preparation the $a_4LRu^{II}OH_2$ complexes. The *trans*-$[Ru(NH_3)_4(py)SO_4]Cl$ and *trans*-$[Ru(NH_3)_4(isn)SO_4]Cl$ were prepared according to the method of Curtis et al.[58] In a typical preparation, 0.5g *trans*-$[Ru(NH_3)_4SO_2Cl]Cl$ was dissolved in 25 mL H_2O at 40°C. 7.5×10^{-3} moles pyridine or isonicotinamide was added slowly, and the solution was stirred for 15 min. The *trans*-$[Ru(NH_3)_4LSO_2]Cl$ (L=py or isn) was then precipitated with 350-500 mL of acetone, collected by filtration, washed with acetone and ether and dried under vacuum for 2-4 h. This solid, $[Ru^{II}(NH_3)_4SO_3py]Cl$ was then

dissolved in a minimum volume of H_2O and filtered. Five to 10 mL of a 1:1 mixture of 30% H_2O_2 and 2 N HCl was added slowly to oxidize the ruthenium complex. The solution was stirred for 10 min and the product was precipitated with 350-500 mL of acetone, collected by filtration and dried under vacuum. Yields were typically ~80%.

Purification of the pyridine and isonicotinamide Ru complexes can be achieved by cation-exchange chromatography. Previous work indicated that *trans*-$[Ru(NH_3)_4(py)SO_4]Cl$ decomposes on the SP-Sephadex. Therefore in order to purify the Ru complex the SO_4 ligand was substituted with chloride. The *trans*-$[Ru(NH_3)_4(py)SO_4]Cl$ and *trans*-$[Ru(NH_3)_4(isn)SO_4]Cl$ complexes were either used as is or converted to the *trans*-$[Ru(NH_3)_4(py)Cl]Cl$ and *trans*-$[Ru(NH_3)_4(isn)Cl]Cl$ complexes according to published procedures.[59] The chloride derivatives could be purified by cation-exchange chromatography (SP-Sephadex C-25, 1g, 4 x 25cm) using a stepwise gradient 0.1 to 0.3M HCl. The pure *trans*-$[Ru(NH_3)_4(LC)I]Cl$ eluted at 0.2-0.25M HCl.

The *trans*-$[Ru(NH_3)_4(pz)SO_4]Cl$ was prepared according to the method of von Kameke et al.[60] The complex is very air sensitive so all manipulations were carried out under positive argon pressure. The complex was purified on a G-25 column after being reduced with zinc amalgam. The Ru complex was allowed to reduce no longer than 30 min because the complex tends to form polymeric impurities.[61] The gel was washed first with several volumes of degassed 0.01M HCl. Purple impurities thought to be Rupz polymers eluted first and then the bright red *trans*-$[Ru(NH_3)_4(pz)OH_2]$. The a_4pzRu decomposes

over time in both oxidation states, so the solution off the column was used immediately to minimize impurities.

Preparation of Ruthenium-Labelled Myoglobin

Native Myoglobin. Native sperm whale Mb (Sigma) was purified by cation-exchange chromatography (CM52, 6x60 cm, 0.05 M Tris, pH 7.8) and the major fraction, Band IV, was used in further studies.

$(NH_3)_5RuMb$. $(NH_3)_5Ru$-labelled Mb was prepared according to previously described procedures.[35-37] Native Mb was reacted with a 15-fold excess of $a_5Ru^{II}(OH_2)$ to form singly and multipy labelled species. The singly-modified derivatives were separated from unreacted and multipy-labelled Mb using preparative IEF (pH 7-10), and the four isomerically pure a_5Ru(His-X)Mb species were isolated using cation-exchange chromatography (CM52, 6x60 cm; Tris buffer pH 7.8).

$(NH_3)_4LRuMb$, L = py or isn. In a typical reaction, 0.3 g of $[a_4LRuSO_4]Cl_2$ or $[a_4LRuCl]Cl_2$, where L=py or isn, were dissolved in ~15-20 mL of μ=0.2, sodium phosphate (NaPi) pH 7 and filtered through a glass frit. The solution was then degassed under argon for approximately 1/2 h and subsequently reduced over Zn amalgam to form the $a_4LRu^{II}OH_2$ complex. Complete reduction of the Ru-py complex occurs in about 1/2 h but the Ru-isn complex takes longer, ~ 2 h.

While the Ru complex was being reduced, a solution of 0.6 g Mb in 15 mL μ=0.2, NaPi, pH 7 was degassed gently under argon for ~ 1/2

h (5X: evacuation 10-15 s, argon 5 min). The reduced ruthenium solution was transferred to the degassed protein solution and the resulting mixture was allowed to react at room temperature. The optimum reaction times were found to be 2-3 h and 7-8 h for the $a_4$pyRuMb and the $a_4$isnRuMb, respectively.

$(NH_3)_4$pzRuMb. For the $a_4$pzRuMb modification, a 10-30 fold excess of reduced Ru complex in 0.01M HCl was added to a previously degassed Mb solution. The protein concentration was ~2 mM in μ=0.2, NaPi, pH 7. The Ru complex was used directly after preparation and purification on a G-25 column since the reduced $a_4$pzRu complex tends to form polymeric impurities if not used immediately. The Ru complex was in 0.01M acid after purification so the protein solution was adjusted to pH 6.5 and the reaction allowed to proceed for 20-24 h.

For the a_4LRuMb reaction mixtures, the excess Ru complex was removed via gel filtration chromatography. Approximately 0.6 g of protein concentrated to 10-15 mL by ultrafiltration could be separated from excess Ru reagent on a 4x27cm G-25 column; $\mu \cong$0.05-0.2, NaPi, pH 7. The modified protein was then oxidized with excess $Co(phen)_3Cl_3$. Prior to separation of the singly-labelled derivatives most of the $Co(phen)_3Cl_3$ was removed and the protein was exchanged into μ=0.05, NaPi, pH 6.

Separation of Singly-Labelled Mb derivatives. The singly-labelled Mb species (a_4LRuMb) were separated from the multiply-labelled Mb [$(a_4LRu)_n$Mb, n=2-4] and native Mb using FPLC (Fast

protein, peptide and polynucleotide liquid chromatography) cation-exchange chromatography. Typically, a prepacked 8 or 20 mL Mono S column (Pharmacia) was used with a pH and ionic strength gradient. The starting buffer (A) was μ=0.05, NaPi, pH 6 and the second buffer (B) was μ=0.05, NaPi, pH 7 + 1M NaCl. One-2 mL of protein was loaded at 5% B at a flow rate of 2-4 mL/min. During a gradient from 5% B to ~30% B the desired singly-labelled Mb species elute. The specific running conditions are listed in Figures 18, 19 and 20.

Preparation of Porphyrin-Substituted Myoglobin

Zinc porphyrin (ZnP) and palladium porphyrin (PdP) substituted Mb derivatives were prepared in a similar fashion to that described previously.[33,35] The iron porphyrin was removed from previously purified native or singly-labelled Mb (15-30 mg in 5-10 mL H_2O, pH 2.9) using acidic butanone extraction to form the apoMb.[62,63] The protein was extracted 4-5 times and then was dialyzed twice against 10mM sodium bicarbonate. The protein solution was then further dialyzed three times against the appropriate sodium phosphate buffer. For most ZnMb species the NaPi buffer (μ=0.1, pH 7) was used except for the $a_4$pyRuMb derivatives in which the pH was decreased to pH 6 in order to stabilize the Ru label. The Ru label of the $a_4$pyRuMb species tends to decompose and/or fall off at high pH. The apoMb samples for the PdMb derivatives were dialyzed against NaPi buffer (μ=0.01, pH 7) for the native and a_5RuMb species and pH 6 for the $a_4$pyRuMb derivative. The apoprotein was kept at 4°C during extraction and dialysis. The protein is not stable without

the heme present and will denature over time so reconstitution was performed immediately after dialysis.

Reconstitution of Porphyrin-Substituted Myoglobin. The reconstitution of the apoMb with zinc porphyrin was performed in the dark using the following procedure.[35] Approximately 3-5 mg of zinc(mesoporphyrin IX) was dissolved in a few drops of 0.1N NaOH (aq), then ~2 mL of μ=0.1, NaPi was added and this solution was added dropwise to the apoMb with stirring. The insertion was allowed to proceed in the dark at 4°C for 6-12 h. Another insertion was made and the solution was again stirred for 6-12 h. To speed up the insertion process the solution was often stirred at room temperature. The Pd porphyrin was inserted into Mb in an almost identical fashion except that the palladium(mesoporphyrin IX) was dissolved in a few drops of DMSO (instead of NaOH), diluted with ~2 mL μ=0.01, NaPi and then added to the apoMb.

Removal of excess porphyrin was achieved by centifugation and then gel filtration of the remaining liquid, (G-25, ~3x22 cm, NaPi). The G-25 column was equilibrated with μ=0.05, NaPi, pH 6 for the ZnMb derivatives and μ=0.01, NaPi, pH 7 for the PdMb derivatives. The Pd derivatives were used without further purification because the Pd porphyrin remains bound to the top of the cation-exchange column. The ZnMb species were further purified using FPLC cation-exchange chromatography. The FPLC separation conditions for the ZnMb derivatives were identical to those used for the separation of the FeMb singly-labelled species.

The ZnMb derivatives were stable at -20°C in the presence of excess $Co(phen)_3Cl_3$ for several months. The PdMb derivatives were used immediately, because after standing the PdP falls out of the heme pocket. All manipulations of the ZnMb and PdMb species were performed in the dark or under reduced lighting conditions. These photoactive porphyrins degrade under bright lights.

Results and Discussion

Preparation of Ru-Modified Myoglobin

The well-characterized complexes of the type *trans*-a_4LRuSO_4 (where a=NH_3, and L=NH_3, pyridine (py), isonicotinamide (isn) and pyrazine (pz)) were chosen to bind to histidine sites on Mb. The advantages of these complexes are that the potential can be fine tuned by varying L, and the *trans* nature of L allows for minimal perturbation of the protein structure. These complexes are also expected to have similar reorganization energies. Brown et al. have estimated the difference in reorganization energy between $(NH_3)_6Ru$ and $(NH_3)_5pyRu$ to be <0.1 eV.[64] With these D-A systems containing measured potentials, the effect of driving force on ET rate can be probed systematically.

The general strategy for attaching a Ru moiety to Mb is to reduce the $a_4LRu^{III}SO_4$ (or $a_4LRu^{III}Cl$) complex forming the $a_4LRu^{II}OH_2$ complex, as shown in equation 6. In the reduced Ru^{II} state the SO_4 (or Cl) ligand is very labile.[59,65]

6) $$a_4LRu^{II}SO_4 + OH_2 \rightarrow a_4LRu^{II}OH_2 + SO_4$$

Figure 16. Absorption spectra of A) oxidized *trans*-$[Ru(NH_3)_4(py)Cl]Cl$, Ru^{III} and B) reduced *trans*-$[Ru(NH_3)_4(py)Cl]Cl$, Ru^{II}.

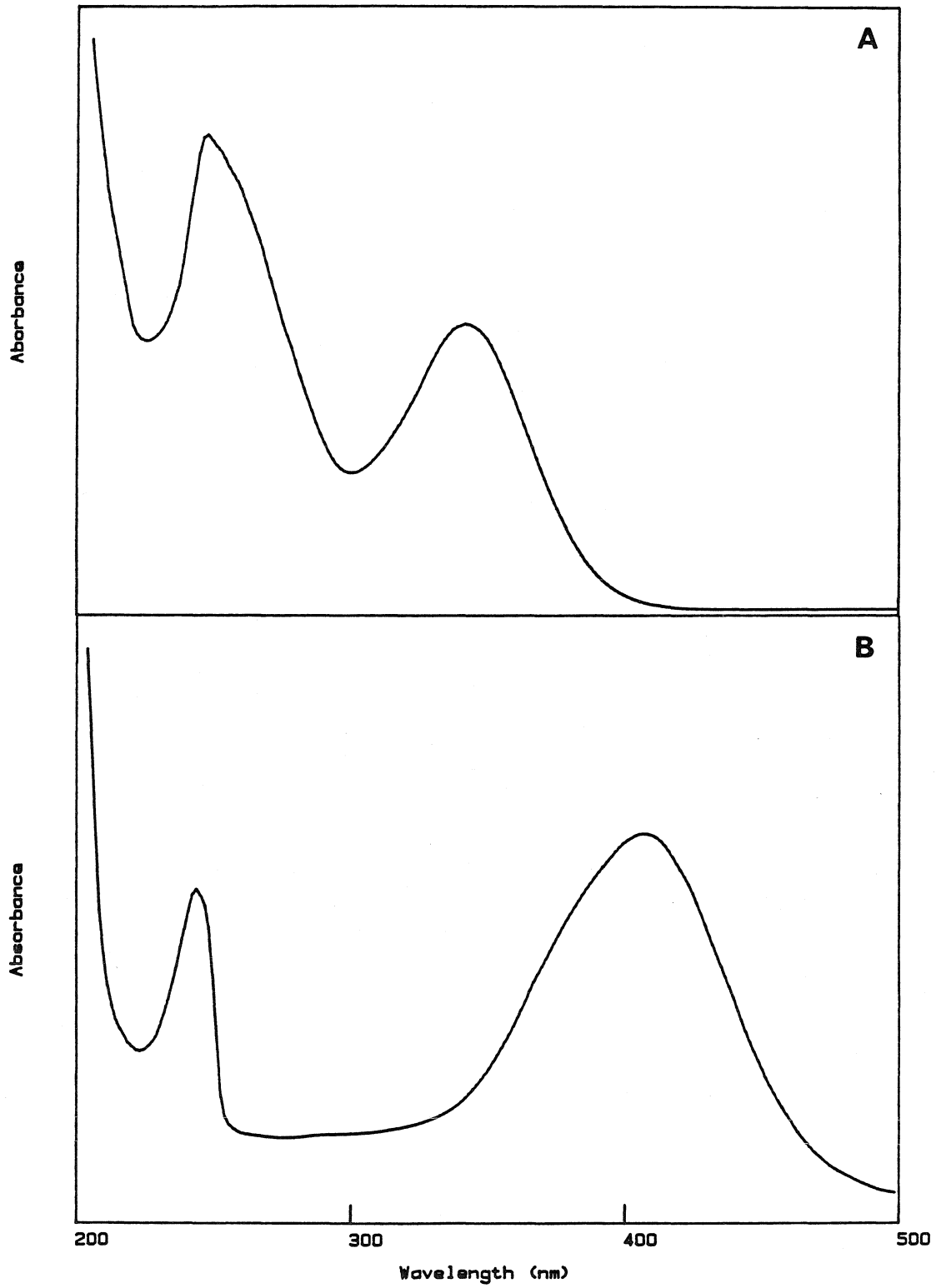
A
B
Aborbance
Absorbance
200
300
400
500
Wavelength (nm)

Figure 17. Absorption spectra of A) oxidized *trans*-$[Ru(NH_3)_4(isn)Cl]Cl$, Ru^{III} and B) reduced *trans*-$[Ru(NH_3)_4(isn)Cl]Cl$, Ru^{II}.

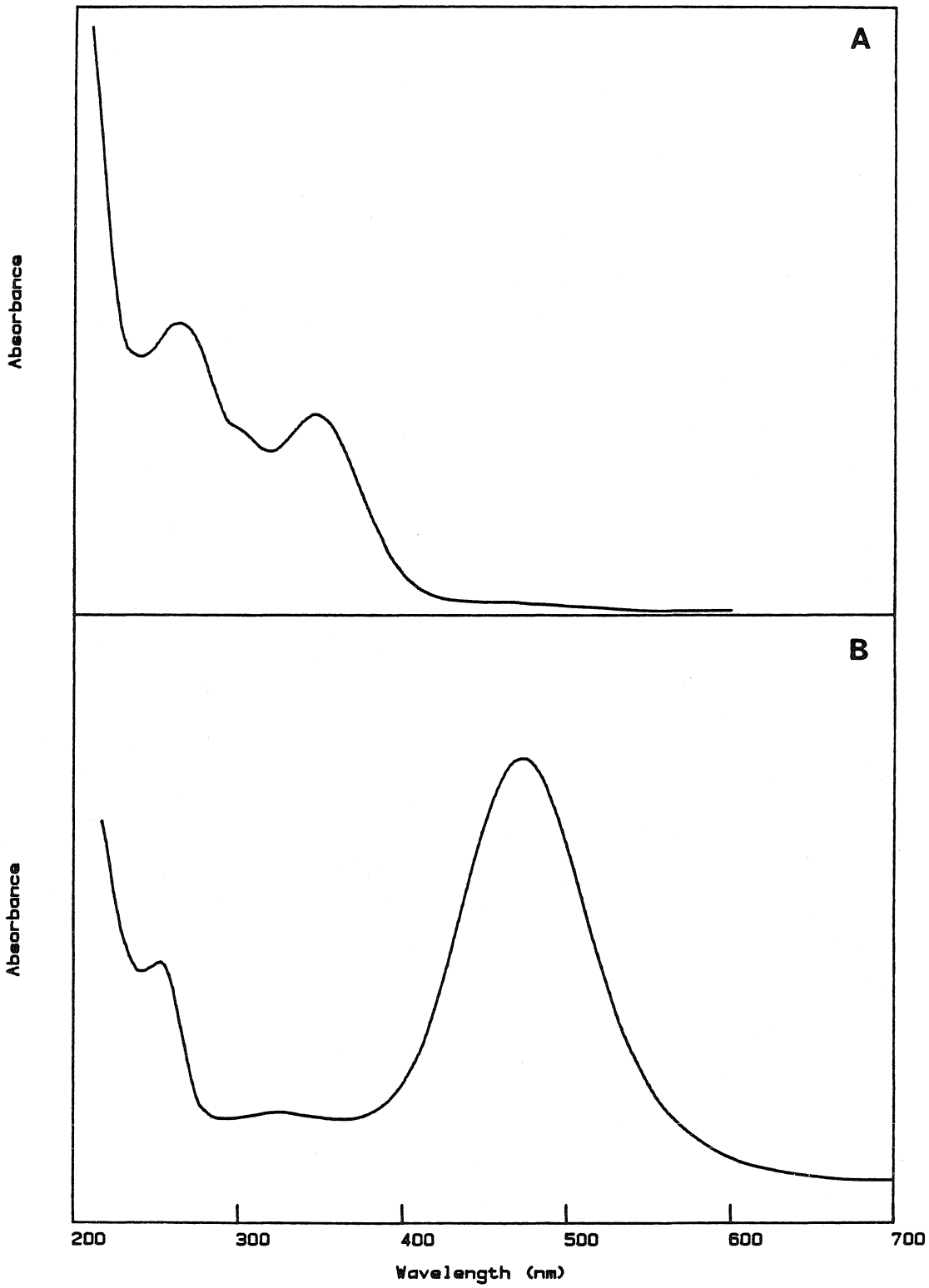
A
B
Absorbance
Absorbance
200
300
400
500
600
700
Wavelength (nm)

The Ru^{II}-aquo complex reacts specifically with a nitrogen donor on the imidazole.[65] After the reaction is complete, the Ru complex is oxidized. The modification procedure takes advantage of the lability of the SO_4 and OH_2 ligands in the Ru^{II} state and the fact that the Ru complexes are substitutionally-inert in the Ru^{III} state.[59,66]

The ruthenium complexes used for modification of Mb were prepared from the starting material $[a_5RuCl]Cl_2$ according to standard procedures described in the previous section.[57-60] Prior to purification of the py and isn-Ru complexes the a_4LRuSO_4 was converted to the a_4LRuCl complex. However, the a_4LRuSO_4 and a_4LRuCl complexes used for modification studies gave similar results. Absorption spectra for the *trans*-$[Ru(NH_3)_4(py)Cl]Cl$ and *trans*-$[Ru(NH_3)_4(isn)Cl]Cl$ complexes are shown in Figures 16 and 17.

The optimum reaction times for Ru-modification were determined by allowing the reactions to proceed for ~20 h and sampling the solution every 30 min for the appearance of the $a_4$pyRuMb species and longer time intervals for the $a_4$isnRuMb and $a_4$pzRuMb. The relative amounts of native, singly-labelled and multiply-labelled Mb were observed by analytical isoelectric focusing or analytical FPLC cation-exchange chromatography. The FPLC system was preferred for analyzing the time course of the reaction because it was faster and could be used as the reaction proceeded. At the optimum reaction time there was a significant fraction of singly-labelled Mb formed but relatively little multiply-labelled species. The optimum reaction time increases with increasing π-acid strength of the ligand *trans* to the OH_2, since the

substitution reaction of the histidine for the OH_2 is slower for the stronger π-acid *trans* ligand.[65] The optimum reaction times for $a_4$pyRu-, $a_4$isnRu- and $a_4$pzRuMb were found to be 2-3 h, 7-8 h and 20-24 h, respectively. For the $a_4$pzRuMb reaction, aliquots taken prior to 20 h indicated that substitution at the surface histidines is very slow, but after 24 h the level of Ru impurities increased rapidly.

Purification of Ru-Labelled Mb. After the labelling reaction is complete, the protein mixture was oxidized with $Co(phen)_3Cl_3$ (E^o=0.4V vs. NHE) and then purified by conventional or FPLC cation-exchange chromatography. Conventional cation-exchange chromatography has been used with the a_5RuMb mixture; however, FPLC was the preferred technique for the other Ru-modified Mb species because it was much faster, 40 min versus several days. Previous work has shown that the $a_4$pyRu moiety tends to fall off while the protein was on a conventional gravity column. The singly-labelled Mb species were separated from the native and multiply-labelled Mb by a pH and ionic strength gradient (Figures 18, 19 and 20). In the $a_4$pyRu- and $a_4$isnRuMb mixtures, the native Mb eluted first and then the singly-labelled species separated into three peaks; Band I, Band II and Band III. The elution profiles for these reaction mixtures are shown in Figures 18 and 19. The multiply-labelled derivatives and residual $Co(phen)_3Cl_3$ eluted in a 1M NaCl wash.

In the $a_4$isnRuMb reaction mixture, the ruthenium(III) tends to autoreduce to Ru(II), so a broad peak often grew in between the

Figure 18. FPLC elution profile for the $a_4$pyRuMb reaction mixture. An 8 mL Pharmacia Mono S cation-exchange column was used. The running program is listed below:

```
  0.0 CONC %B    0.0
  0.0 ML/MIN    3.00
  0.0 CM/ML     0.20
  2.0 VALVE.POS 1.2
  5.0 VALVE.POS 1.1
  8.0 CONC %B    0.0
 28.0 CONC %B    8.5
 88.0 CONC %B   24.0
 88.0 CONC %B    100
104.0 CONC %B    100
104.0 CONC %B    0.0
120.0 CONC %B    0.0
```

In the figure the dotted line is the buffer gradient and Band I, II and III are the singly-labelled Mb derivatives.

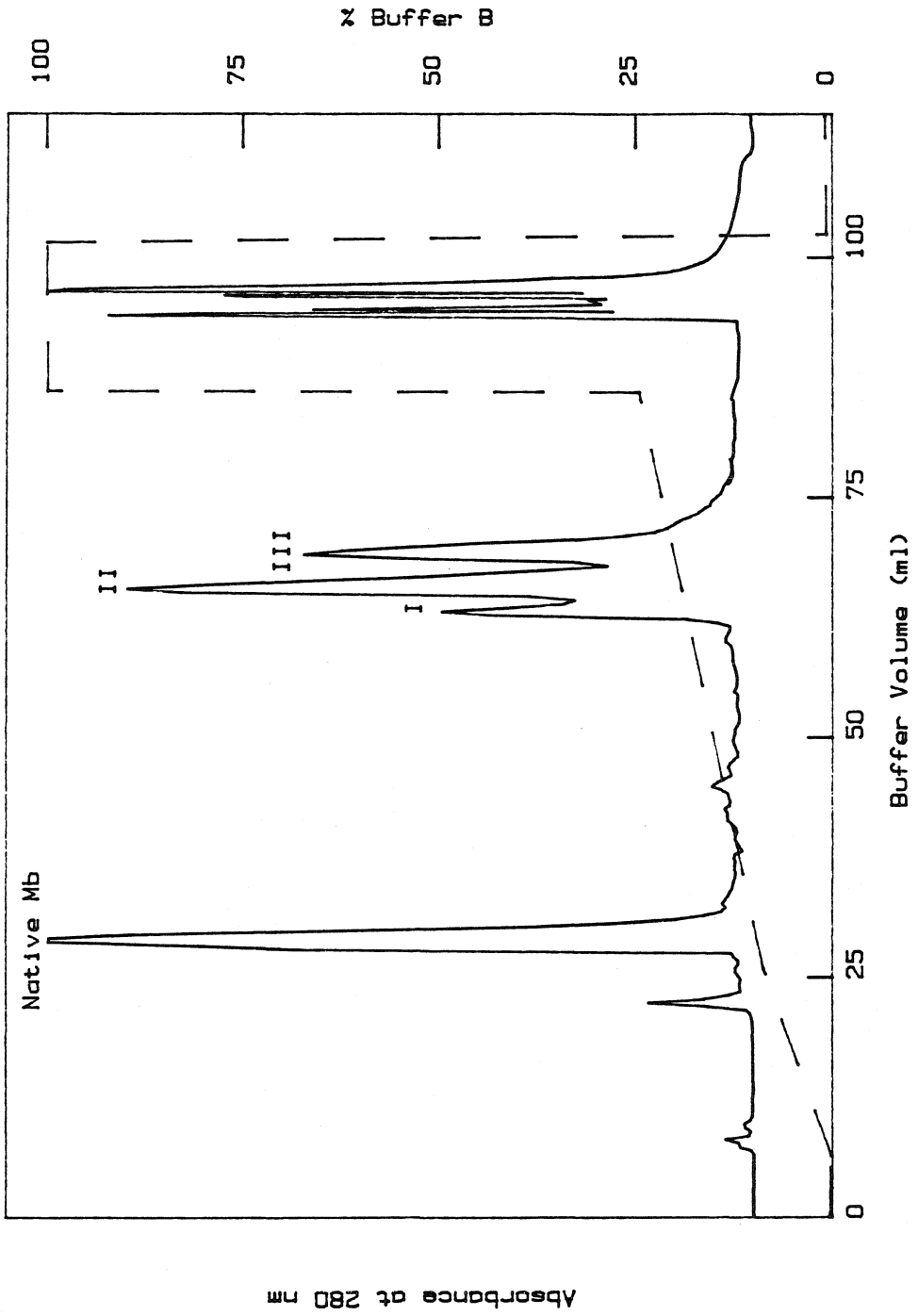
% Buffer B
100
75
50
25
0
Native Mb
I
II
III
0
25
50
75
100
Buffer Volume (ml)
Absorbance at 280 nm

Figure 19. FPLC elution profile for the $a_4$isnRuMb reaction mixture. A 20 mL Pharmacia Mono S cation-exchange column was used. The running program is listed below:

```
  0.0 CONC %B    5.0
  0.0 ML/MIN    6.00
  0.0 CM/ML     0.10
  5.0 VALVE.POS 1.2
 10.0 VALVE.POS 1.1
 16.0 CONC %B    5.0
 60.0 CONC %B   13.5
120.0 CONC %B   22.0
135.0 CONC %B   25.0
135.0 CONC %B    100
167.0 CONC %B    100
167.0 CONC %B    0.0
195.0 CONC %B    0.0
```

In the figure the dotted line is the buffer gradient and Band I, II and III are the singly-labelled Mb derivatives.

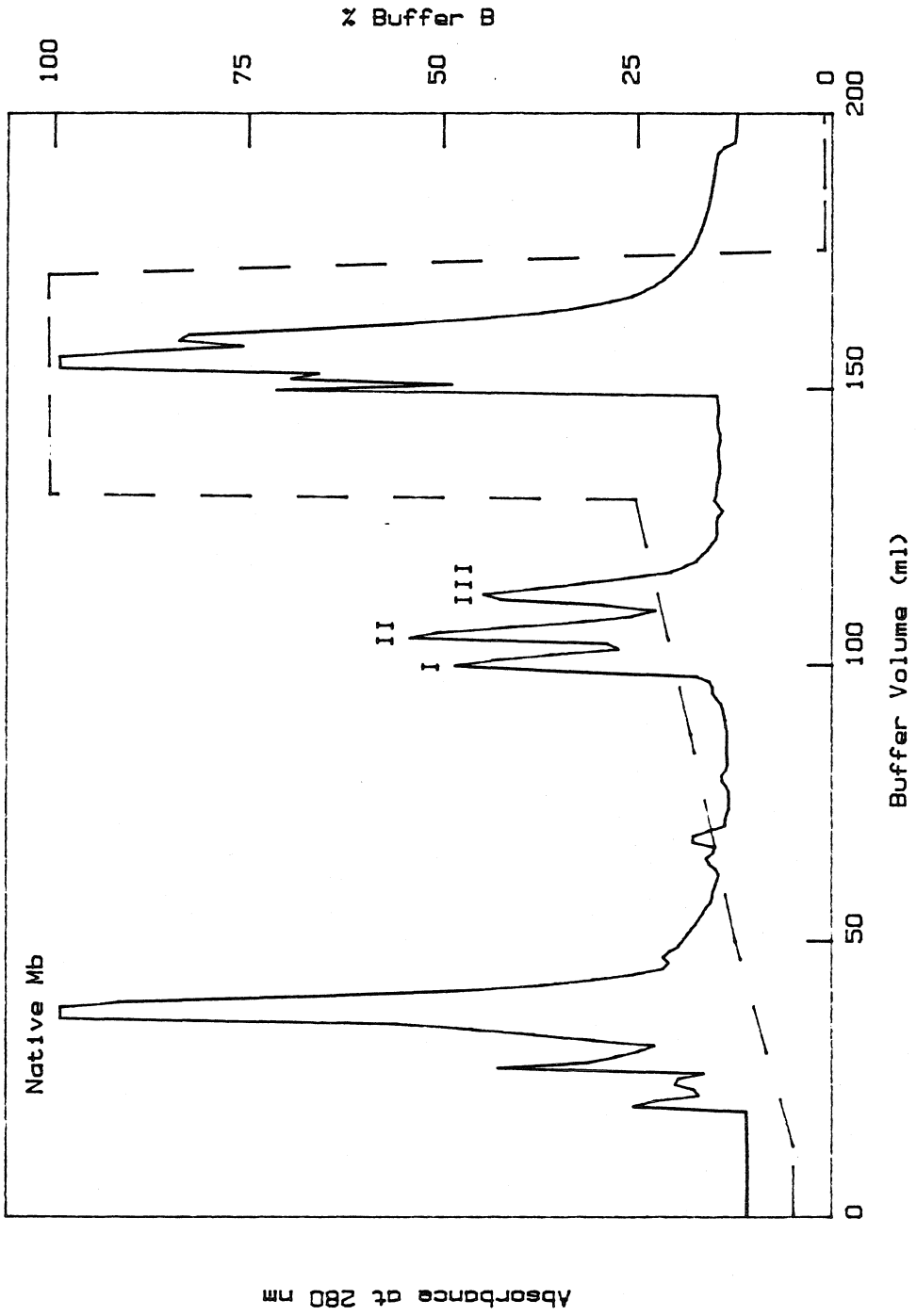
% Buffer B
100
75
50
25
0
200
150
100
50
0
Buffer Volume (ml)
Native Mb
I
II
III
Absorbance at 280 nm

Figure 20. FPLC elution profile for the $a_4$pzRuMb reaction mixture. A 20 mL Pharmacia Mono S cation-exchange column was used. The running program is listed below:

```
  0.0 CONC %B    0.0
  0.0 ML/MIN    6.00
  0.0 CM/ML     0.10
  5.0 VALVE.POS 1.2
 10.0 VALVE.POS 1.1
 16.0 CONC %B    0.0
 60.0 CONC %B   13.5
120.0 CONC %B   22.0
135.0 CONC %B   25.0
135.0 CONC %B    100
167.0 CONC %B    100
167.0 CONC %B    0.0
195.0 CONC %B    0.0
```

In the figure the dotted line is the buffer gradient, Band A is native Mb and Band B is the singly-labelled (Ru^{II}) Mb derivatives.

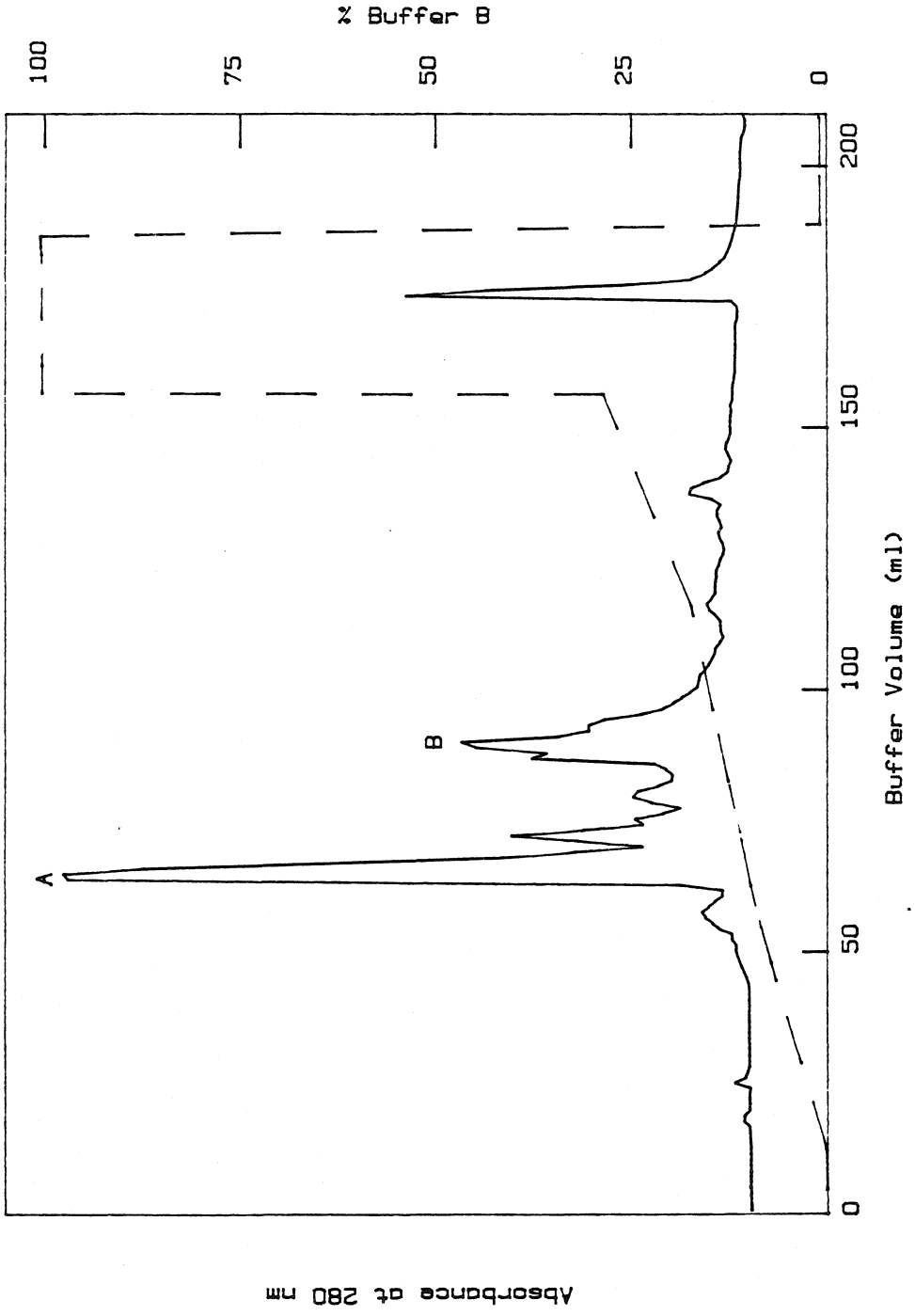
% Buffer B
100
75
50
25
0
200
150
100
50
0
Buffer Volume (ml)
A
B
Absorbance at 280 nm

native Mb and the singly oxidized species on the FPLC elution profile. Keeping the column clean prevented the Ru from becoming reduced on the column.

The $a_4$pzRuMb elution profile is shown in Figure 20. Peak A corresponds to native Mb and peak B is singly-labelled $a_4$pzRu^{II}Mb. The singly-labelled derivatives were isolated in the reduced form, because the $a_4$pzRu^{III}Mb species are not stable. Upon oxidation of the attached Ru (E^o=0.56 V) with $IrCl_6^{2-}$ (E^o=0.9 V),[67] the $a_4$pzRu complex fell off the protein; only native Mb was observed in the FPLC trace.

Porphyrin Substitution of Mb

An important feature of Mb is that the heme is noncovalently bound and can be removed easily. Many exogenous porphyrins can be inserted and have been shown to be stable.[68] To permit electron transfer studies at high driving forces, photoactive porphyrins that contain highly reducing excited states (palladium and zinc(mesoporphyrin IX)) have been inserted into Mb. Figure 21 shows the absorption spectrum of zinc-porphyrin substituted Mb (ZnMb) where the Zn porphyrin has been completely inserted and the protein has been purified. Figure 22 displays the absorption spectrum of PdMb. The Soret in the ZnMb and PdMb derivatives has shifted (from 409.5 nm in metMb) to 414 and 390 nm, respectively.

Figure 21. Absorption spectrum of Zn-substituted Mb.

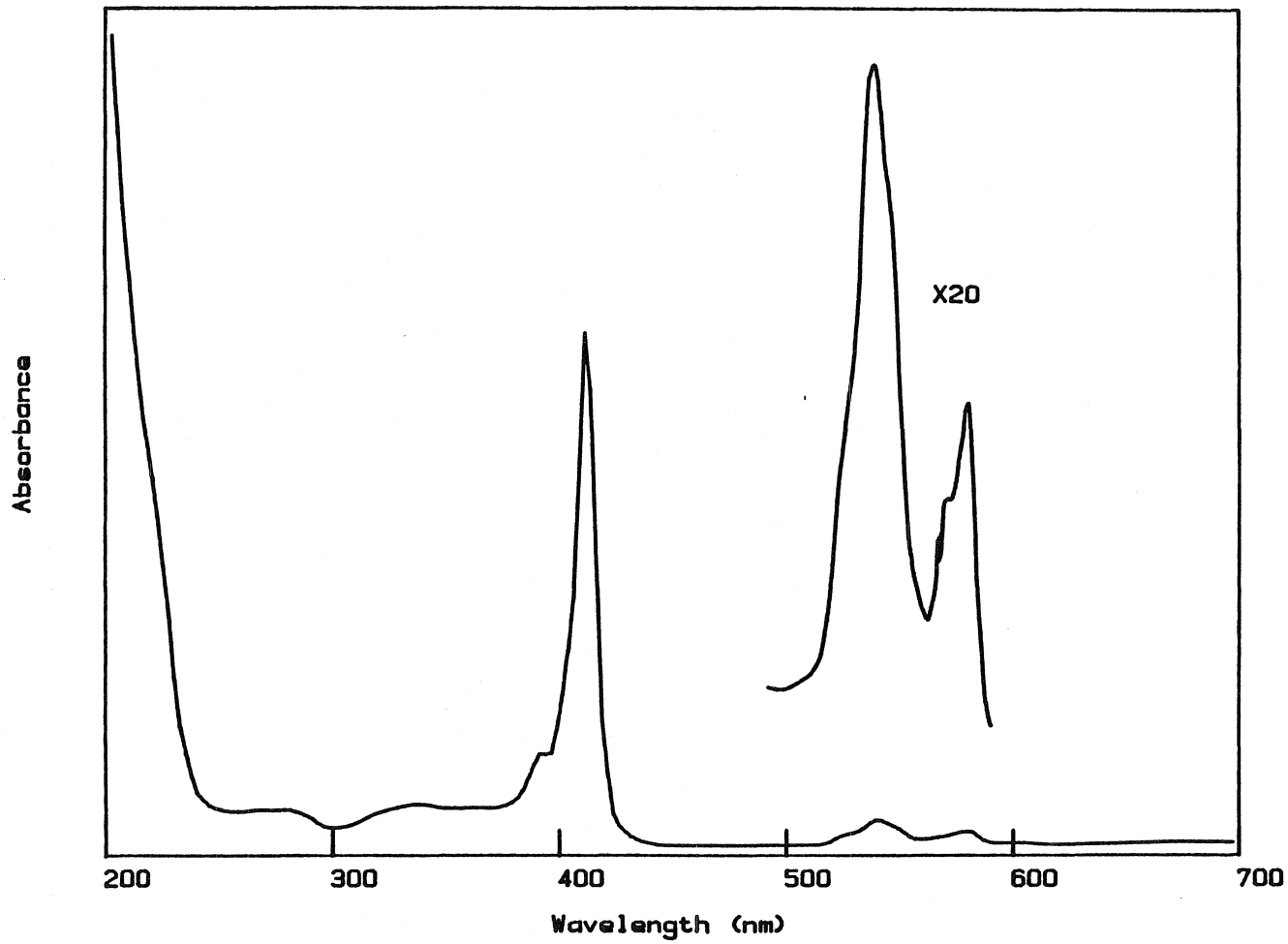
Absorbance
X20
200
300
400
500
600
700
Wavelength (nm)

Figure 22. Absorption spectrum of Pd-substituted Mb.

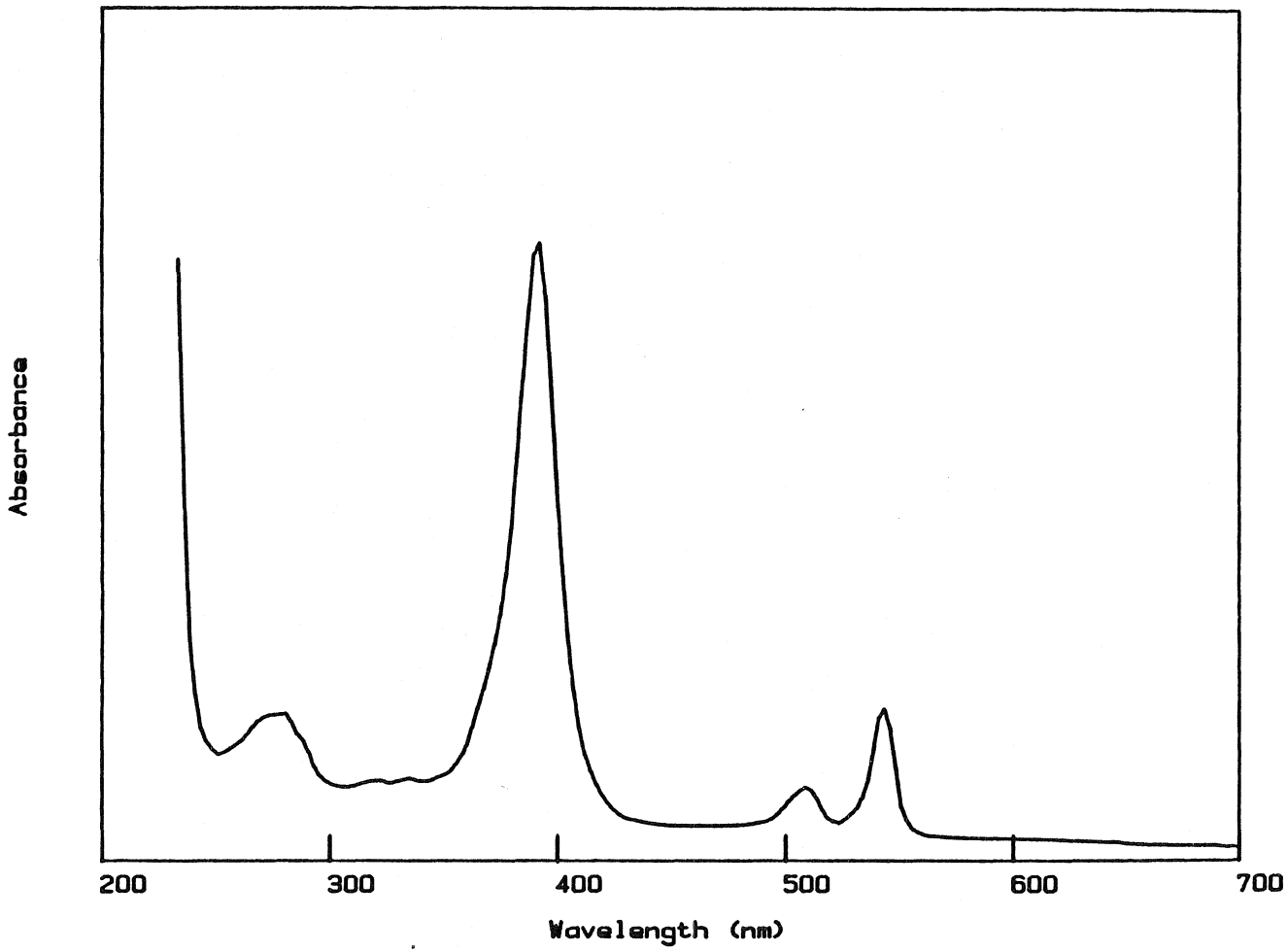
Absorbance
200
300
400
500
600
700
Wavelength (nm)

Characterization of the Ru-labelled Mb derivatives

As noted earlier, there are four surface histidines (12, 116, 81, 48) that have previously been labelled with the pentaammineruthenium moiety.[35-37] The site of Ru attachment was identified in this case by peptide mapping. The a_5RuMb histidine 48 labelling site was confirmed by x-ray crystallography. Analysis of the crystallographic data indicates that the peptide backbone of native Mb and a_5Ru(His-48)Mb are nearly identical, see Figure 15.[49]

Proton NMR Spectroscopy. To identify the labelling site in the new RuMb derivatives, proton nuclear magnetic resonance (NMR) spectroscopy has been used. By comparison of the NMR spectra of the known a_5RuMb species (characterized by peptide mapping, see Appendix) with the unknown $a_4$pyRu- and $a_4$isnRuMb species, the histidines that are labelled in the new Mb derivatives have been identified.

Histidine residues give rise to resonances from the C-2 and C-4 protons of the imidazole in the 6-9 ppm region.[69] In metMb C–2 proton resonances for seven histidines are observed: histidines 119, 116, 12, 81, 48, 113 and 36.[70,71] The four histidines that have been labelled in a_5RuMb are 12, 116, 81 and 48. The paramagnetic Ru attached to an imidazole (Figure 23) is expected to broaden and shift the corresponding proton resonance, thereby eliminating the NMR peak. These shifted resonances have been observed at -35 ppm.[72]

The histidine resonances had been assigned previously for sperm whale Mb by Botelho et al.[70] and Carver et al.[73] Initial

Figure 23. Schematic of an imidazole with a_4LRu- attached. The C-2 and C-4 protons are indicated.

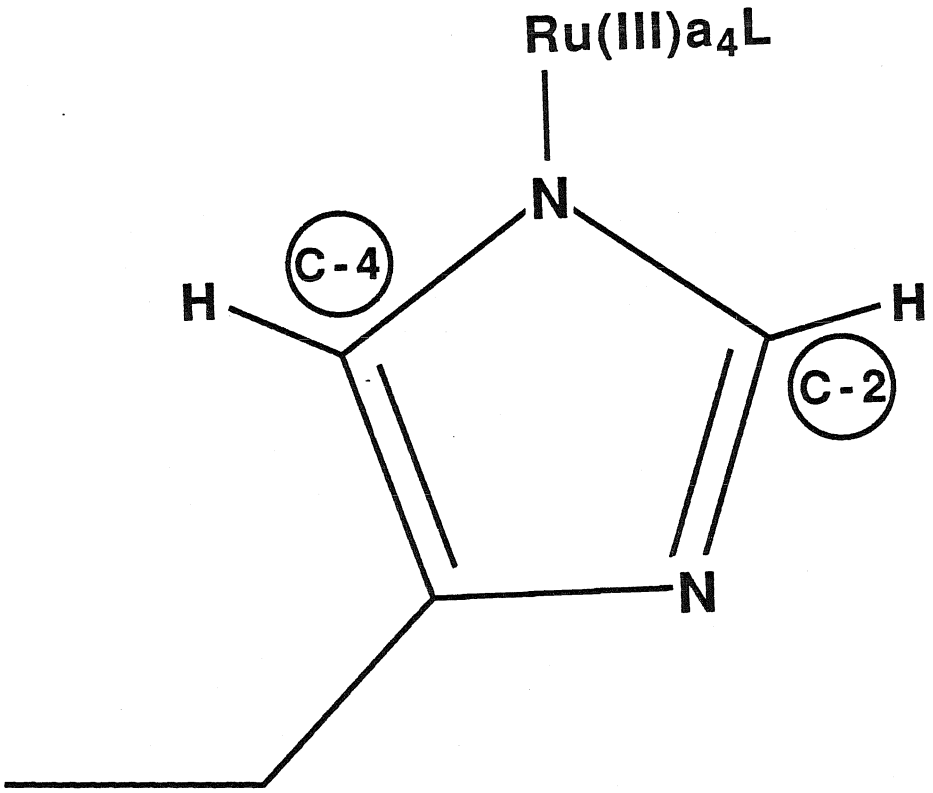
Ru(III)a4L
N
C-4
H
H
C-2
N

studies of a_5RuMb derivatives in our laboratory indicated that several of these assignments were incorrect. More recently, Wright has reassigned the proton resonances in carbonylMb (COMb) using two-dimensional NMR techniques.[74] The $Fe^{II}CO$ form of the protein is diamagnetic, and therefore it is difficult to compare the metMb spectrum with the COMb spectrum. Since the COMb spectrum had been correctly assigned, this form of the a_4LRuMb proteins was prepared to try to identify the histidine labelling sites. In the Ru-labelled COMb both the Ru and Fe are reduced. It was observed that the Ru label is not stable in the reduced state. Therefore, NMR studies were performed with the metMb. Comparison of the NMR spectra of new derivatives with those of the known a_5RuMbs, was used to identify $a_4$pyRu- and $a_4$isnRu- binding sites in Mb.

NMR spectra were obtained for the met forms of native Mb and all a_5Ru-, $a_4$pyRu- and $a_4$isnRu-Mb derivatives at and around pH 4.7, Figures 24-39. The low pH region was chosen because the seven C–2 histidine resonances are well-resolved. Figure 24 shows the C-2 histidine resonances of native Mb from pH 4.7 to ~5. The resonances (a through e) shift upfield as the pH is increased. Peak g remains unchanged and at ~pH 4.8 peak f moves upfield of peak g.

In the NMR spectrum of a Ru-labelled Mb, it is anticipated that one of the seven histidine residues (corresponding to the Ru-labelled histidine) will disappear. This is clearly what is observed for a_5Ru(His-48)Mb (Figure 25). In Figure 25, peak e in the NMR spectrum of RuMb disappears, indicating that this peak e should be assigned to histidine 48. All other peaks in the modified Mb

Figure 24. Proton NMR spectra of native metMb in the range of 7.0 to 9.0 ppm. The labelled peaks, a-g, correspond to the C-2 protons of the seven histidines that can be observed. As the pH is increased, the peaks a-f shift upfield of g, g remains unchanged and f shifts upfield of g. A) pH 4.7, B) pH 4.8, C) pH 4.9 and D) pH 5. Mb concentration in this and all subsequent experiments is 1-4mM; T=298K, 400 MHz (unless otherwise stated).

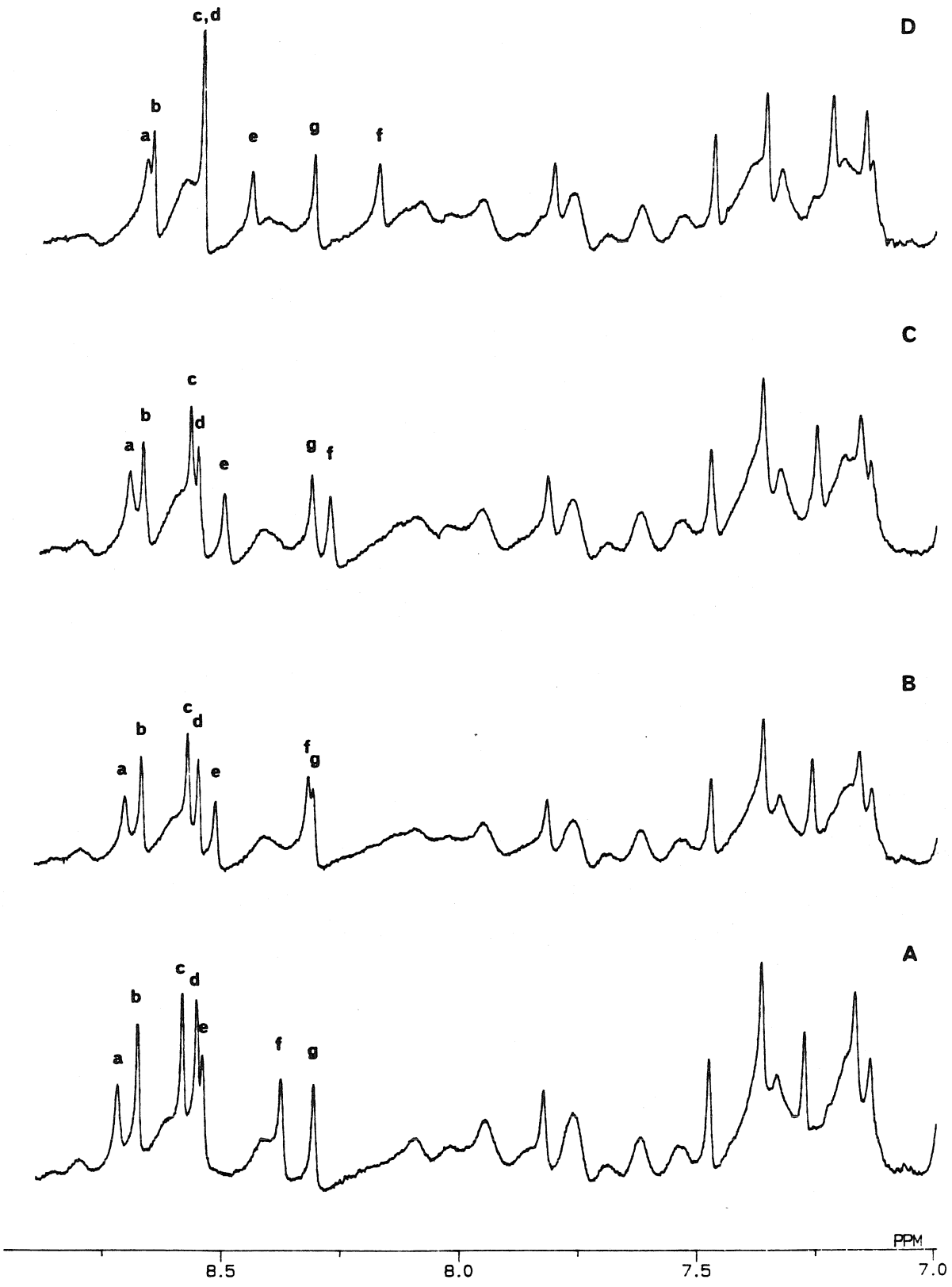
D
c,d
b
a
e
g
f
C
c
b
d
a
e
g
f
B
c
d
b
f
g
a
e
A
c
d
b
e
a
f
g
PPM
8.5
8.0
7.5
7.0

Figure 25. Proton NMR spectra at pH 4.7 of A) native Mb and B) a_5Ru(His-48)Mb. The starred position corresponds to the C-2 resonance (e) that is absent (histidine 48) in the a_5Ru(His-48)Mb spectrum. 500 MHz spectra.

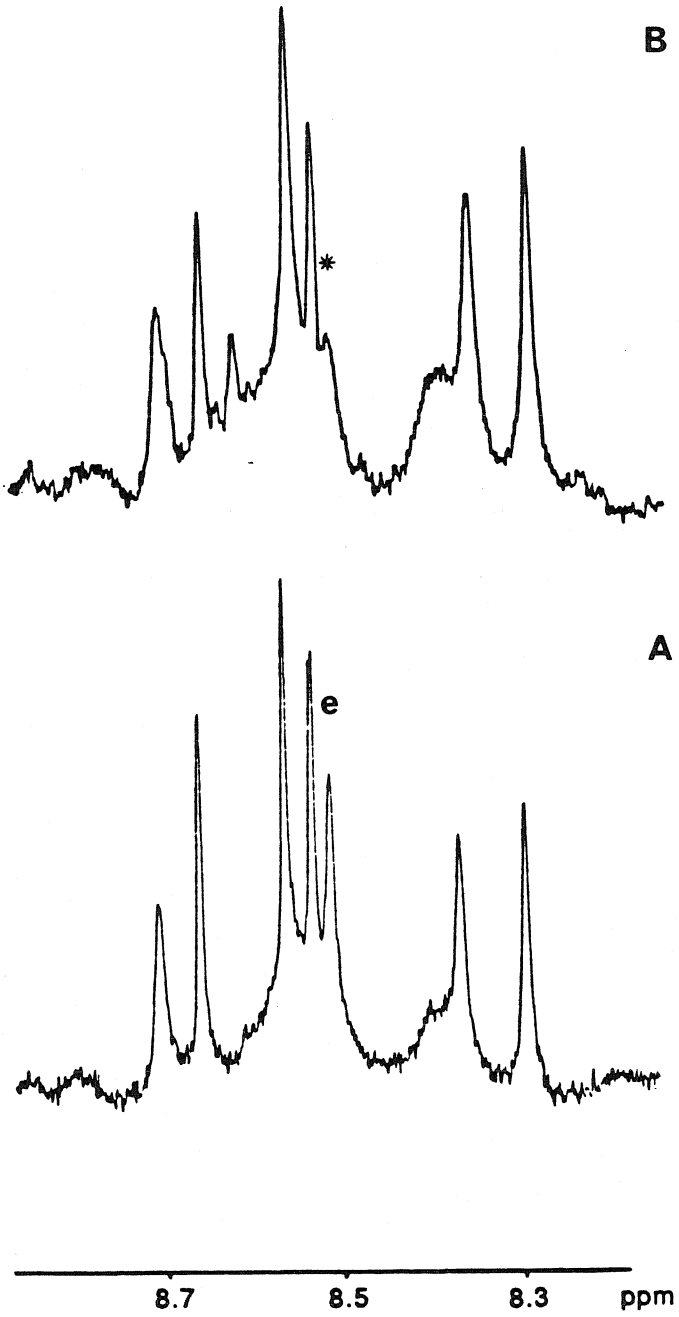
B
*
A
e
8.7
8.5
8.3
ppm

spectrum appear at identical chemical shifts to the native. The NMR spectrum of a_5Ru(His-81)Mb (Figure 26) also shows one peak missing (peak d), indicating that this resonance corresponds to histidine 81. A pH dependence (Figure 27) shows peak d absent at several pHs. As with a_5Ru(His-48)Mb, all remaining peaks in the modified Mb spectrum remain unchanged.

The NMR spectra of a_5Ru(His-12)Mb and a_5Ru(His-116)Mb are more complicated than those discussed previously. One histidine peak disappears, but other peaks also shift slightly and it is difficult to ascertain exactly which peak has disappeared. Figures 28 and 29 show the NMR spectra of a_5Ru(His-12) compared with native Mb and as a function of pH. Peaks d, e, f and g are in the same position in the modified Mb as in the native Mb. Out of the remaining three peaks, one has disappeared and the other two have shifted upfield. At all three pH values (Figure 29), the first two residues of the modified Mb spectra are shifted upfield of peaks a and b of the native Mb. Residues in the 7 to 8 ppm region are also shifted. From these results, histidine 12 could be either peak a, b or c. The NMR spectrum of a_5Ru(His-116)Mb shown in Figure 30 shows again that assigning the labelled histidine to an NMR resonance is not always easy. This spectrum shows peaks b, d, e and g unchanged, but the other peaks are not present. It is possible that the absent resonances are due to histidines 113, 116 and 119. A ruthenium attached at 116 may affect all three histidines since 113 and 119 are nearby (~10-15 Å).

Figure 26. Proton NMR spectra at pH 4.9 of A) native Mb and B) a_5Ru(His-81)Mb. The starred position corresponds to the C-2 resonance (d) that is absent (histidine 81) in the a_5Ru(His-81)Mb spectrum.

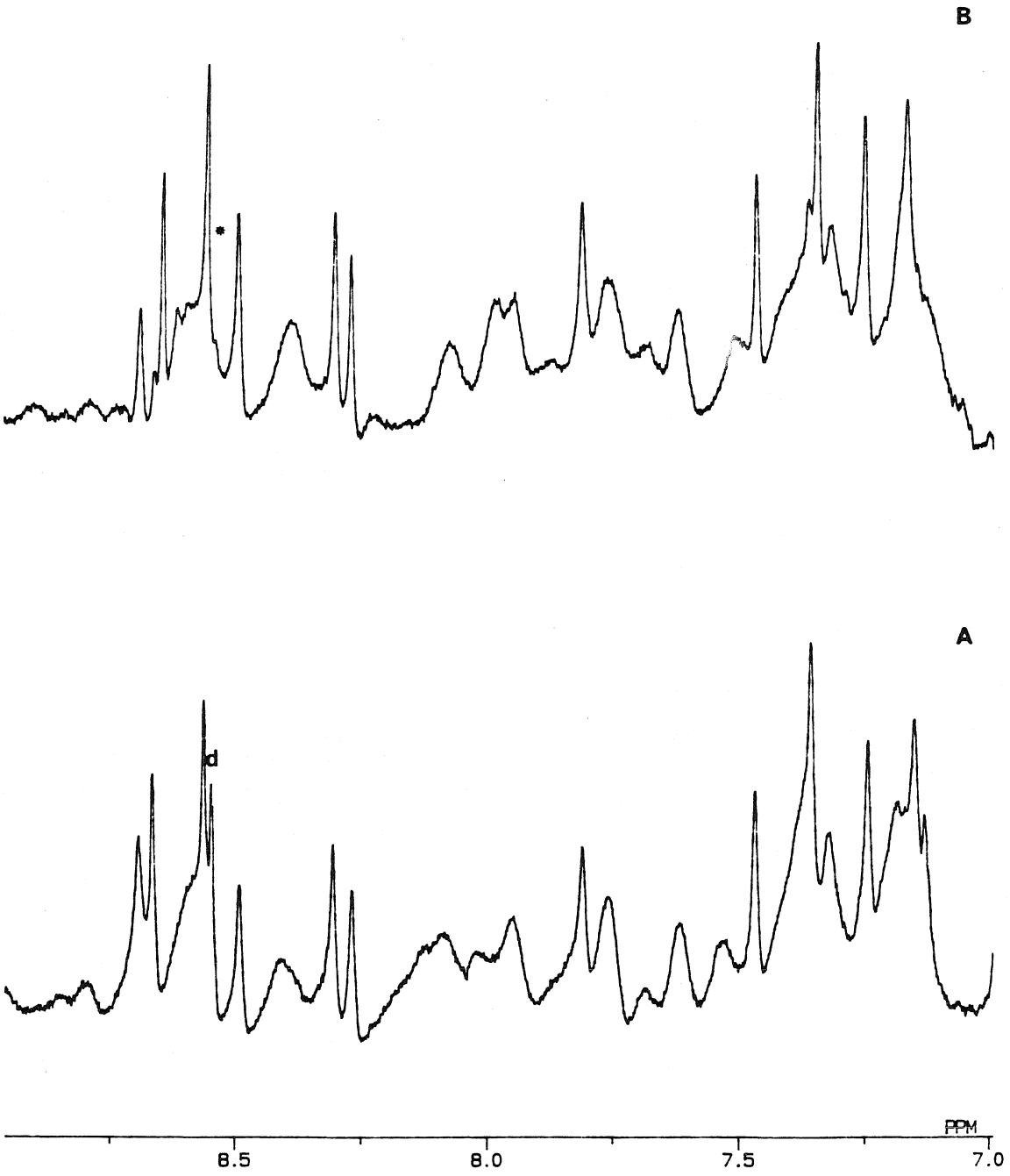
B
*
A
d
PPM
8.5
8.0
7.5
7.0

Figure 27. Proton NMR spectra of a_5Ru(His-81)Mb. A) pH 4.7, B) pH 4.8 and C) pH 5 The starred positions indicate resonances that are absent (relative to the native Mb spectra.)

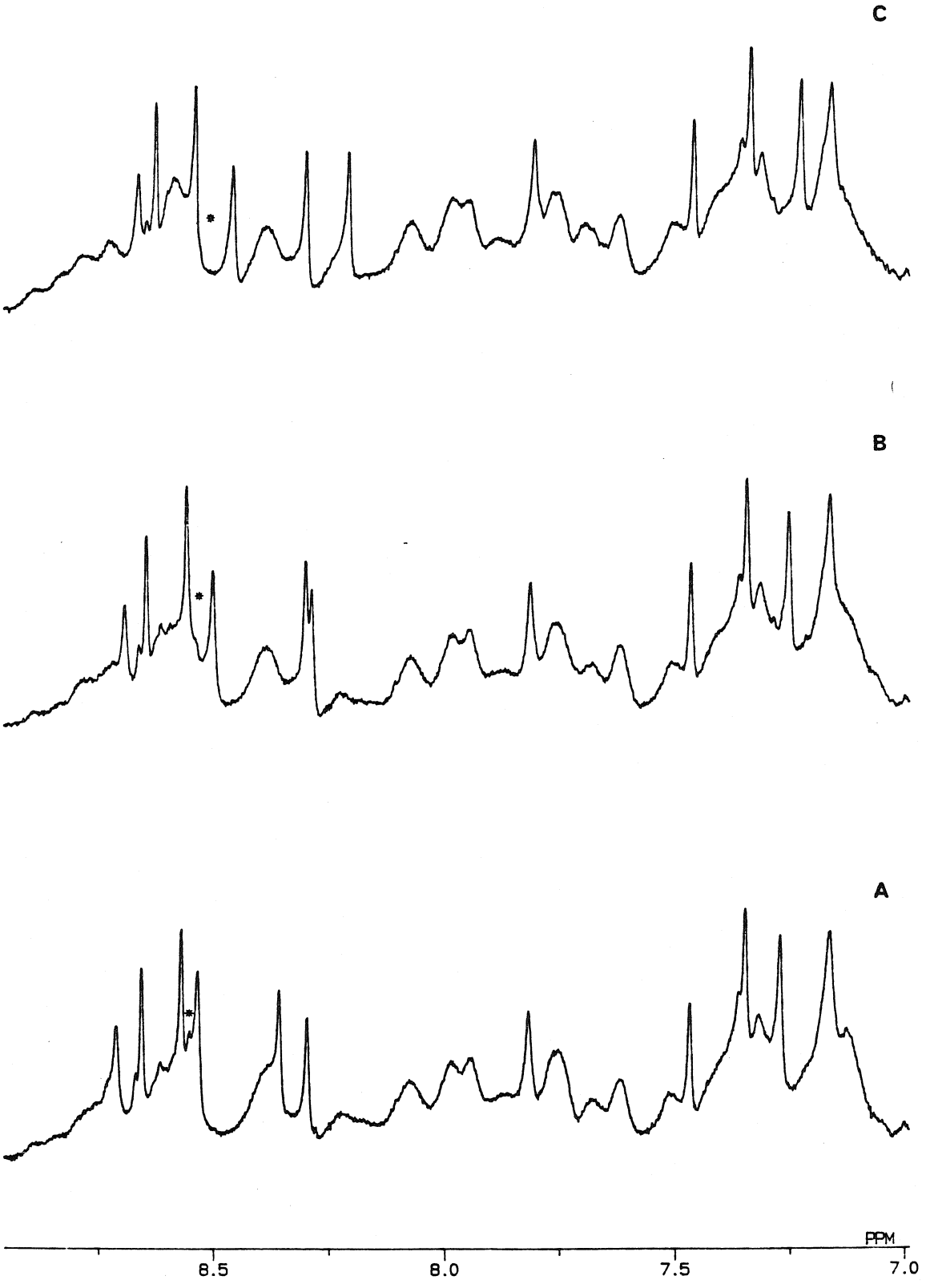
C
B
A
PPM
8.5
8.0
7.5
7.0

Figure 28. Proton NMR spectra at pH 4.7 of A) native Mb and B) a_5Ru(His-12)Mb. Peaks a, b, and c from the native Mb spectrum have shifted in the a_5Ru(His-12)Mb spectrum. The starred peaks (in the a_5Ru(His-12)Mb spectrum) correspond to the shifted resonances.

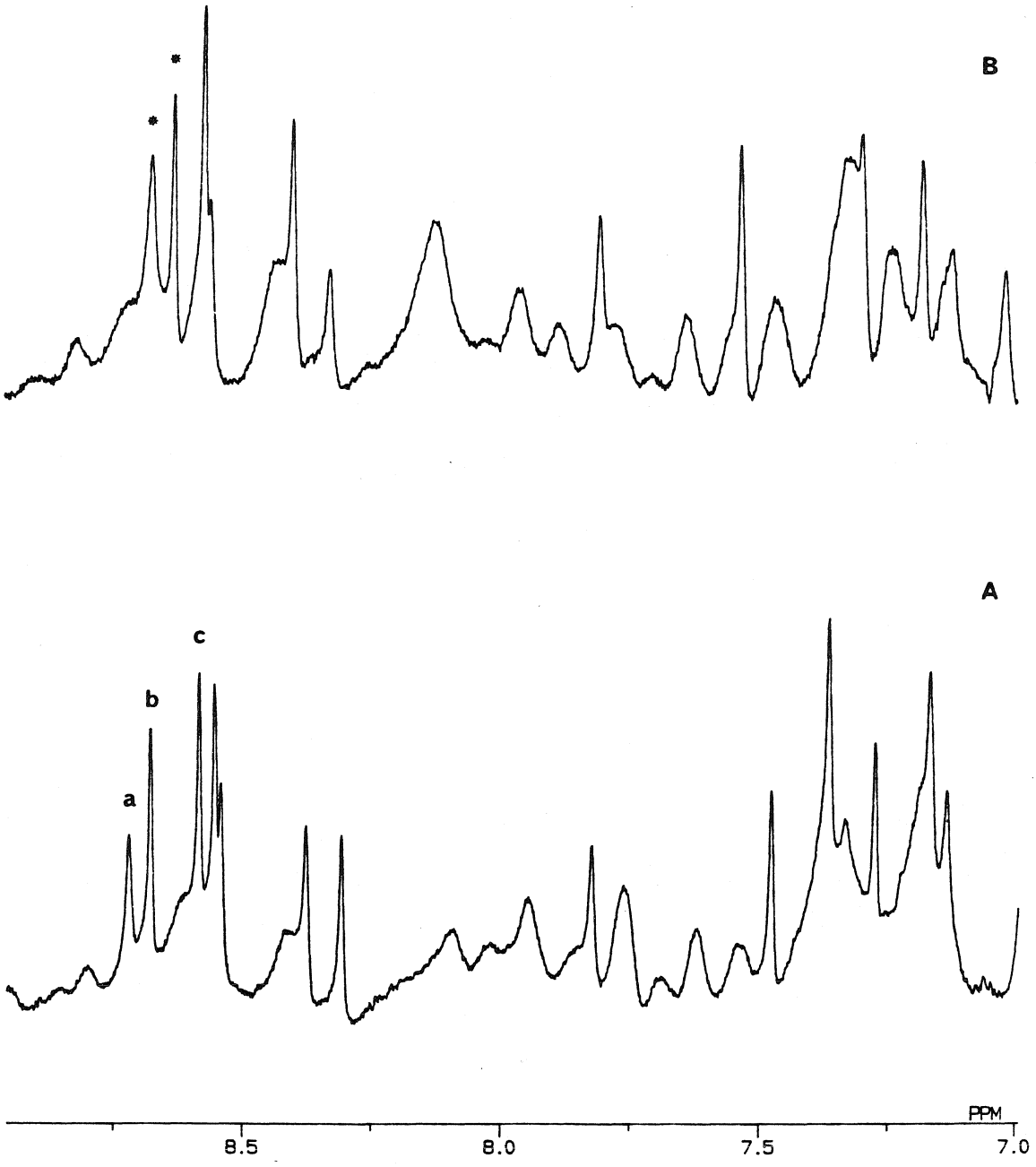
B
*
*
A
a
b
c
PPM
8.5
8.0
7.5
7.0

Figure 29. Proton NMR spectra of a_5Ru(His-12)Mb. A) ~pH 4.6, B) pH 4.8 and C) pH 4.9.

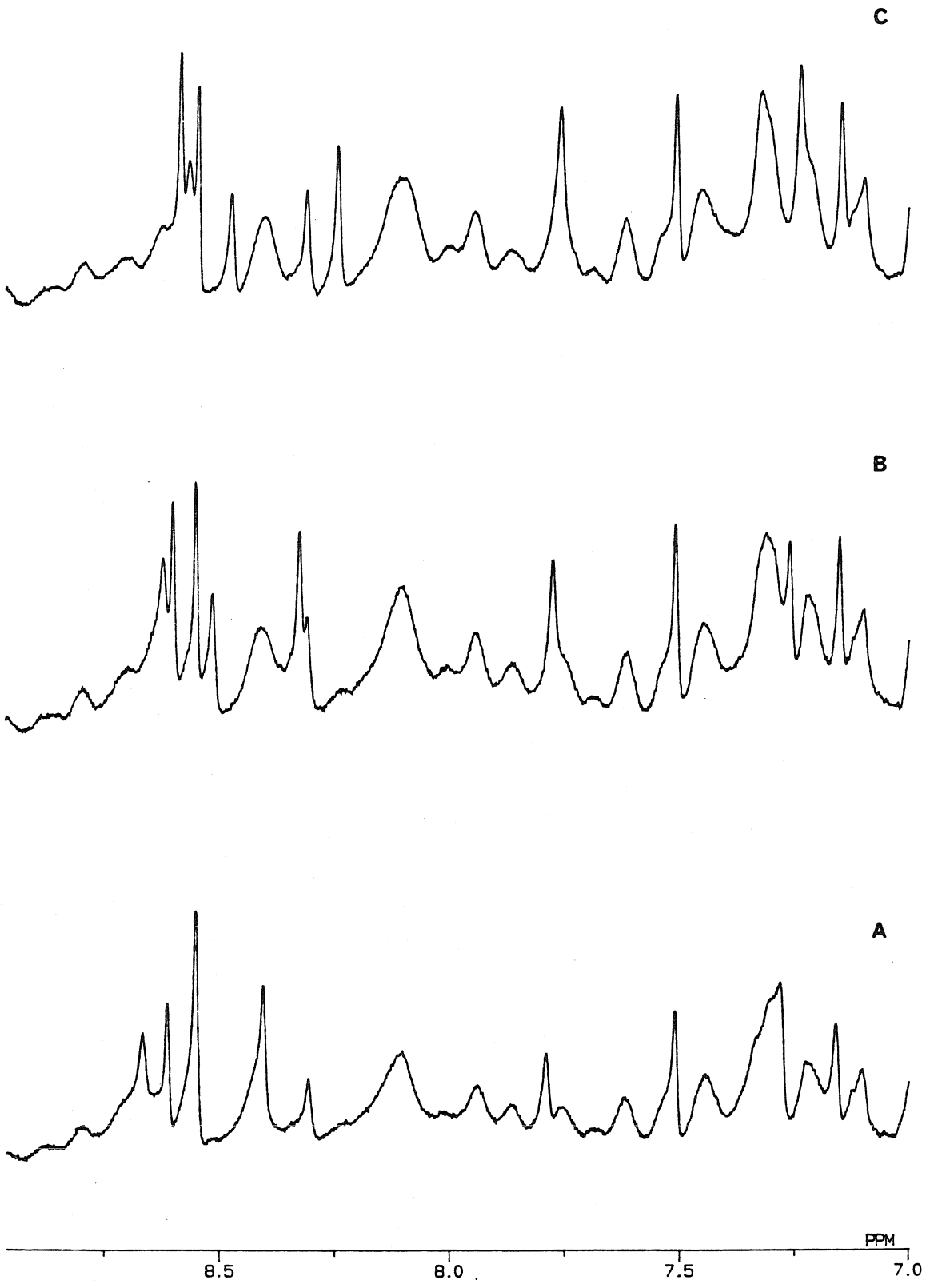
C
B
A
PPM
8.5
8.0
7.5
7.0

Figure 30. Proton NMR spectra at pH 4.7 of A) native Mb and B) a_5Ru(His-116)Mb. The stared positions correspond to the peaks a, c and f from the native Mb spectrum that are not present in the a_5Ru(His-116)Mb spectrum. 500MHz spectra.

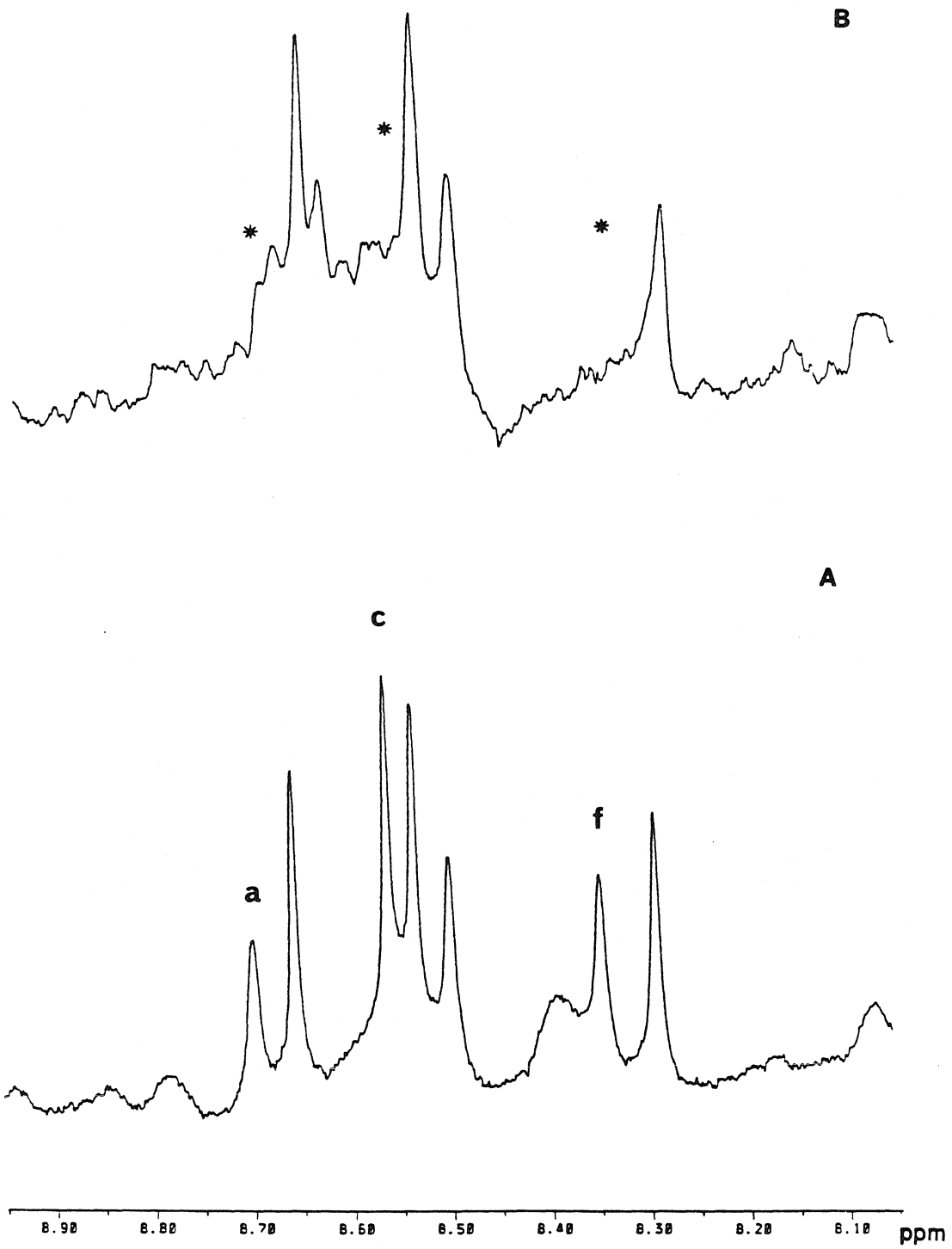
B
*
*
*
A
c
a
f
8.90
8.80
8.70
8.60
8.50
8.40
8.30
8.20
8.10
ppm

The results of the NMR studies on the a_5RuMb derivatives indicate that histidine 48 and 81 can be assigned to peaks e and d, respectively. Histidine 12 could be peak a, b or c. The NMR results of a_5Ru(His-116)Mb indicate that histidine 116 could be peak a, c or f. It is apparent that the His-48 and His-81 labelling sites in the new derivatives will probably be the easiest to identify.

Figure 31 compares the NMR spectrum of $a_4$pyRu(Band III)Mb, (the third and final singly-labelled $a_4$pyRuMb derivative off the cation exchange column) and the spectrum of native Mb. Peak e, corresponding to histidine 48, is missing, indicating that this new derivative is labelled at histidine 48. NMR spectra of Band III from the $a_4$isnRuMb mixture (Figures 32 and 33) also show peak e missing, indicating that it is the 48-labelled derivative. Spectra in Figure 32 and 33 also contain a peak at ~7.2 ppm that is present in the native Mb and missing in the modified Mb. It probably corresponds to the C–4 proton on histidine 48. All three 48-labelled Mb derivatives (a_5Ru-, $a_4$pyRu- and $a_4$isnRu-) elute off the column as the final singly-labelled band.

Both the $a_4$pyRu(Band II)- and $a_4$isnRu(Band II)Mb NMR spectra (Figures 34, 35) do not have a clear resonance missing and the imidazole region is rather broad. Peak d seems to be diminished but most of the other features are similar to native Mb spectra. These results lead to the conclusion that Band II for both these Ru labels may contain more than one singly-labelled species that elute together on the cation-exchange column. Histidine 81, which corresponds to peak d, is probably the ligand in one of the

Figure 31. Proton NMR spectra at pH 4.7 of A) native Mb and B) $a_4$pyRu(Band III)Mb. The starred position in B corresponds to the resonance (peak e, histidine 48) that is not present in the $a_4$pyRu(Band III)Mb spectrum. The labelling site in $a_4$pyRu(Band III)Mb is identified as histidine 48. 500MHz spectra.

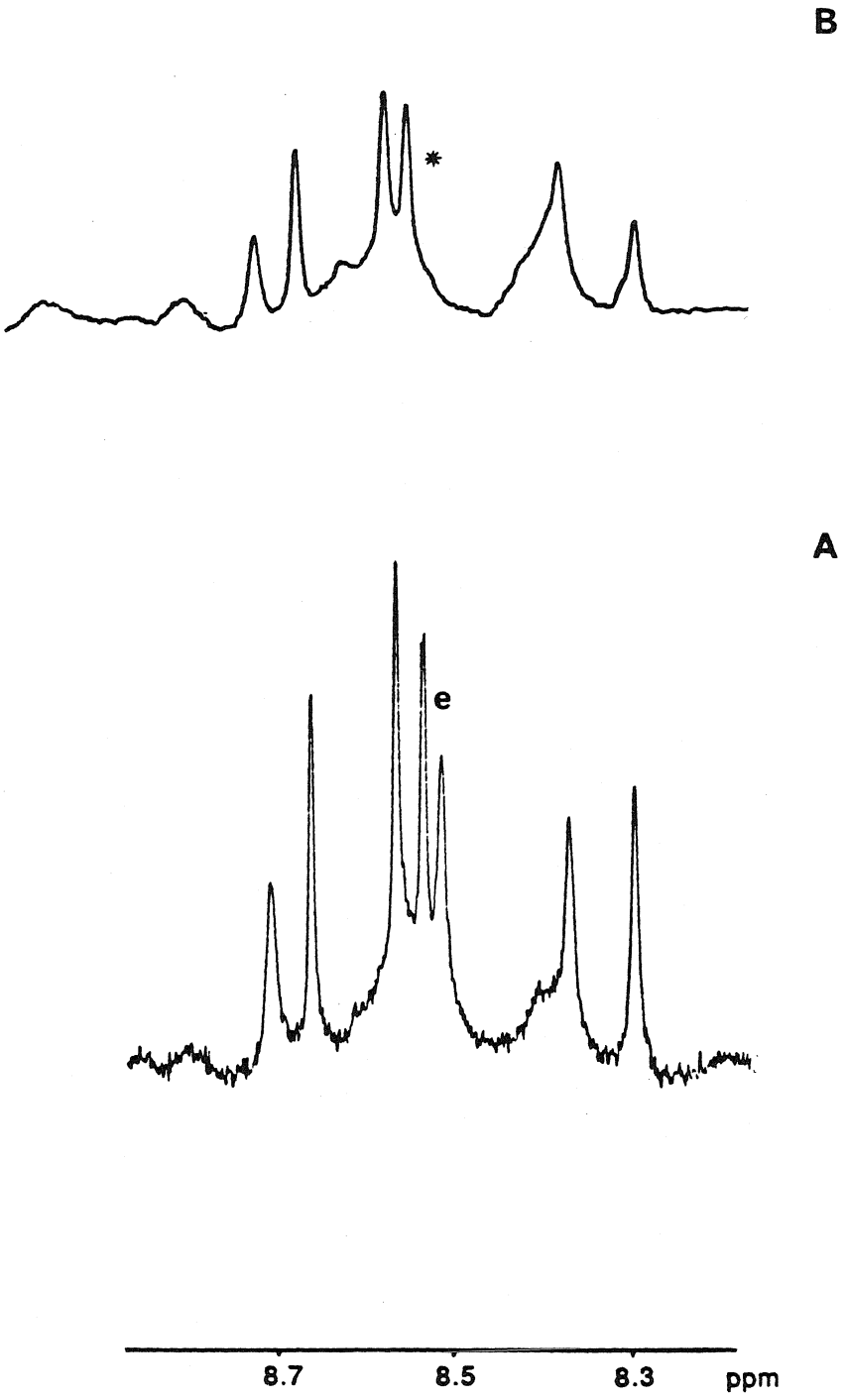
B
*
A
e
8.7
8.5
8.3
ppm

Figure 32. Proton NMR spectra at pH 4.75 of A) native Mb and B) $a_4$isnRu(Band III)Mb. The starred position in B corresponds to the resonance (peak e, histidine 48) from native Mb that is not present in the $a_4$isnRu(Band III)Mb spectrum. The labelling site in $a_4$pyRu(Band III)Mb is identified as histidine 48.

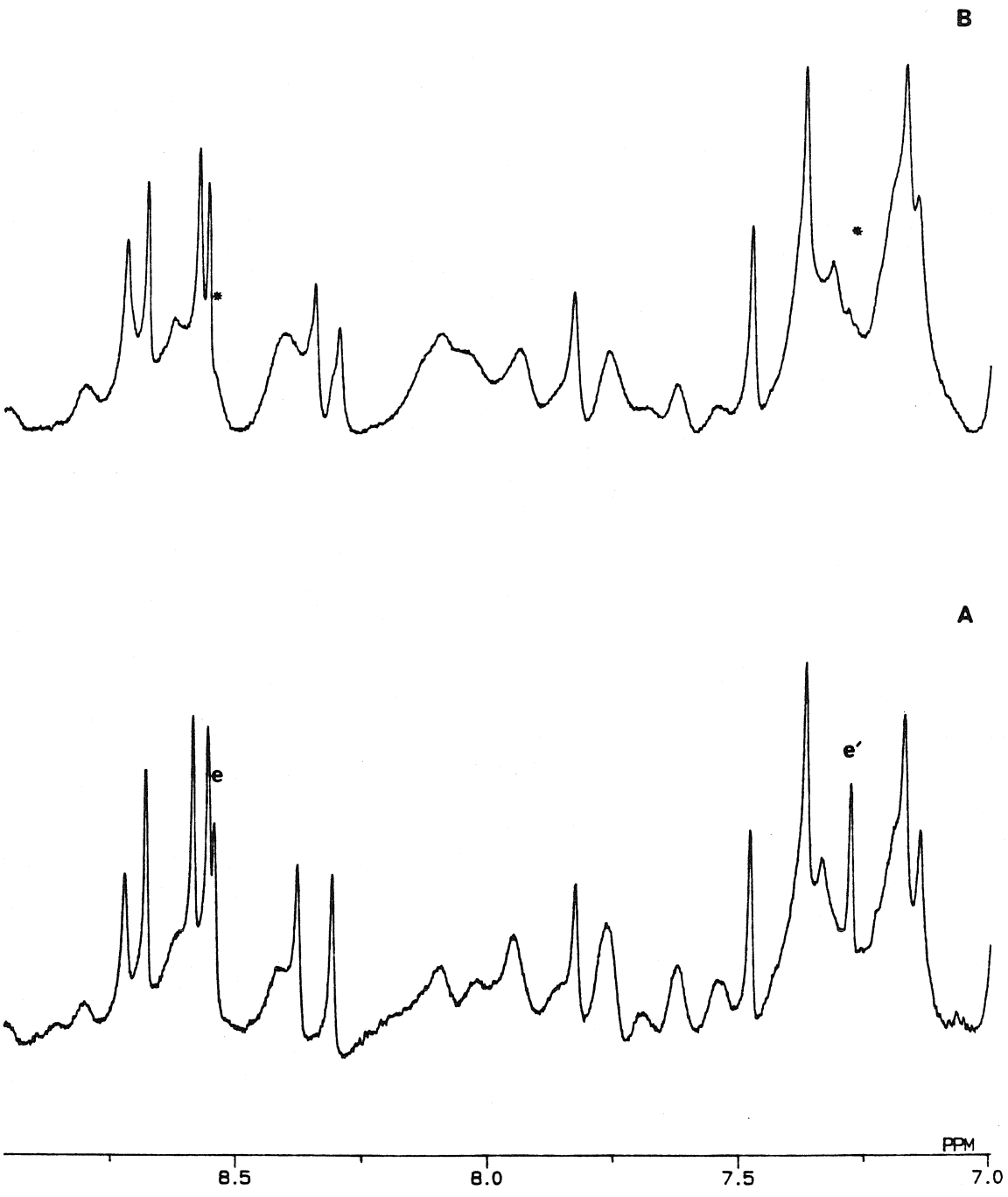
B
*
*
A
e
e´
PPM
8.5
8.0
7.5
7.0

Figure 33. Proton NMR spectra of $a_4$isnRu(Band III)Mb. A) pH 4.75, B) pH 4.9 and C) pH 5. The starred position corresponds to the histidine 48 position.

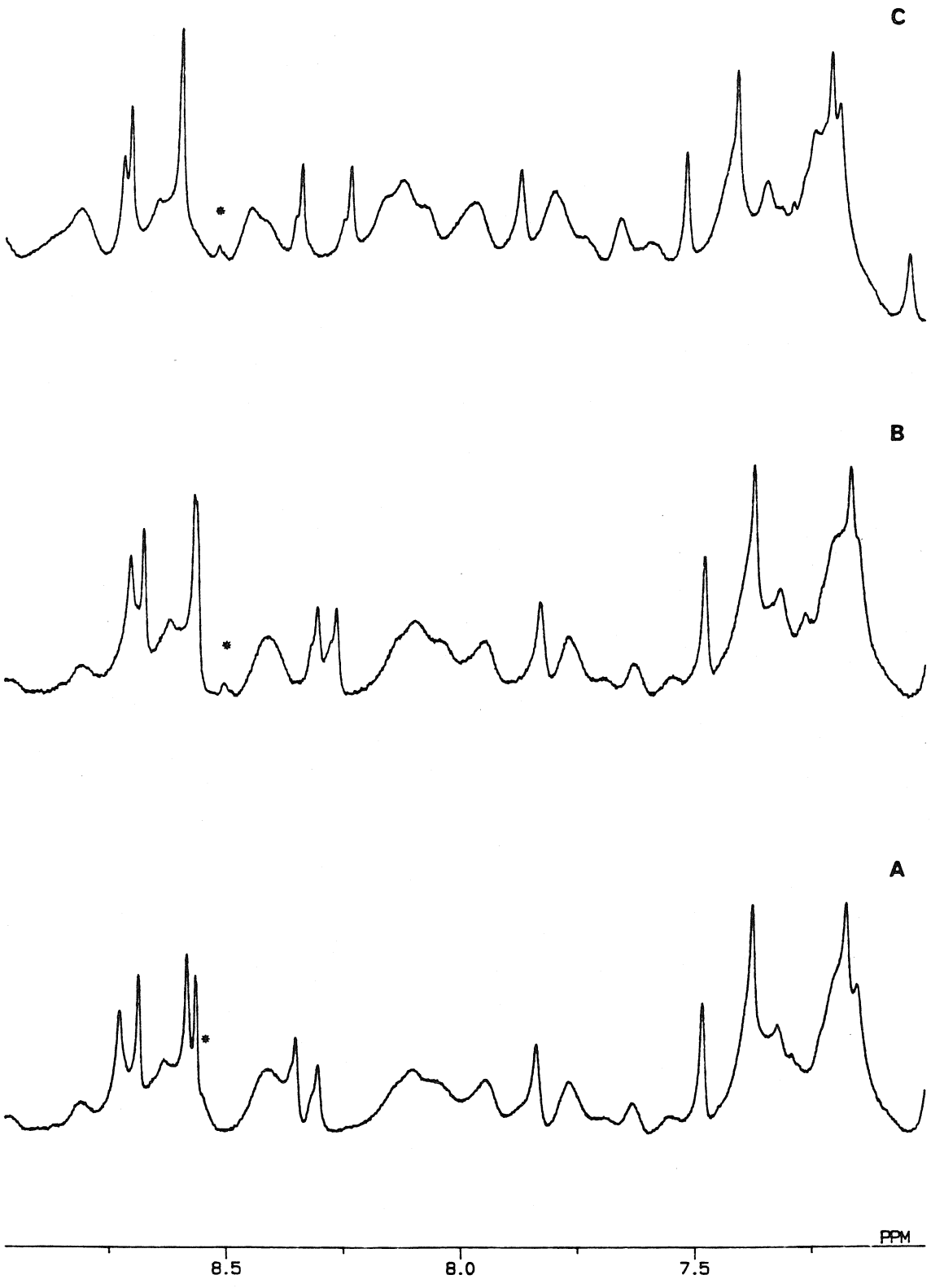
C
B
A
PPM
8.5
8.0
7.5

Figure 34. Proton NMR spectra at pH 4.8 of A) native Mb and B) $a_4$pyRu(Band II)Mb. The starred position in B corresponds to resonance d, which is reduced in intensity relative to native Mb. These spectra indicate that Band II contains a singly-modified Mb species that is labelled at histidine 81 and at least one other singly-labelled derivative.

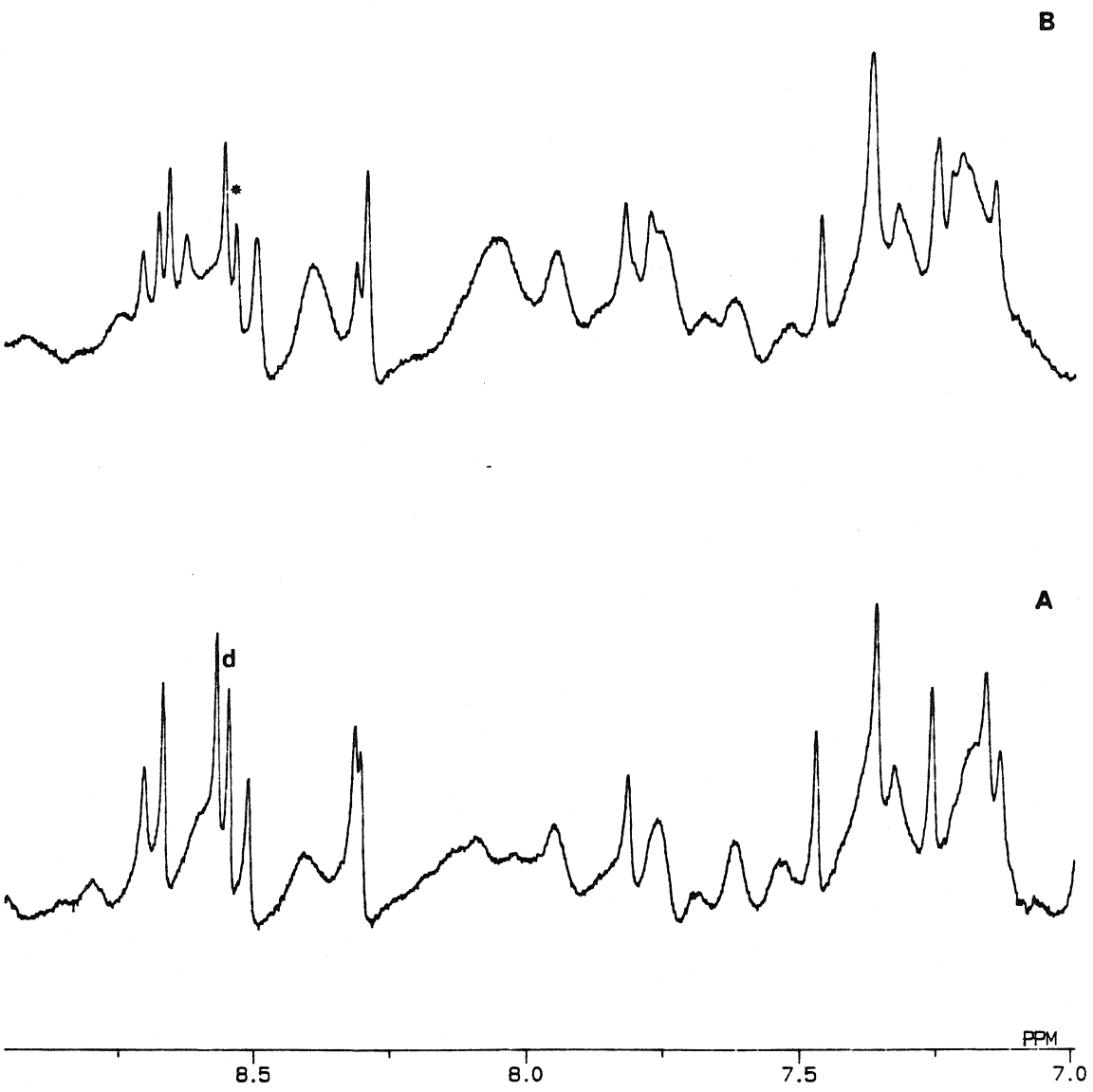
B
*
A
d
PPM
8.5
8.0
7.5
7.0

Figure 35. Proton NMR spectra at pH 4.8 of A) native Mb and B) $a_4$isnRu(Band II)Mb. The features of the $a_4$isnRu(Band II)Mb spectrum are almost identical to those of the $a_4$pyRu(Band II)Mb spectrum.

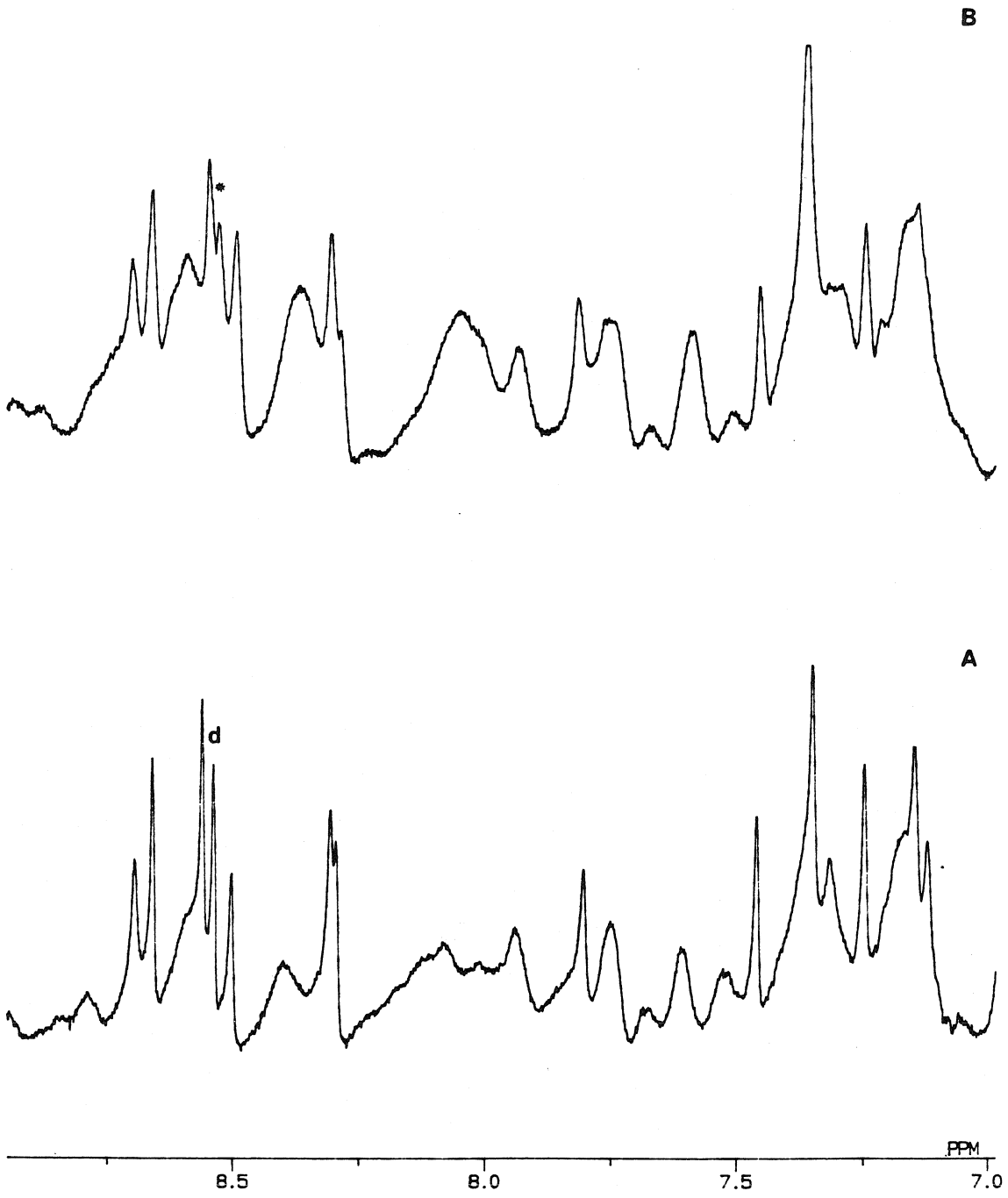
B
*
A
d
PPM
8.5
8.0
7.5
7.0

derivatives in the Band II mixture. Further work will be needed to separate and characterize the Band II species.

Figures 36 and 37 show the NMR spectra of $a_4$pyRu(Band I)Mb. The general features of the modified spectra are that peaks f, g and d (from the native Mb spectra) are unchanged after labelling with Ru. The remaining peaks in the C-2 region have shifted upfield from their original positions. Resonances have also shifted in the 7-8 ppm region. The NMR spectra of a_5Ru(His-12)Mb (Figure 28) and $a_4$pyRu(Band I)Mb are similar but not identical.

The NMR spectra of $a_4$isnRu(Band I)Mb are shown in Figures 38 and 39. Again, peaks f, g and e have not shifted relative to native Mb, but the other peaks in the C-2 region have shifted upfield. The 7-8 ppm region looks similar to the corresponding region in $a_4$pyRu(Band I)Mb, that is, several peaks have shifted in this region relative to native. The two likely possibilities for the labelling site in $a_4$pyRu(Band I)- and $a_4$isnRu(Band I)Mb are histidine 12 and histidine 116, since histidine 48 and 81 derivatives are included in Bands II and III. The tentative assignment of the labelling site is histidine 12, because the NMR spectra of the Band I derivatives are more similar to the a_5Ru(His-12)Mb spectra than to the a_5Ru(His-116)Mb spectrum. Several peaks are shifted upfield of peaks a and b, and histidine peaks f and g are consistently unaffected by the Ru reagent in the a_5Ru(His-12)Mb and the Ru(Band I)Mbs. a_5Ru(His-12)Mb is also the first band off the column in the purification of the a_5RuMb derivatives.

Figure 36. Proton NMR spectra at pH 4.7 of A) native Mb and B) $a_4$pyRu(Band I)Mb. Peaks a, b, c and e from the native Mb spectrum have shifted in the $a_4$pyRu(Band I)Mb spectrum. The starred peaks (in B) correspond to the shifted resonances.

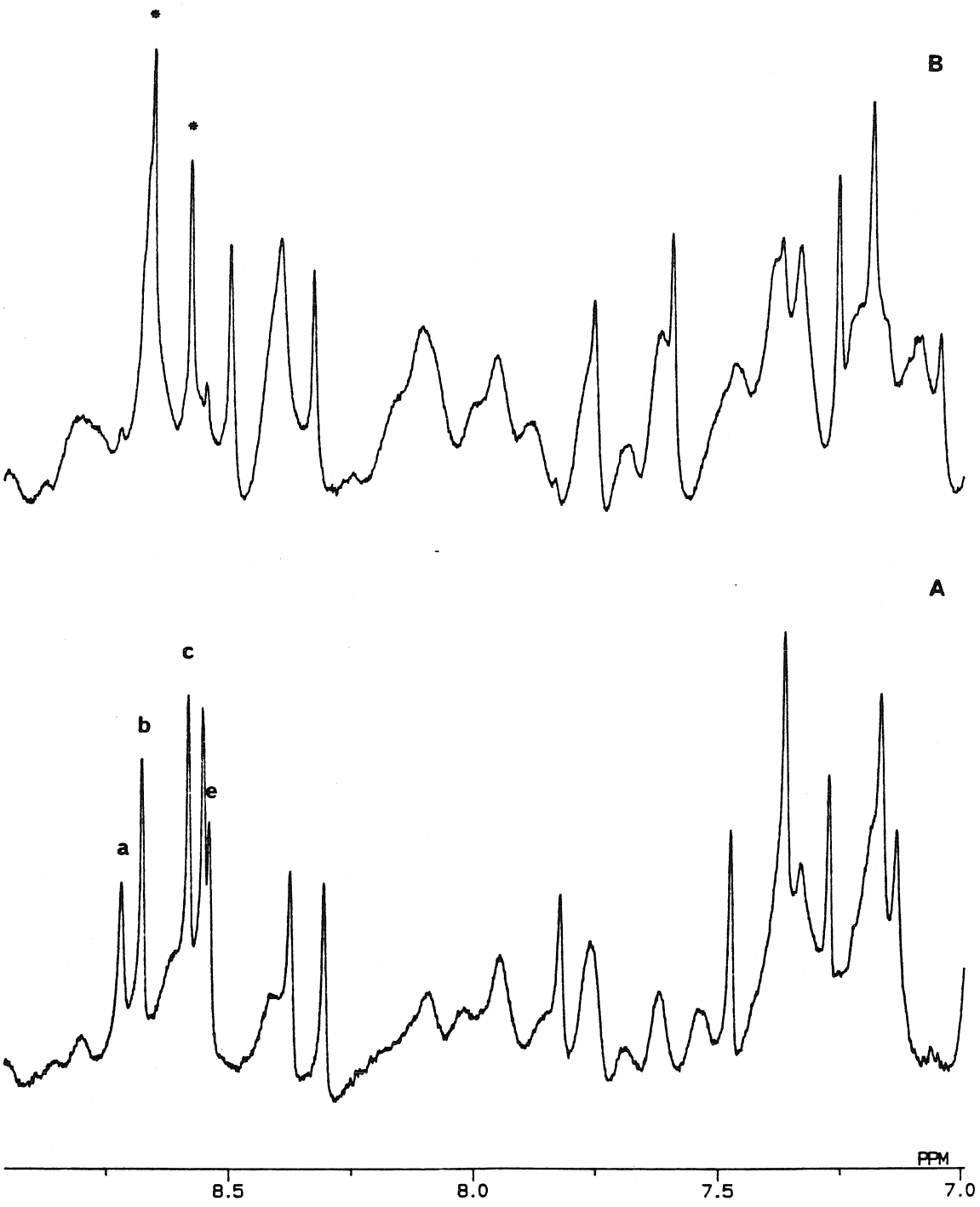
*
*
B
A
c
b
e
a
PPM
8.5
8.0
7.5
7.0

Figure 37. Proton NMR spectra of $a_4$pyRu(Band I)Mb. A) pH 4.6, B) pH 4.7 and C) pH 4.8.

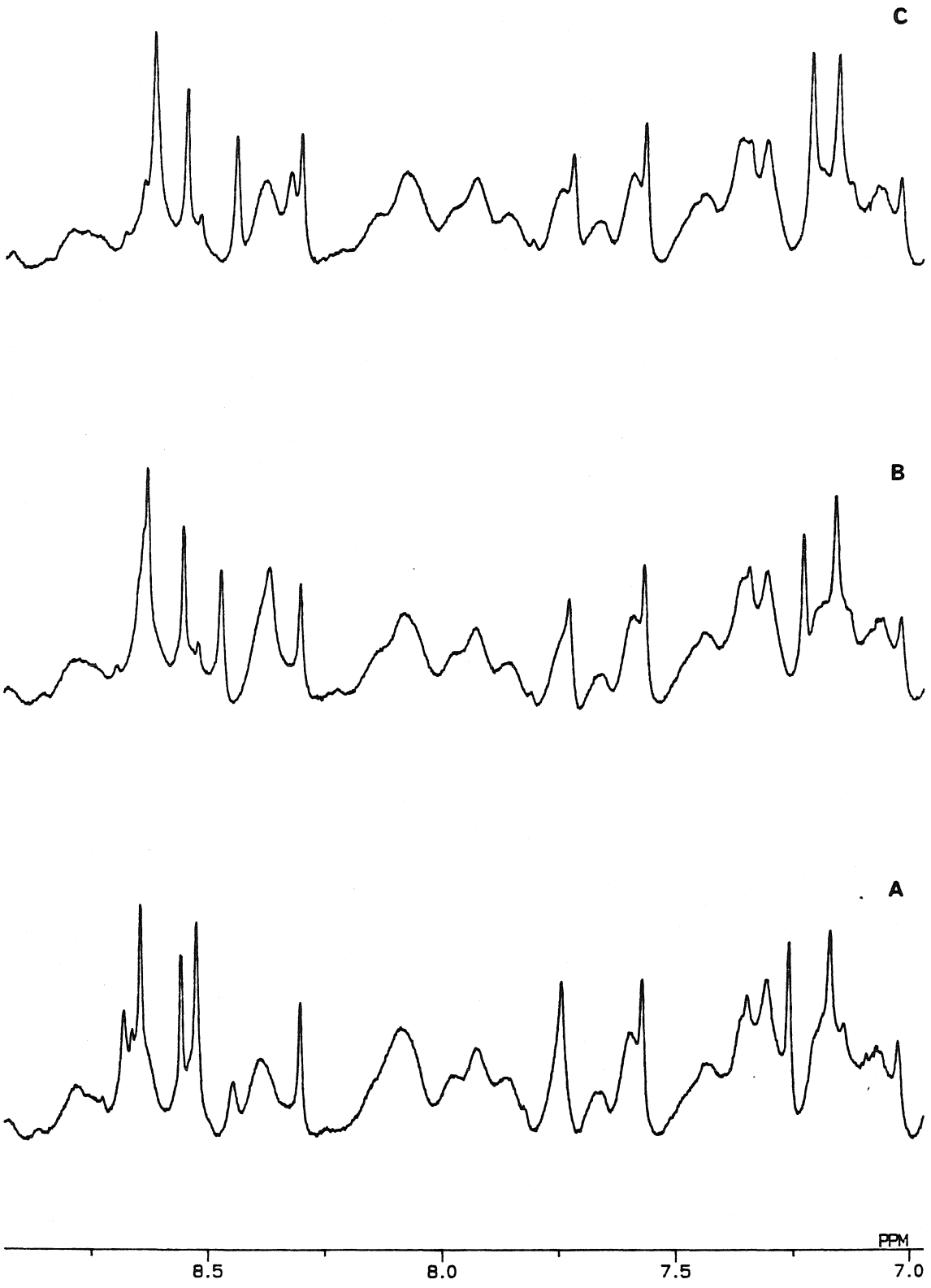
C
B
A
PPM
8.5
8.0
7.5
7.0

Figure 38. Proton NMR spectra at pH 4.7 of A) native Mb and B) $a_4$isnRu(Band I)Mb. Peaks a, b, c and d from the native Mb spectrum have shifted in the $a_4$isnRu(Band I)Mb spectrum. The starred peaks (in B) correspond to the shifted resonances.

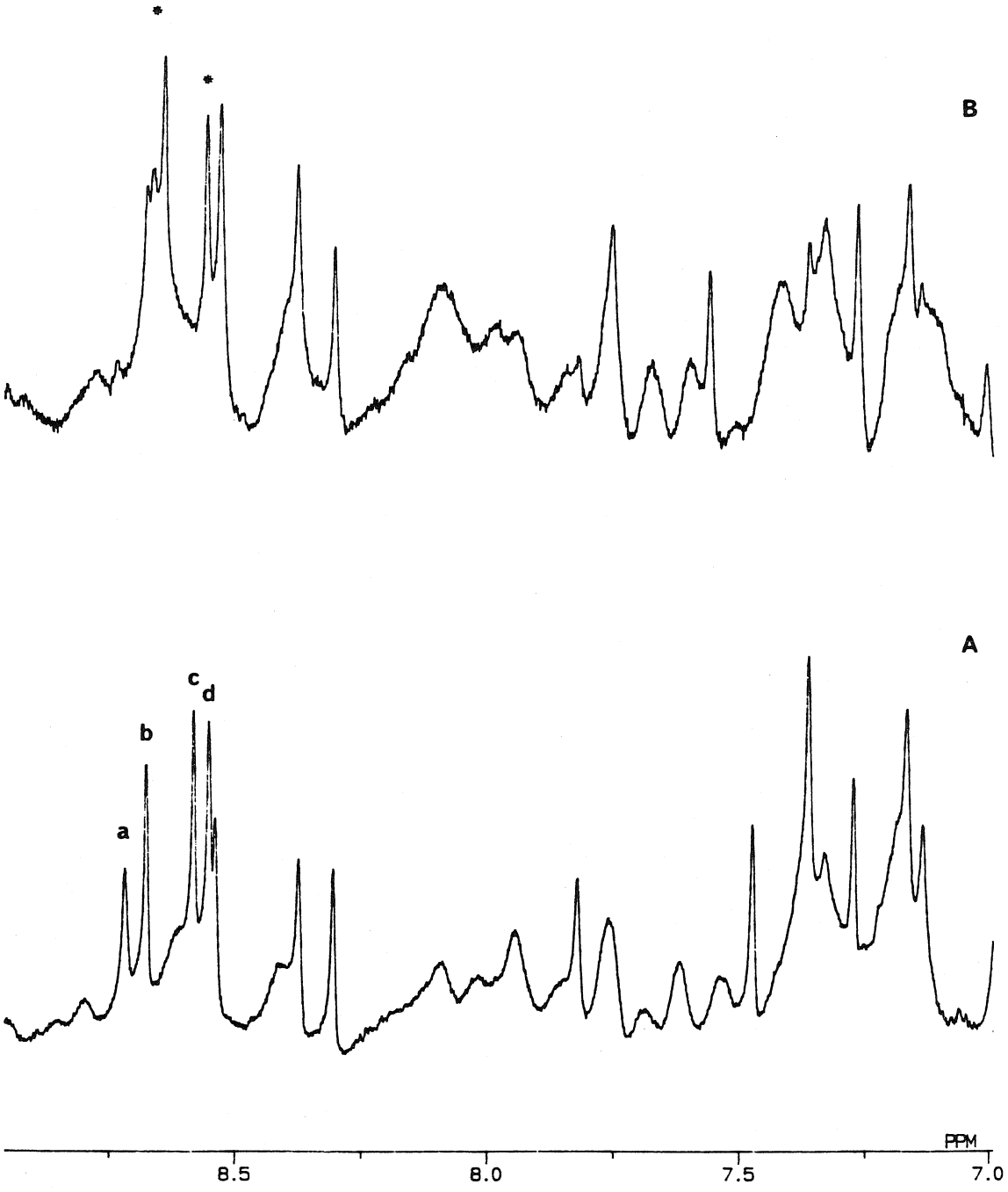
*
*
B
A
a
b
c
d
PPM
8.5
8.0
7.5
7.0

Figure 39. Proton NMR spectra of $a_4$isnRu(Band I)Mb. A) pH 4.7, B) pH 4.8 and C) ~pH 5.

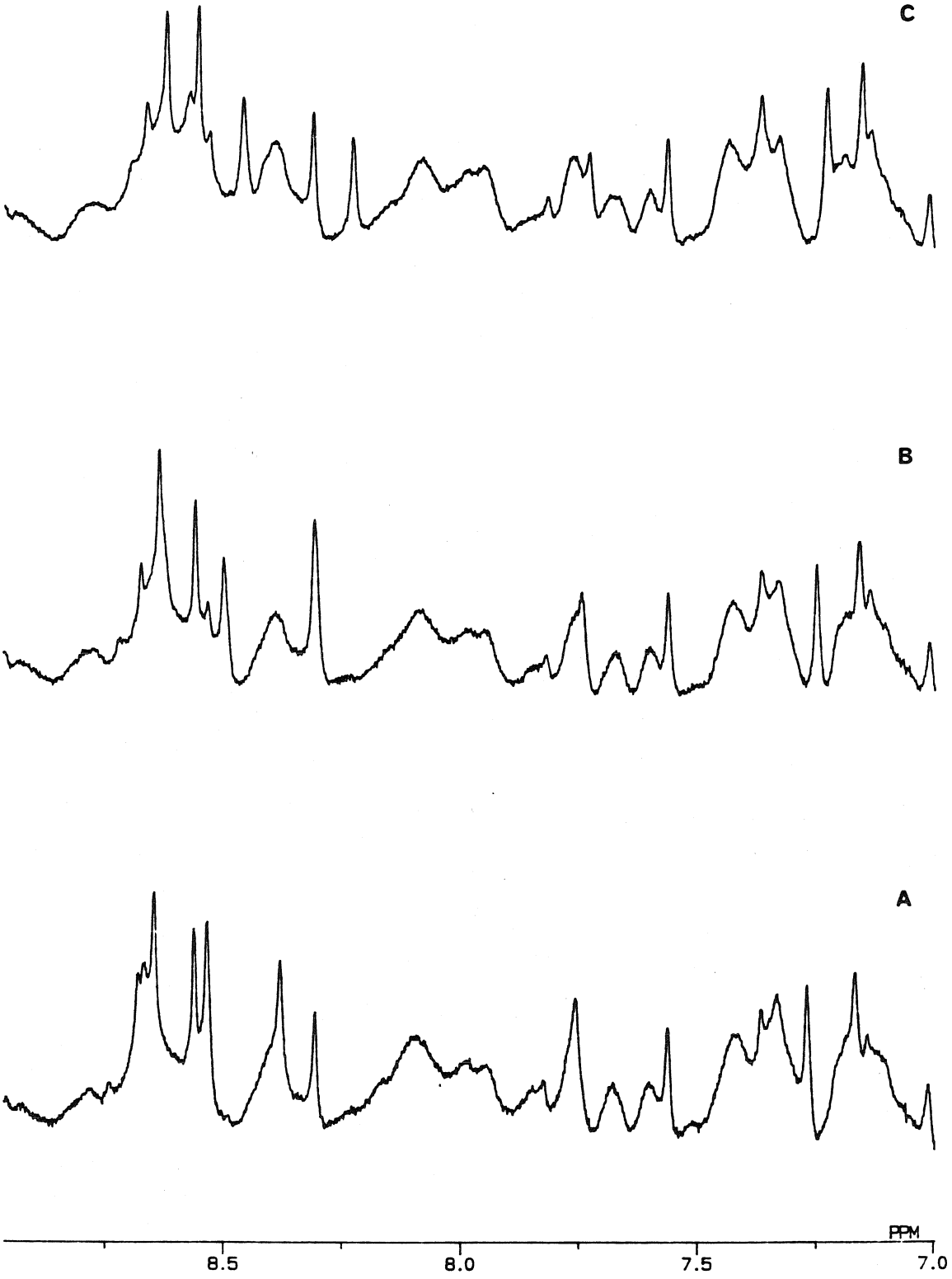
C
B
A
PPM
8.5
8.0
7.5
7.0

Electrochemistry. The Ru complexes attached to the protein have reversible redox potentials; this allows accurate characterization of the electron-transfer driving force (Chapter 3). In a_5Ru-labelled Mb[36,37] and cytochrome c,[39] the reduction potentials of the attached ruthenium have been determined using differential pulse polarography (DPP). This technique has also been used to measure the reduction potentials in the new Ru-labelled Mb species. The measurements were obtained using 1-3mM protein solutions plus 4,4' bipyridine. (4,4' bipyridine was added to facilitate electron transfer at the electrode.) Representative voltamograms for the singly-labelled Mb species are shown in Figures 40, 41 and 42. The $Ru^{III/II}$ reduction potentials are 340, 420 and 560 ± 10 mV vs NHE at 25°C for the $a_4$pyRu-, $a_4$isnRu- and $a_4$pzRuMb, respectively. These values are an average of several scans. These potentials correspond fairly well to those of the a_5LRu model complexes (L=py, isn or pz; see Table II).

The Mb $Fe^{III/II}$ reduction potentials for native and a_5RuMb have been measured previously by spectroelectochemistry[36,37] and found to be 65 and 60 mV vs. NHE, respectively. It is apparent that labelling of a surface histidine with a_5Ru does not change the heme potential significantly. It is assumed that the other Ru complexes do not influence the heme potential; the Fe potential of Ru-labelled Mbs is estimated to be 65 ± 5 mV.

Figure 40. Smoothed differential pulse voltammogram of 1mM $a_4$pyRuMb plus 10mM 4,4' bipyridyl in NaPi buffer (μ=0.1, pH 7). The potential ($E^o(Ru^{III/II})$) at maximum current is 340 mV vs. NHE. A scan rate of 2 mV s^{-1} and a 0.5 s drop time were used. The conditions for subsequent experiments were identical.

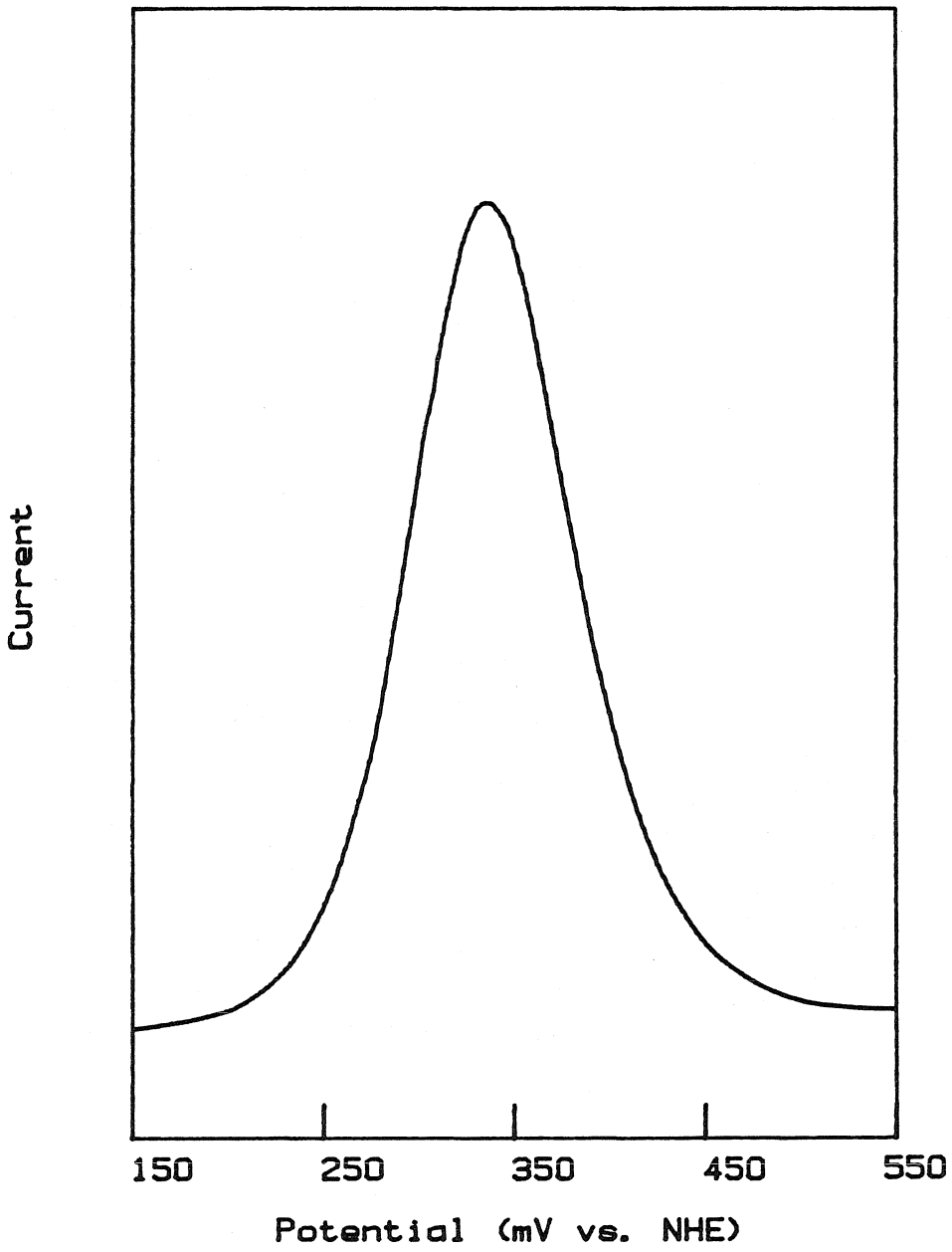
Current
150
250
350
450
550
Potential (mV vs. NHE)

Figure 41. Smoothed differential pulse voltammogram of the Ru center in $a_4$isnRuMb. The potential at maximum current is 420 mV vs. NHE.

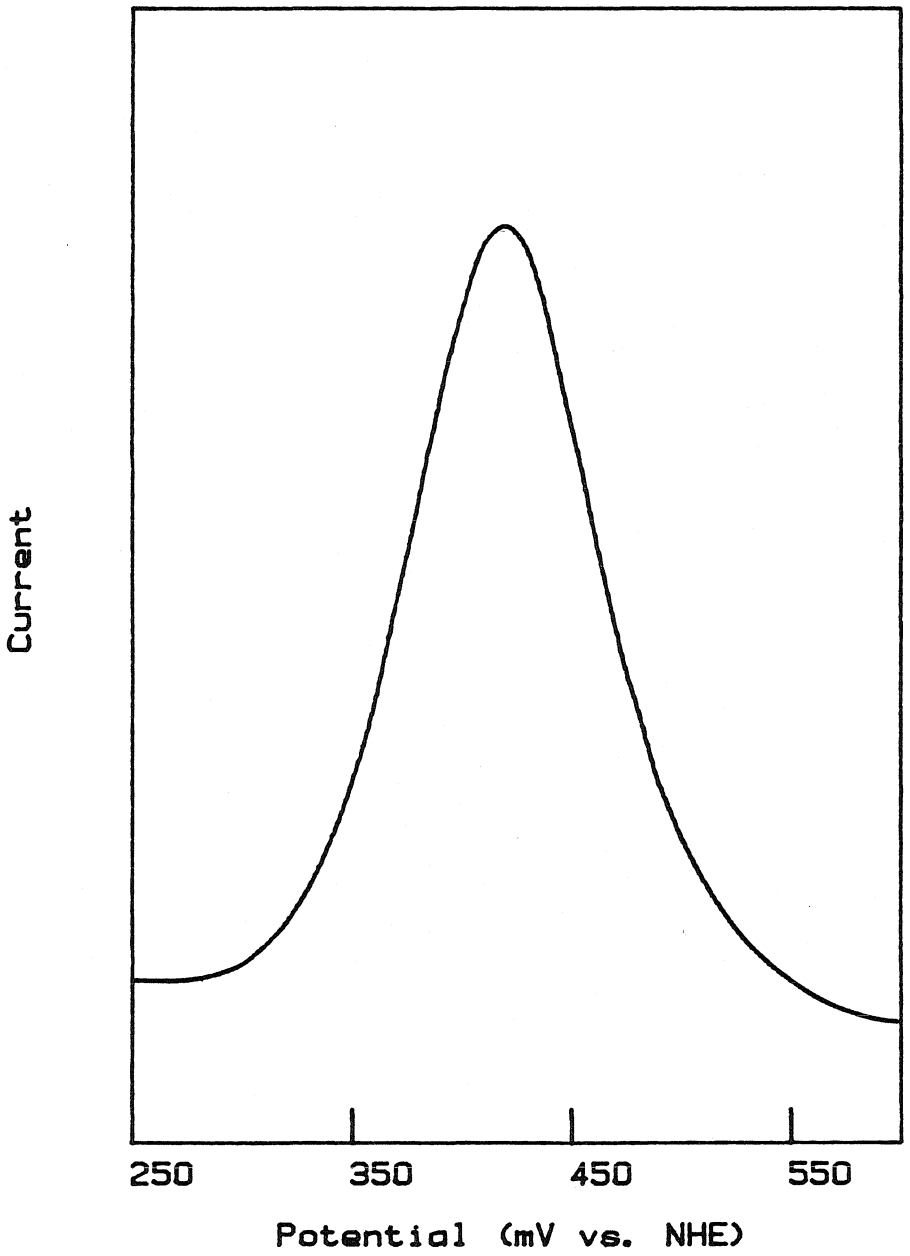
Current
250
350
450
550
Potential (mV vs. NHE)

Figure 42. Smoothed differential pulse voltammogram of the Ru center in $a_4$pzRuMb. The potential at maximum current is 560 mV vs. NHE.

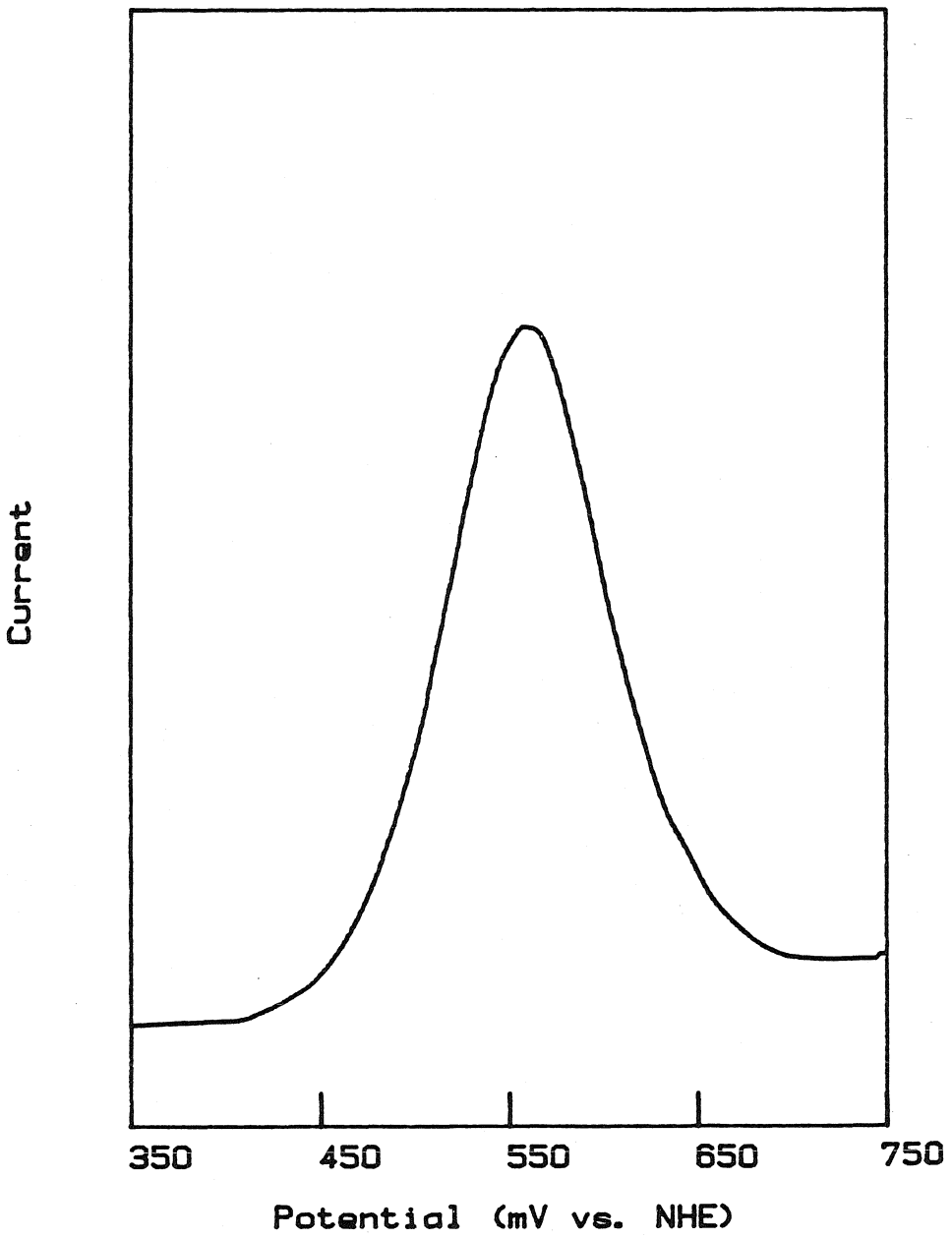
Current
350
450
550
650
750
Potential (mV vs. NHE)

Chapter III.

Electron Transfer in Ruthenium-Labelled Myoglobin

Introduction

The general strategy for studying the effect of reaction free energy on k_{ET} and determining the reorganization energy for a donor/acceptor system is to create a series of homologous ET systems. The reaction free energy can be tuned by varying the potential of the donor and/or the acceptor. Ideally, as the reaction free energy changes, other important factors such as distance, medium and reorganization energy can be kept constant. These conditions are achieved in the two-site Ru-labelled Mb derivatives.

There are two strategies that have been used to create a series of variable driving force systems using the protein matrix of myoglobin as the spacer. The general donor/acceptor model consists of heme-containing myoglobin labelled at histidine 48 with a $(NH_3)_5Ru$ moiety (Figure 43).[35,36] This two-site system is rigid and has a fixed ET distance of 13 Å. The first approach that has been used to change the ET driving force in the Ru(His-48)Mb system involves changing the Ru complex that is attached to histidine 48.[34] To systematically tune the potential of the attached Ru-ammine complex, the ligand *trans* to the imidazole was varied from NH_3 to pyridine and finally to isonicotinamide:

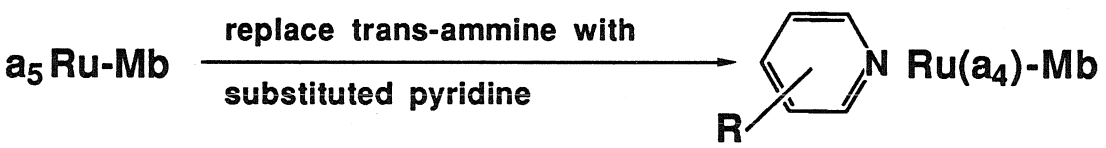

In this fashion a range in potential of 340 mV can be achieved. The important advantages of this method include: 1) The potential of the

Figure 43. Cutaway view of the donor and acceptor sites in a_4LRu(His-48)Mb.

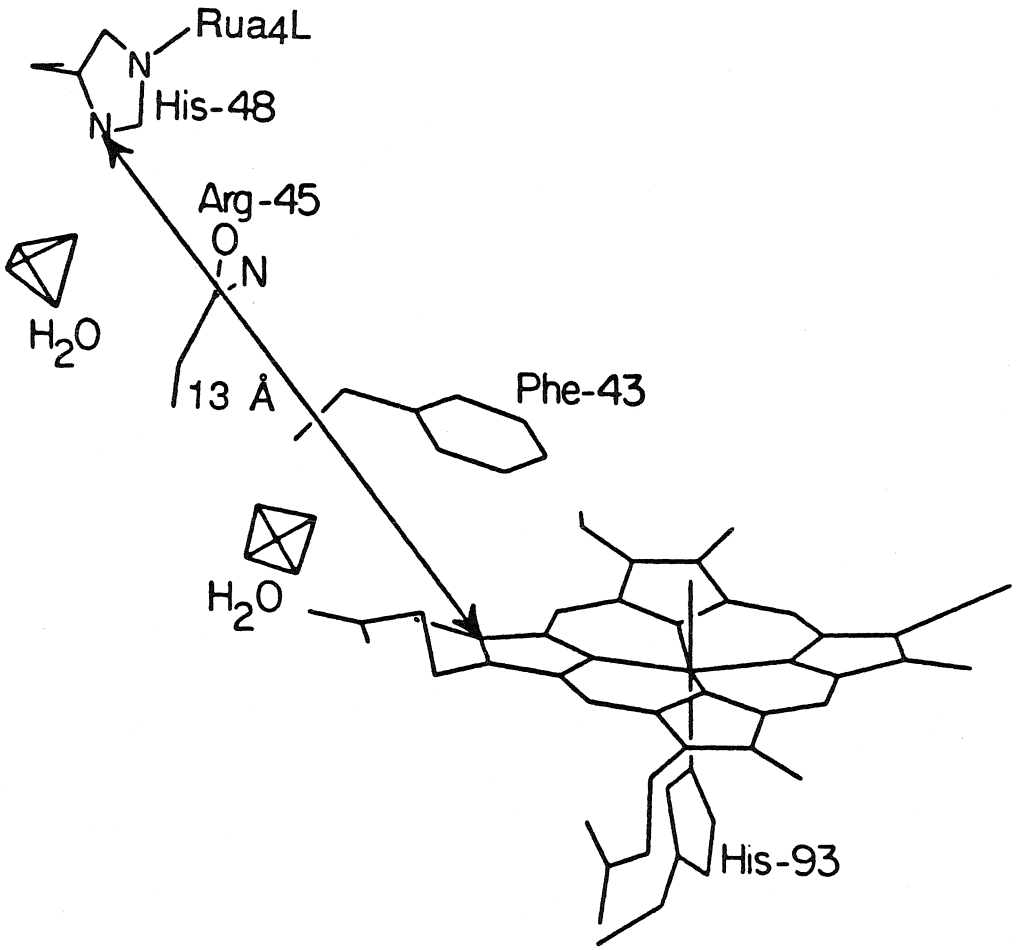
Rua4L
N
His-48
N
Arg-45
O
N
H_2O
13 Å
Phe-43
H_2O
His-93

attached Ru complex is reversible and can be measured directly, and 2) There are minimal changes to the system other than variation in redox potential. In particular, the fact that the ligand being varied is *trans* to the imidazole suggests that the structure of the protein will not be disturbed.[75] Also, the change in reorganization energy that is expected in going from a_5Ru- to $a_4$pyRuMb is estimated to be small, <0.1 eV.[64] Since the protein is relatively incompressible the distance between the donor and acceptor is fixed.[11,35]

The second strategy that has been used to manipulate the reaction free energy in the Ru(His-48)Mb system is to remove the heme and substitute various other porphyrins.[33,35] This approach of tuning ΔG^o by metal substitution has been used previously by McLendon et al. to vary the ET driving force in a series of cyt c/cyt b_5 protein-protein complexes. In Mb the reaction free energy can be increased significantly when a photoactive porphyrin, such as Zn or Pd porphyrin (ZnP, PdP) is substituted for the Fe heme. Both ZnP and PdP have long-lived, highly-reducing excited states, $E^o(ZnP^{*/+})$~0.8 V and $E^o(PdP^{*/+})$~0.6 V.[76,77] Using these porphyrins and the various attached Ru complexes, the reaction free energy can be extended from near zero to ~1.2 V.

One disadvantage of the photoactive porphyrin Mb systems is that the excited state potentials cannot be measured directly, and therefore there is uncertainty in the absolute reaction free energy. This problem is partially circumvented because the Ru complexes allow for the same well-defined changes in ΔG^o at low driving forces and at the higher driving forces. For example, in the case of

FeMb and ZnMb there are two sets of ET systems that have the same changes in ΔG^o, one at low driving force (FeMb) and one at high driving force (ZnMb). The change in porphyrin may also lead to a small change in ET distance or reorganization energy. Since the excited states of Zn and Pd porphyrins are more delocalized than the donor or acceptor state of an Fe porphyrin, the ET distance is probably somewhat longer for the FeMb than for the Zn and PdMb. In Fe porphyrin, there is also a ligation change upon reduction (water dissociates)[48] that is not present in the Zn or PdMb. This means that the reorganization energy of FeMb should be greater than that of ZnMb (or PdMb). With these differences in mind, an investigation of the ET rates in this series of Ru-labelled Mb derivatives was performed.

Experimental

Materials

Nickel(II)[hexamethyltetraazacyclodecane]·$2ClO_4$ ($Ni^{II}Me_6ane$) was prepared by published procedures.[78]

3-Bromopropionic acid (RBr) was purchased from Aldrich and purified by vacuum sublimation prior to use. The RBr was stored under vacuum with dessicant.

Tris(2,2'bipyridyl)ruthenium(II)chloride·hexahydrate ($Ru(bpy)_3^{2+}$) was obtained from Aldrich and was stored in a dark container.

Sodium dithionite was obtained from MCB. The deuterium

oxide used was 99.8 atom %D and was purchased from Aldrich. Acetonitrile obtained from Mallinckrodt was used without further purification. All buffer salts and other materials were of reagent grade quality.

Water used in all preparations had been passed through a Barnstead NANOpure water purification system (Model 2794).

Purified protein derivatives were prepared as indicated in Chapter 2.

Methods

Preparation of Flash Photolysis Samples

A 10 mL solution of 6.5×10^{-5} M $Ru(bpy)_3^{2+}$, 1×10^{-2} M RBr and 5×10^{-3} M $Ni(Me_6ane)$ in μ=0.1, NaPi, pH 7 was degassed on a high vacuum line equipped with a a diffusion pump. Five freeze-pump-thaw cycles were performed on each solution. The RuMb (3-6 mg in 2 mL μ=0.1, NaPi, pH 7) was gently degassed on an argon/vacuum line via three cycles of evacuation 10 s, argon 2 min. The degassed protein solution and $Ru(bpy)_3^{2+}$ solution were brought into an argon filled inert atmosphere box (Vacuum Atmospheres).

Under the argon atmosphere the protein solution was reduced with two drops of sodium dithionite (~2 mg in 1 mL) to form the $Ru^{II}Fe^{II}$-protein. The dithionite was removed by ultrafiltration; the protein was concentrated to 0.5 mL and then diluted with ~5 mL μ=0.1, NaPi, pH 7. After four cycles of this exchange process the Mb solution was transferred to a capped 1mm UV cell, brought out of

the box, and from the absorption spectrum the protein concentration was determined; at 556 nm, $\varepsilon=1.2\times10^4$ cm^{-1} M^{-1}.[79]

In the argon atmosphere box 0.1-0.3 mL of Mb (corresponding to 5×10^{-6} M in 10 mL) was transferred to the degassed $Ru(bpy)_3^{2+}$ solution in the flash cell. After the protein was added the flash experiment was performed immediately to prevent autooxidation of the protein.

Preparation of Laser Photolysis and Emission Samples

All ZnMb and PdMb samples were degassed thoroughly on a vacuum/argon line for 30 min to 2 h. The ZnMb samples were prepared in a 1 cm pathlength vacuum cell; 3-5 μM protein in 5 mL μ=0.1, NaPi, pH 7. The PdMb samples were prepared in a similar fashion using ~15 μM protein in μ=0.01, NaPi, pH 7.

Instrumentation

Flash Photolysis

The flash photolysis experiments were performed on an apparatus that has been described previously.[80] The apparatus consisted of a Xenon Corporation N851C flashlamp fired by a micropulser (Energy=36-100J/flash, $\tau_{1/2}\cong5\mu s$). The flashlamp was filtered with a Corning glass filter that eliminated ultraviolet light. The protein solution was enclosed in a 15 cm pathlength vacuum cell with quartz windows. The output of a tungsten lamp was the monitoring beam and detection of the signal utilized an Oriel 7240 1/4 meter monochromator (556 or 568 nm) and a Hamamatsu R928

photomultiplier. The tungsten lamp was filtered (wavelength cutoff 525 nm) to prevent continuous irradiation of the Mb Soret and the $Ru(bpy)_3^{2+}$. The signal was stored in a Biomation 805 transient waveform recorder, displayed on a Tetronix 549 storage oscilloscope and plotted on a strip chart recorder.

Transient Emission

The pulsed laser system that was used to measure transient emission in the PdMb samples has been described previously.[39] The excitation source was a Quanta Ray DCR-1 Nd:YAG laser that was frequency doubled with a harmonic generator (Quanta Ray HG-1) followed by a prism harmonic separator (Quanta Ray PHS-1) to produce a 532 nm pulse of 8 ns (fwhm) duration at 10 Hz. Light emitted from the sample was collected at 90° to the excitation beam with a collimating lens (f/1.3) and focused with a second lens onto the entrance slit of a MacPherson 0.35 m monochromator. The PdMb luminescence was monitored at 670 nm and detected by a Hamamatsu R928 photomultiplier tube. The signal was passed through either a LeCroy model VV101ATB amplifier or a Tetronix FET amplifier with a 5kΩ resistor to a Biomation 6500 waveform recorder. The LeCroy amplifier was used in cases where the lifetime was 1 ms or shorter. The FET amplifier yielded a much better signal-to-noise ratio and could be used for measurements when the lifetimes were about 1 ms or longer. Laser triggering, data acquisition and data analysis were controlled with a Digital PDP 11/03-L computer.

Transient Absorption

The transient absorption measurements on the RuMbZn samples were performed at Brookhaven National Laboratories. The experimental system has been described previously.[41,81] The excitation source was a mode-locked, frequency doubled Nd:YAG laser (532 nm, 30 ps fwhm). The probe light used was a 75-W xenon arc lamp (Photon Technology International); the lamp was run cw at ~40W. The detection apparatus utilized a double 1/4 meter monochromator and a Hamamatsu R928 photomultiplier tube (PMT). The PMT signal fed into a quasidifferential amplifier and then into a CAMAC-controlled LeCroy TR8828B transient digitizer. The data collected were an average over more than 25 laser pulses and were analyzed on a PDP 11/73 computer.

Results and Discussion

Electron-Transfer Rates for $(NH_3)_4$LRuMbFe; L=NH_3, pyridine.

The electron-transfer rates for the a_5Ru- and $a_4$pyRu-labelled at histidine 48 in Mb have been determined using a flash photolysis technique.[34,36] The general strategy required to observe intramolecular electron transfer in a two-site protein is to utilize an external reductant (or oxidant) that will rapidly and selectively reduce (or oxidize) one redox center on the protein. In this fashion a mixed valence species, i.e., $Ru^{II}MbFe^{III}$ or $Ru^{III}MbFe^{II}$, can be formed and the intramolecular ET can be observed ($Ru^{II}\rightarrow Fe^{III}$ or $Fe^{II}\rightarrow Ru^{III}$). Two conditions must be satisfied in order to observe intramolecular

ET: 1) The bimolecular ET step that creates the mixed-valence species must be much faster than the intramolecular ET, and 2) The back ET reaction from the protein to the external reductant (or from the oxidant to the protein) must be blocked.

In a_5Ru(His-48)MbFe the reduction potentials of the Fe and Ru are closely matched, and therefore the ET rate can be measured in either direction. In $a_4$pyRu(His-48)MbFe, however, the difference in reduction potentials between the surface $a_4$pyRu (340 mV) and heme (65 mV) is 275 mV and this requires that the ET rate must be measured from the Fe^{II} to the surface Ru^{III}. To generate the mixed-valence Fe^{II}/Ru^{III} protein species and monitor the subsequent ET, a methodology was developed in our laboratory.[34] This procedure is outlined in Figure 44 and discussed below.

Flash photolysis generates the excited state of tris(2,2'-bipyridine)ruthenium(II), $Ru(bpy)_3^{2+*}$, which is a powerful oxidant; E^o $(Ru(bpy)_3^{2+*/1+})$ =0.84 V. This species is subsequently quenched via rapid bimolecular ET from the reduced Ru^{II}-MbFe^{II} protein complex to yield primarily Ru^{III}-MbFe^{II}. The intramolecular ET process, Ru^{II}-MbFe^{III} $\rightarrow$ Ru^{II}-MbFe^{III}, can then be observed if the $Ru(bpy)_3^{+}$ is efficiently removed from the system. Removal of $Ru(bpy)_3^{+}$ prevents the very favorable back reaction (k_{BET}, Figure 44) which would rapidly regenerate Ru^{II}-MbFe^{II}. A suitable scavenger system consists of nickel(II)hexamethyltetraazacyclodecane ($Ni^{II}Me_6$ane) and 3-bromopropionic acid (RBr).[82,83] In this system, $Ni^{II}Me_6$ane is reduced by $Ru(bpy)_3^{+}$ to form the Ni^{I} species, which then reacts irreversibly with RBr. The $Fe^{II}\rightarrow Ru^{III}$ ET is measured by

Figure 44. Experimental flash photolysis technique for measuring $Ru^{III}PFe^{II} \rightarrow Ru^{II}PFe^{III}$ electron transfer.

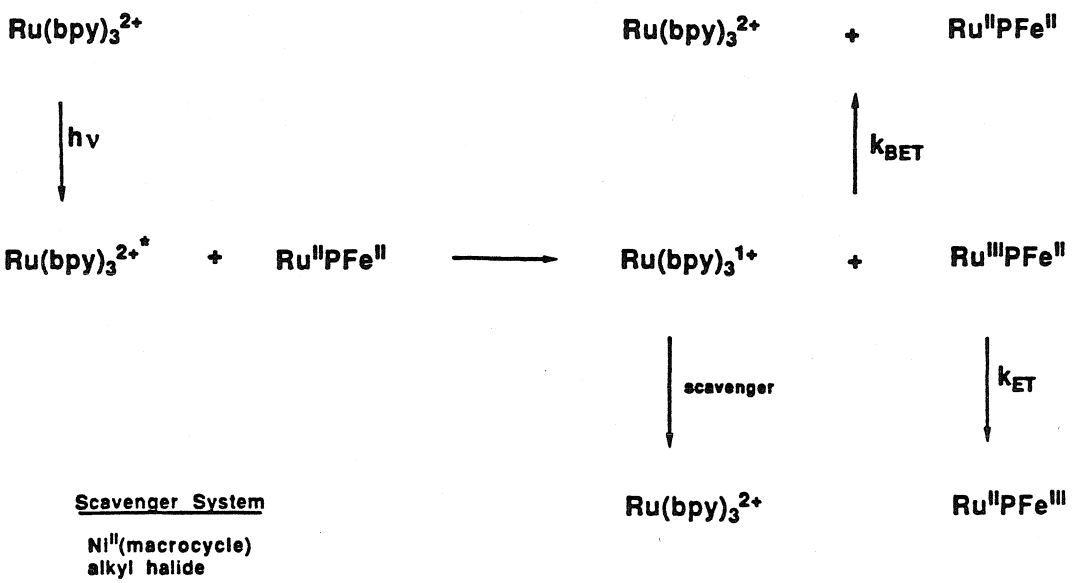
Ru(bpy)3 2+
hν
Ru(bpy)3 2+*
+
RuIIPFeII
Ru(bpy)3 1+
+
RuIIIPFeII
kBET
scavenger
kET
Ru(bpy)3 2+
RuIIPFeIII
Scavenger System
NiII(macrocycle)
alkyl halide

monitoring the bleaching of the heme absorption at 568 or 556 nm. At these wavelengths the absorption of $Fe^{II}Mb$ is greater than the absorption of $Fe^{III}Mb$.

Using this technique we have measured the Fe^{II} to Ru^{III} ET kinetics in both the a_5Ru(His-48)MbFe and the a_4pyRu(His-48)MbFe donor/acceptor systems. The changes in the heme absorption of a_5Ru- and $a_4pyRuMbFe$ systems upon flash photolysis are shown in Figures 45 and 47, respectively. After the microsecond flash, an initial rapid oxidation of the heme is observed due to direct bimolecular oxidation of the heme by $Ru(bpy)_3^{2+*}$; this is followed by a slower further oxidation that is attributed to intramolecular ET: $a_4LRu^{III}MbFe^{II} \rightarrow a_4LRu^{II}MbFe^{III}$, where L=a or py. A first-order plot of the experimental data gave a straight line with an observed rate constant of 0.058±0.004 s^{-1} for $a_5RuMbFe$ and 2.5±0.5 s^{-1} for $a_4pyRuMbFe$, Figures 46 and 48. The kinetics were found to be independent of concentration, indicating that bimolecular ET contributions are not significant.

The observed rate of ET for a_5Ru(His-48)MbFe, $Fe^{II} \rightarrow Ru^{III}$, is within experimental error of the ET rate previously determined for the reverse process; k_{obs} ($Ru^{II} \rightarrow Fe^{III}$) is 0.060±0.004 s^{-1}. Crutchley et al. measured Ru^{II} to Fe^{III} ET using a similar flash photolysis technique.[36] In this system, the mixed-valence Ru^{II}-PFe^{III} was produced upon flash photolysis of the fully-oxidized protein ($Ru^{III}PFe^{III}$) and $Ru(bpy)_3^{2+}$. $Ru^{II}PFe^{III}$ and $Ru(bpy)_3^{3+}$ were produced by oxidative quenching (rapid bimolecular ET from $Ru(bpy)_3^{2+*}$ to the protein), EDTA scavenged the $Ru(bpy)_3^{3+}$ and intramolecular ET was

Figure 45. Change in optical density of the heme absorption at 556 nm following flash photolysis of a μ=0.1 M, pH 7, NaPi solution containing a_5Ru^{II}(His-48)$MbFe^{II}$ (5 μM), $Ru(bpy)_3^{2+}$ (65 μM), $Ni^{II}Me_6$ane (5 mM) and RBr (20 mM).

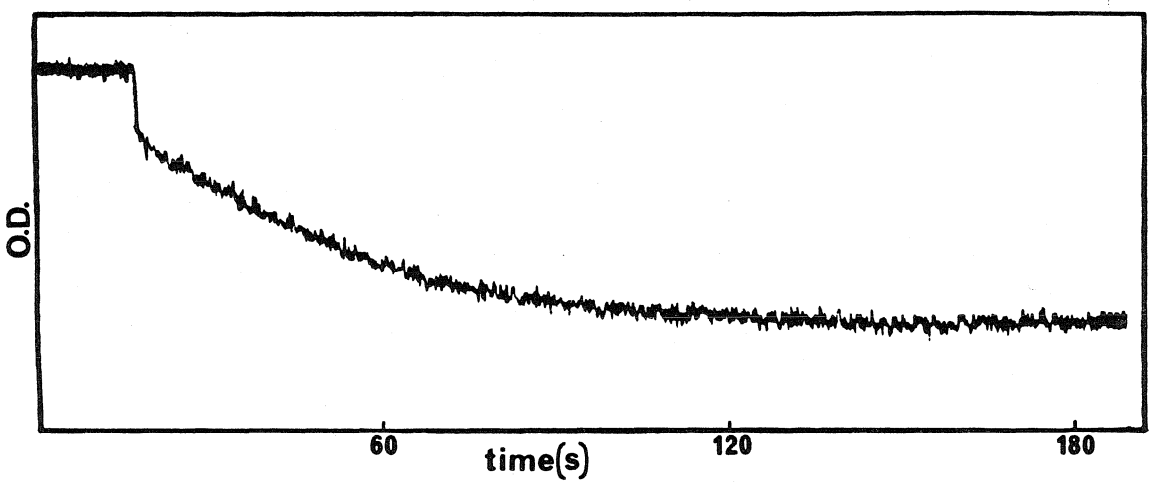
O.D.
60
120
180
time(s)

Figure 46. First-order plot of the experimental data from Figure 45.

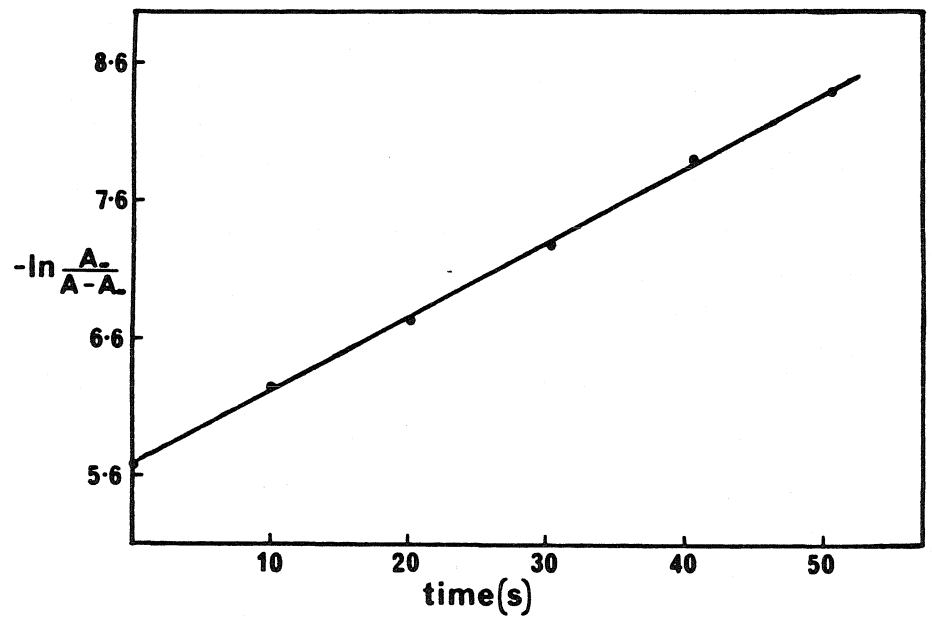
8·6
7·6
6·6
5·6
$-\ln \frac{A_\infty}{A-A_\infty}$
10
20
30
40
50
time(s)

Figure 47. Change in optical density of the heme absorption at 568 nm following flash photolysis of a μ=0.1 M, pH 7, NaPi solution containing $a_4pyRu^{II}(His\text{-}48)MbFe^{II}$ (5 μM), $Ru(bpy)_3^{2+}$ (65 μM), $Ni^{II}Me_6ane$ (5 mM) and RBr (20 mM).

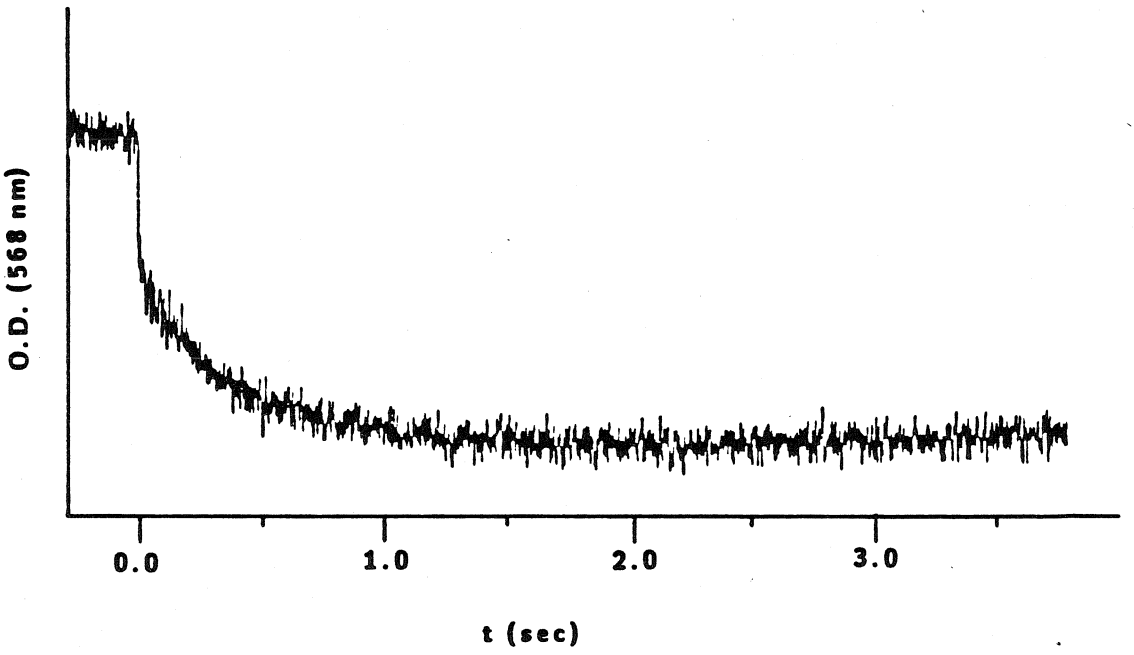
O.D. (568 nm)
0.0
1.0
2.0
3.0
t (sec)

Figure 48. First-order plot of the experimental data from Figure 47.

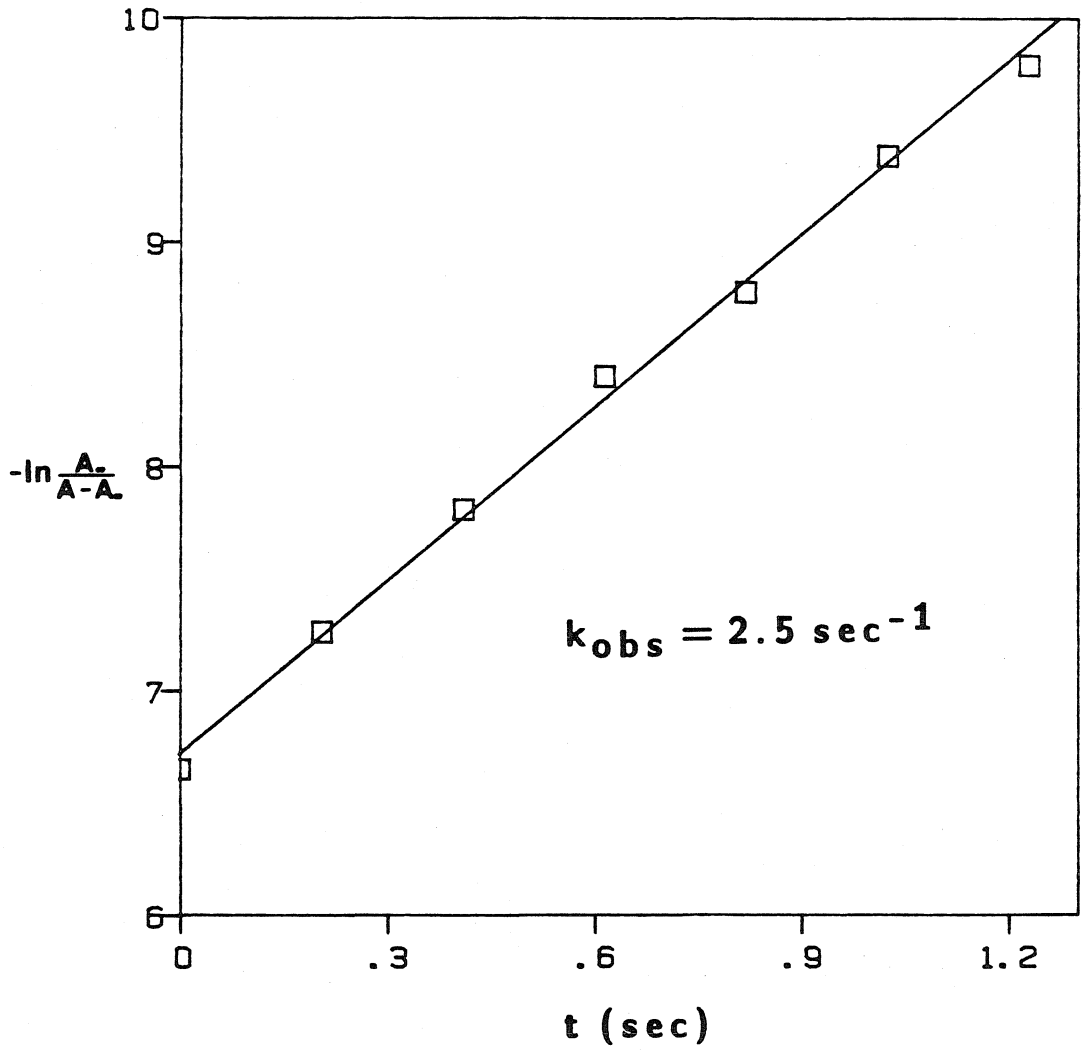
10
9
8
7
6
$-\ln \frac{A_\infty}{A-A_\infty}$
0
.3
.6
.9
1.2
t (sec)
$k_{obs} = 2.5\ sec^{-1}$

measured spectrophotometrically by monitoring the reduction of the heme.

A reversible unimolecular process should yield an observed rate constant that is equal to the sum of the forward (k_f) and reverse (k_r) rates. This is expected for the ET reaction in a_5Ru(His-48)MbFe where ΔE^o=20mV:

$$a_5Ru^{III}(His\text{-}48)MbFe^{II} \rightarrow a_5Ru^{II}(His\text{-}48)MbFe^{III} \quad k_{obs}=k_f + k_r$$

The observation that the rate constant (k_{obs}) is independent of the initial [$Ru^{III}PFe^{II}$]:[$Ru^{II}PFe^{III}$] ratio demonstrates that long-range ET in a_5Ru(His-48)MbFe is reversible. At 25°C the forward and reverse ET rates are calculated to be 0.04 and 0.02 s^{-1}, respectively.

The driving force, ΔE^o, for $Fe^{II} \rightarrow Ru^{III}$ ET in $a_4$pyRu(His-48)MbFe is 275 mV and therefore $k_f >> k_r$ and $k_f \cong k_{obs}$. With this 255 mV increase in driving force, the $Fe^{II} \rightarrow Ru^{III}$ ET rate increases from 0.04 to 2.5 s^{-1}. This change in ET rate with reaction free energy indicates that the ET rates in these systems are not controlled by conformational gating. In contrast to the reversible ET in Mb, Isied et al.[84] have reported directional ET in ruthenium-labelled cytochrome c derivatives. They found that ET occurs from the surface Ru to the heme iron but not in the reverse direction. Two systems were studied, a_5Ru(His-33)cyt c and $a_4$isnRu(His-33)cyt c, that had approximately the same ET driving force, 0.11 and 0.18 V, respectively. In these two systems the potentials suggest that ET should occur from Ru^{II} to Fe^{III} in the a_5Rucyt c derivative and from Fe^{II} to Ru^{III} in $a_4$isnRucyt c. The ET rate was measured to be 50 s^{-1}

in $a_4$isnRucyt c, but ET from Fe^{II} to Ru^{III} in $a_4$isnRucyt c was found to be $>10^5$ times slower.

It has been suggested that the directionality results from a conformational change in the protein upon reduction that prohibits ET in the Fe→Ru direction. Recently, however, Meade et al.[75] have prepared a series of a_4LRu-modified Fe and Zn cyt c derivatives (L=NH_3, pyridine or isonicotinamide) that range in driving force from ~0 to 1.0 V. They have found a dependence on reaction free energy that yields ET rates from 2 to 10^6 s^{-1}. They have also measured a Fe^{II}→Ru^{III} ET rate in $a_4$isnRucyt c that is ~10 s^{-1}. These results are consistent with our findings on Ru-labelled Mb.

Our ET rate data for a_5Ru- and $a_4$isnRu(His-48)MbFe can also be used to evaluate the reorganization energy, λ. Using Marcus theory, the reorganization energy of a donor/acceptor system can be determined if the ET rate dependence on driving force is known (equation 3). The free energy at which the ET rate is a maximum, i.e., the peak of a Marcus free energy curve, is equal to λ. Figure 49 shows the rate data for the two RuMbFe systems and two plotted Marcus free energy curves ($\ln k_{ET}$ vs. $-\Delta G^o$) corresponding to λ values of 1 and 2 eV. The two data points can be fit equally well by the curves for λ=1 and 2 eV. It is clear that ET rates at much higher driving forces must be obtained. For example, at a driving force of ~1 eV the ET rate predicted for a λ=2eV system is much greater than the rate predicted for a λ=1eV system. By synthesizing high driving force systems in which the electronic coupling and reorganization energy are held constant, a better estimate of λ can be made.

Figure 49. Lnk vs. $-\Delta G^{o}$ plot of the two experimental RuMbFe ET rates and two calculated Marcus curves for λ=1 eV and λ=2 eV.

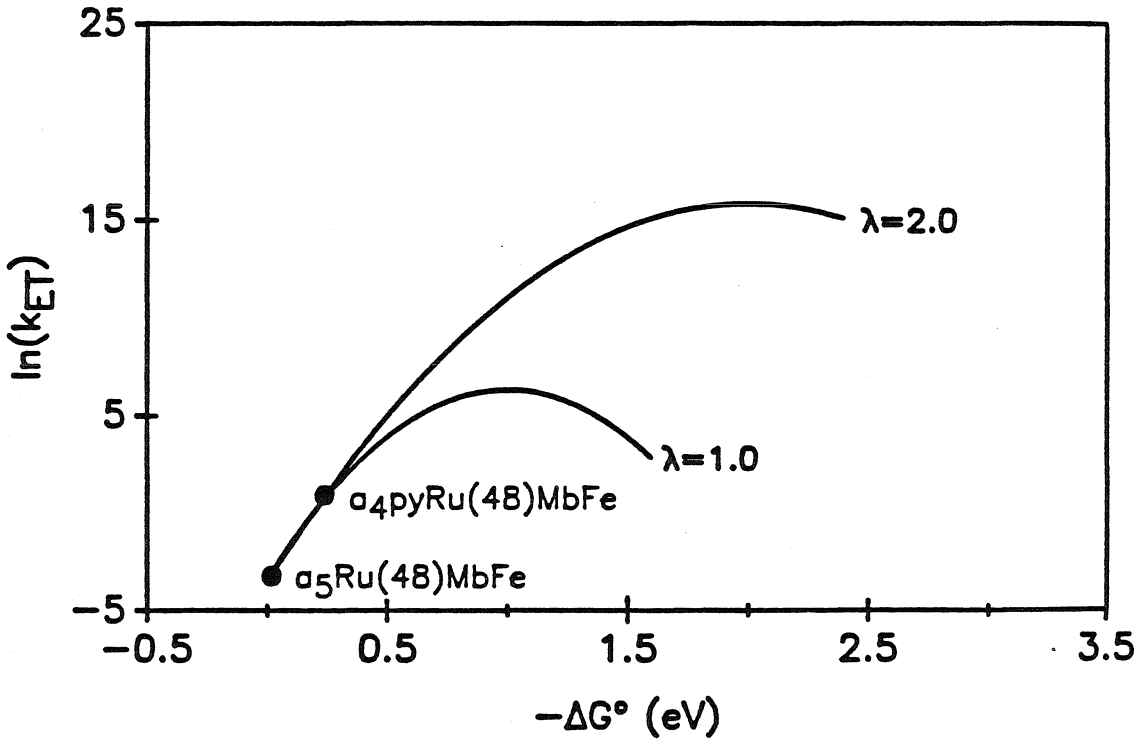
25
15
5
−5
ln(kET)
λ=2.0
λ=1.0
a4pyRu(48)MbFe
a5Ru(48)MbFe
−0.5
0.5
1.5
2.5
3.5
−ΔG° (eV)

ET studies in Donor/Acceptor Systems with Large Reaction Free Energies

The goal of our next study was to prepare high driving force systems; i.e., we want to increase the reaction free energy while keeping other factors constant. To try to maintain the same distance and approximately the same reorganization energy as in Ru-MbFe, the new derivatives were prepared by removing the heme in the Ru(His-48)Mb and replacing it with a photoactive porphyrin, either Pd(mesoporphyrin IX) (PdP) or Zn(mesoporphyrin IX) (ZnP). Both PdP and ZnP have long-lived, highly reducing excited states and are therefore suitable for ET studies at high driving forces. With this approach the overall ET driving force is increased significantly and the same well-defined ΔG^o step between the Ru-labelled Mb derivatives is maintained.

Reduction Potentials of the Photoactive Porphyrins

The excited-state reduction potentials of ZnP and PdP cannot be measured directly. They can be estimated, however, from the porphyrin oxidation potential and the triplet energy. The excited-state potential of a metalloporphyrin (MP) is equal to the difference between the ground state MP oxidation potential ($MP^{o/+}$) and the triplet-state energy. The triplet energy has been determined from emission measurements of Pd and Zn-substituted Mb at low temperatures. The values reported are 1.90 and 1.78 eV for Pd and ZnMb, respectively.[76,85] The ground state oxidation potentials for the Pd and ZnMb were estimated from measurements of different Pd

and Zn porphyrins in several organic solvents. Therefore, there is some uncertainty associated with this estimate; $E^{o}(ZnP^{+/o})$ = 0.98(10) V and $E^{o}(PdP^{+/o})$ = 1.26(10) V. The excited-state reduction potentials used for PdMb and ZnMb are 0.64 (10) and 0.80 (10) V vs. NHE, respectively. Similar reduction potentials to that calculated for ZnMb have been reported for Zn-cyt c[7,41] and Zn-substituted hemoglobin.[8] The reduction potentials for all Mb donors and acceptor are listed in Table III.

ET in Ru-Modified PdMb Systems

In the MbPd systems, a_5Ru(His-48)MbPd and $a_4$pyRu(His-48)MbPd, the ET rates were determined directly by monitoring the quenching of the PdP emission as shown in scheme II:

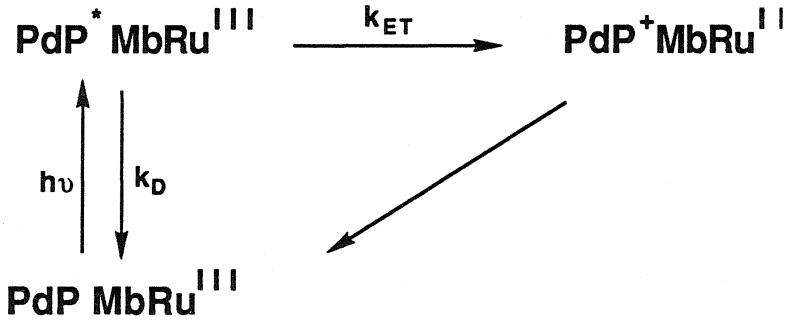

Scheme II

Electronically excited MbPd (MbPd*) was produced via pulsed laser excitation and the emission intensity was monitored at 670 nm. After excitation electron transfer occurs from PdP* to the surface bound Ru. Although other deactivation pathways such as energy transfer exist, they have been ruled out because they are energetically unfavorable.[41] Kinetic analysis of the scheme above yields an observed first-order rate constant for the decay of MbPd*

Table III. Reduction potentials for the redox sites in ruthenium-labelled myoglobin.

Redox Couple	E^o (V vs. NHE)
$a_5Ru^{III/II}$-Mb	0.085[36]
$a_4pyRu^{III/II}$-Mb	0.340
$a_4isnRu^{III/II}$-Mb	0.420
$Fe^{III/II}$-Mb	0.065[36]
$ZnP^{+/o}$-Mb	0.98(10)[76,77]
$ZnP^{+/*}$-Mb	-0.8(10)[76,77]
$PdP^{+/*}$-Mb	-0.64(10)[33]

that is equal to k_d+k_{ET}.

The decay in emission intensity for native PdMb is shown in Figure 50. The decay follows first-order kinetics with a k_D of $1.0(5)x10^3$ s^{-1}. Both the a_5Ru^{III}- and a_4pyRu^{III}(His-48)-modified MbPd derivatives exhibit enhanced emission quenching. This is expected for ET from the PdP excited state to the surface Ru since the driving forces for $Ru^{III}(48)MbPd^* \rightarrow Ru^{II}(48)MbPd^+$ are 0.72(10) and 0.98(10) V for a_5Ru- and a_4pyRu derivatives, respectively. The quenching of a_5Ru(His-48)MbPd* closely follows first-order kinetics with an observed rate constant equal to $1.1(5)x10^4$ s^{-1} (Figure 51). Since $k_{obs}=k_{ET} + k_D$, the ET rate constant is $9.1(5)x10^3$ s^{-1}. The ET rate measured by transient absorption techniques at 390 nm was identical.

The kinetics for a_4pyRu(His-48)MbPd* were biphasic and an ET rate of $9.0(5)x10^4$ s^{-1} was determined for the major (fast) component, Figure 52. The minor (slow) component is probably due to residual native PdMb. The contribution of native PdMb is not surprising since the a_4pyRu- moiety tends to fall off more rapidly than a_5Ru. The preparation time for the PdMb derivatives is ~48 h and they cannot be further purified via cation-exchange chromatography because these derivatives are stable only at low ionic strength. At high ionic strength and on cation-exchange resin (CM52, Mono S) the Pd porphyrin is removed from the protein. The Pd porphyrin is expected to be more weakly bound in the heme pocket since it is unlikely that it will coordinate to the axial ligand. The a_4pyRu(His-48)MbPd was used immediately after preparation.

Figure 50. Time-resolved decay of the emission intensity for native MbPd monitored at 670 nm. k_D=1000 s^{-1}.

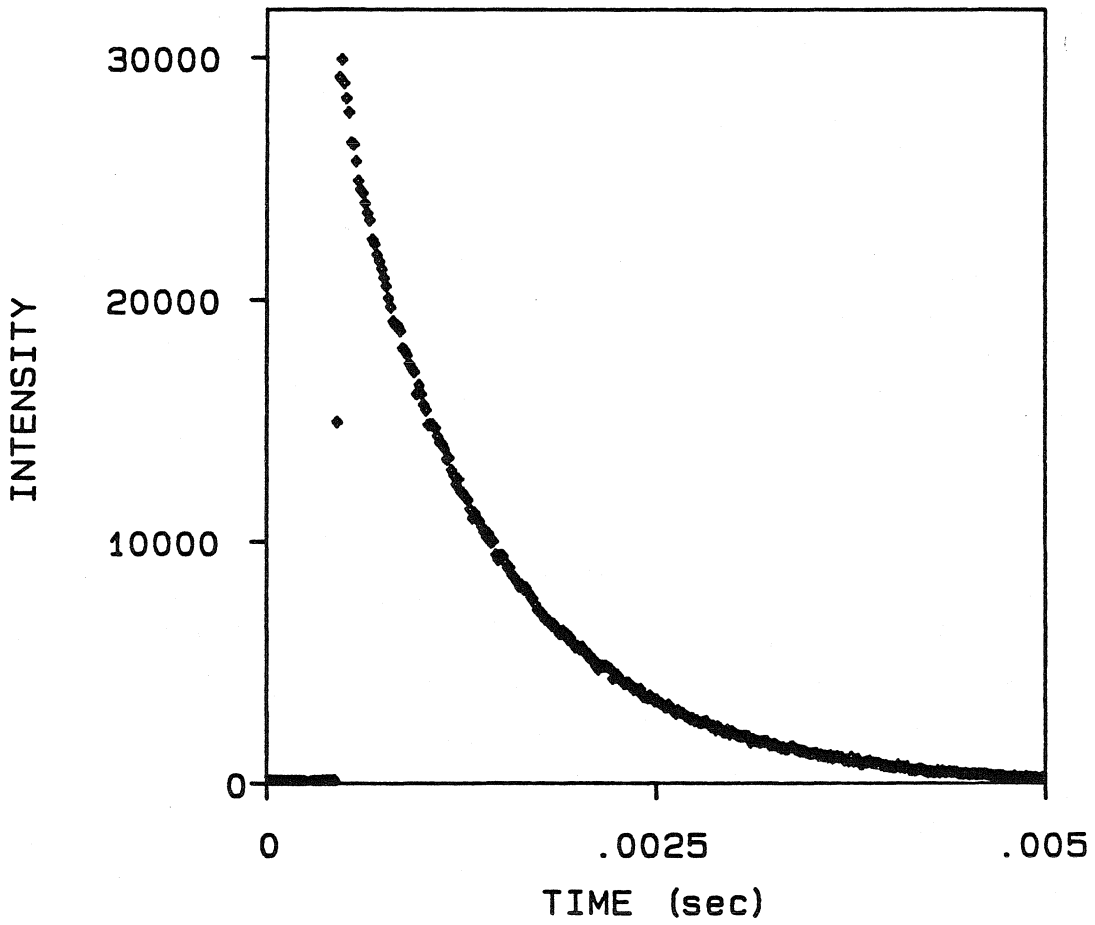
30000
20000
10000
0
INTENSITY
0
.0025
.005
TIME (sec)

Figure 51. Time-resolved decay of the emission intensity for a_5Ru(His-48)MbPd monitored at 670 nm.

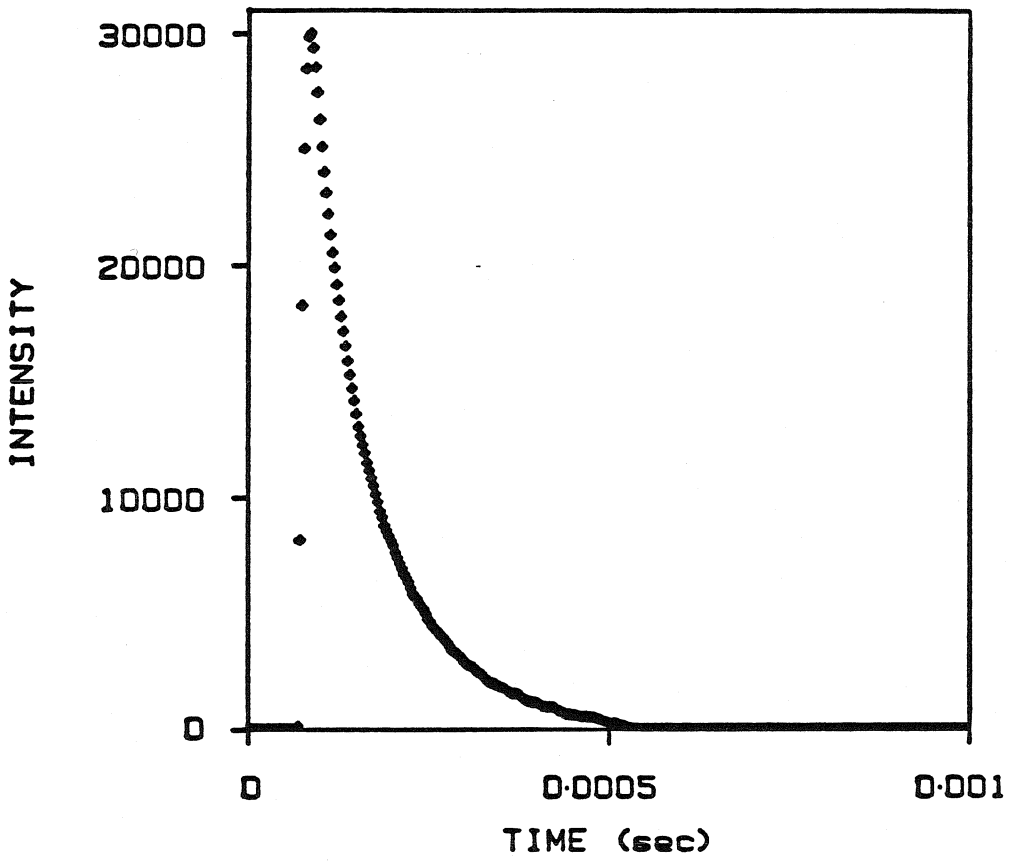
30000
20000
10000
0
INTENSITY
0
0·0005
0·001
TIME (sec)

Figure 52. Time-resolved decay of the emission intensity for $a_4$pyRu(His-48)MbPd monitored at 670 nm.

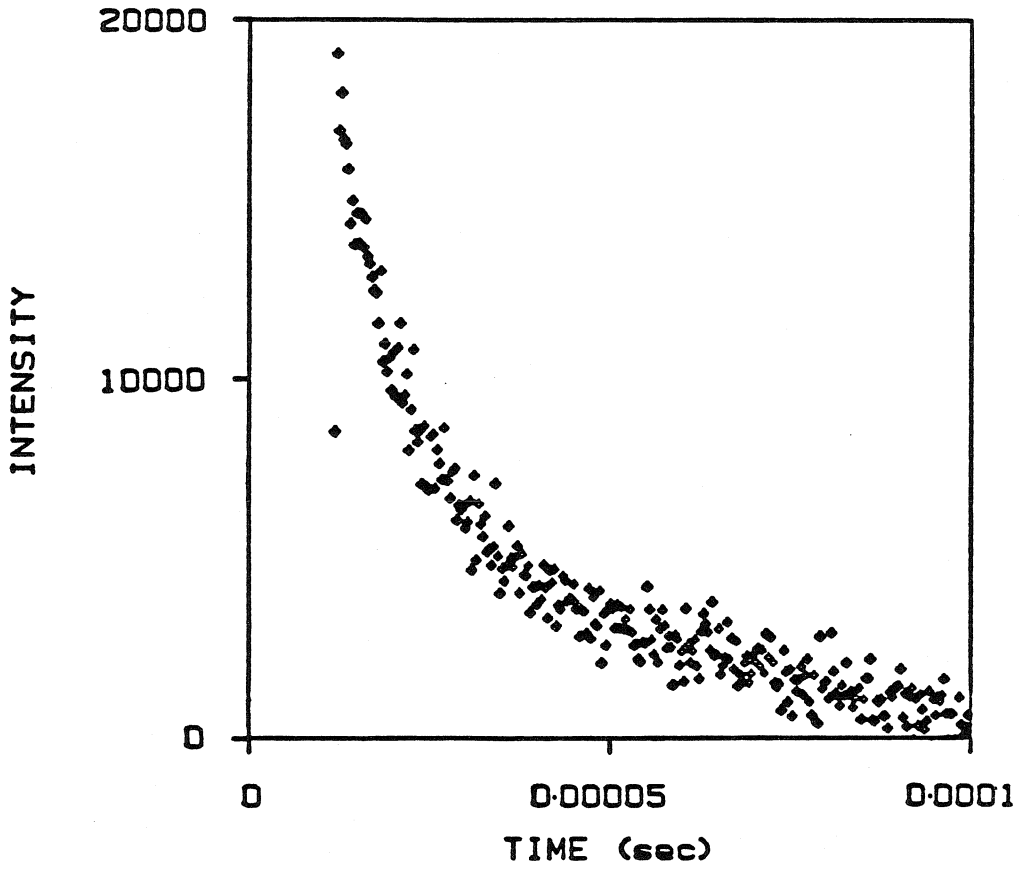
20000
10000
0
INTENSITY
0
0·00005
0·0001
TIME (sec)

ET in Ru-Modified ZnMb Derivatives

ZnMb derivatives with a_4LRu attached at histidine 48, (L=a, py, or isonicotinamide) were also prepared in order to increase the range of reaction free energy available. The excited-state Zn potential is ~150 mV greater than the PdP potential. The ZnMb species are also more stable and can be purified after Zn insertion via FPLC cation-exchange chromatography to yield very pure samples. One disadvantage of the ZnMb versus the PdMb is that ZnMb emits very weakly at room temperature and therefore the ET rate cannot be measured by emission quenching. The ET rates in the ZnMb derivatives were measured by transient spectroscopy.

The ET scheme for the RuMbZn systems is similar to that described previously for RuMbPd.

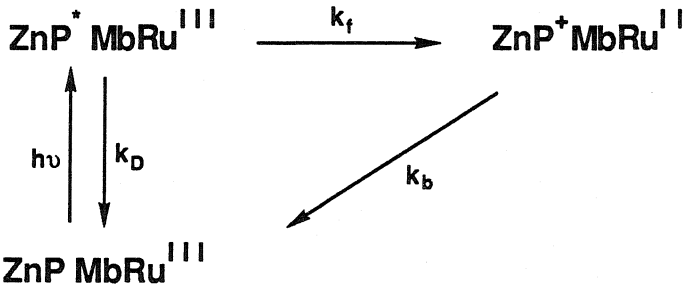

Scheme III

Upon excitation, the excited-state ZnP (ZnP^*) is formed, and then it decays via nonradiative decay and ET pathways. The ZnP radical cation (ZnP^+), the product of the first ET step, is a strong oxidant ($E^o \cong 1$ eV) and back electron transfer occurs rapidly from the reduced surface Ru to ZnP^+. As with the PdMb species, energy transfer is expected to be energetically unfavorable.[41]

The change in absorption after laser excitation was monitored both at 450 and at 670 nm. At 450 nm the change in absorbance (ΔA) is due mainly to ZnP^* and at 670 nm the ΔA due to ZnP^+ is observed.[41] By monitoring the absorbance due to the radical cation (i.e., watching it grow in and disappear), both an excited-state forward rate (k_f) and a ground-state reverse ET rate (k_b) have been measured.

Kinetic analysis of a system such as that in Scheme III has been previously solved and rate expressions have been derived for the excited-state ZnP and ZnP radical cation.[54]

a) $[RuMbZnP^*]_t = A_o exp[-(k_d+k_f)t]$

b) $[RuMbZnP^+]_t = A_o K\{exp[-(k_d+k_f)t] - exp(-k_b t)\}$

A_o= $[RuMbZnP^*]$ at t=0, and K is a preexponential term equal to $k_f/(k_b-k_f-k_d)$.

The second rate expression consists of two first-order terms; one contains the intrinsic decay and the forward rate constant, k_D+k_f, and the other contains the reverse ET rate constant, k_b. The experimental measurements that have monitored ΔA at 450 nm should be first order with the observed rate constant equal to the sum of the intrinsic decay and the forward ET rate constant. However, it has been observed that the radical cation contributes about 10% of the signal, so generally the observed decays are second order. By monitoring at 670 nm, the kinetics should be biexponential and will yield both the forward and the reverse ET rate constants.

The intrinsic decay measured in native ZnMb, k_D = 40 s^{-1}, was in agreement with that reported previously.[35] k_D is independent of concentration from 5-50 μM. The $ZnP^* \rightarrow Ru^{III}$ ET rate for a_5Ru(His-48)MbZn has also been measured previously by transient absorption to be 7.0(8)x10^4 s^{-1}. The exponential increase measured at 414 nm was due to ground-state ZnP. The observed decay was first order with $k_{obs}=k_f$ since $k_b >> k_f$.

Our measurement of the triplet-state decay for a_5Ru(His-48)MbZn at 450 nm yielded a first-order rate constant that was slightly higher; k_f = 8.7(5)x10^4 s^{-1} (Figure 53a). In order to measure the reverse reaction, we also probed the transient kinetics at 670 nm where the absorbance of ZnP^+ predominates, Figure 53b. The absorption at 670 nm grows in and then decays with a first-order rate constant equal to that measured at 450 nm. The curve fit with a biexponential functon when k_2 is fixed at 8.7x10^4 yields k_1=1.5x10^5 s^{-1}. k_1 corresponds to the thermal reverse ET step, $Ru^{II}MbZnP^+ \rightarrow Ru^{III}MbZnP$. This kinetic behavior is consistent with an A→B→C reaction series in which the rate constant for the B to C step is greater than the rate constant for the A to B step. [86]

The driving force for the forward ET process is increased by 275 mV from a_5RuMbZn when $a_4$pyRu is attached at histidine 48; therefore, k_f is expected to increase. Figure 54 shows the decay curves after laser excitation of $a_4$pyRu(His-48)MbZn monitored at both 450 and 670 nm. Biphasic behavior is observed in both of the curves. Monitoring the quenching of ZnP^* (450 nm, Figure 54a)

Figure 53. Transient kinetics of a_5Ru(His-48)MbZn. A) ΔA monitored at 450 nm; smooth curve through the data is a single exponential decay function with a rate constant of 8.7×10^4 s^{-1}. B) ΔA monitored at 670 nm; smooth curve is a biexponential function with rate constants of 1.5×10^5 and 8.7×10^4 s^{-1}.

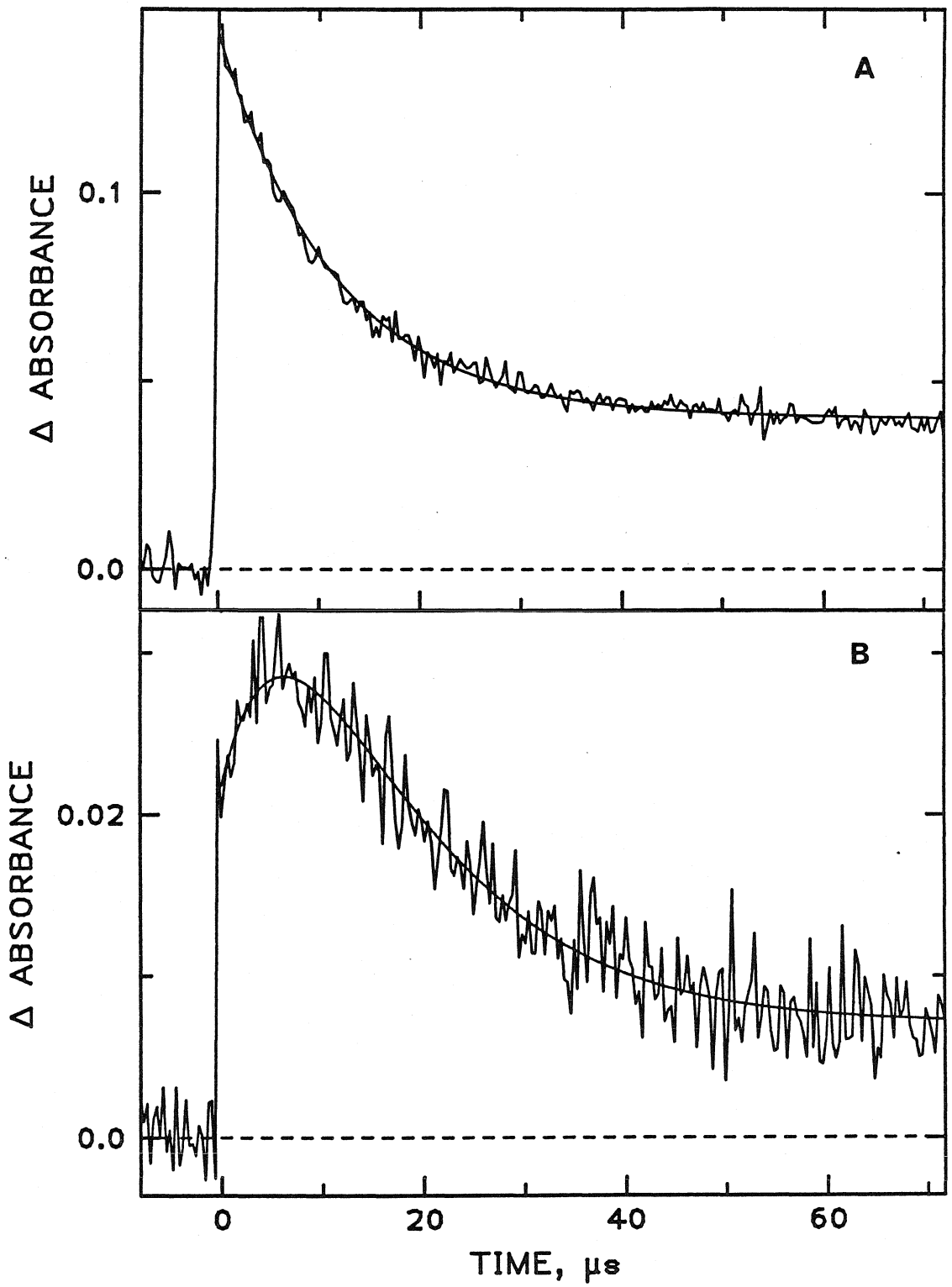
A
B
Δ ABSORBANCE
0.1
0.0
Δ ABSORBANCE
0.02
0.0
0
20
40
60
TIME, μs

Figure 54. Transient kinetics of $a_4$pyRu(His-48)MbZn. A) ΔA monitored at 450 nm; smooth curve through the data is a biexponential decay function with a rate constants of 2.0×10^5 and 2.1×10^4 s^{-1}. B) ΔA monitored at 670 nm; smooth curve is a biexponential function with rate constants of 2.0×10^5 and 2.6×10^4 s^{-1}.

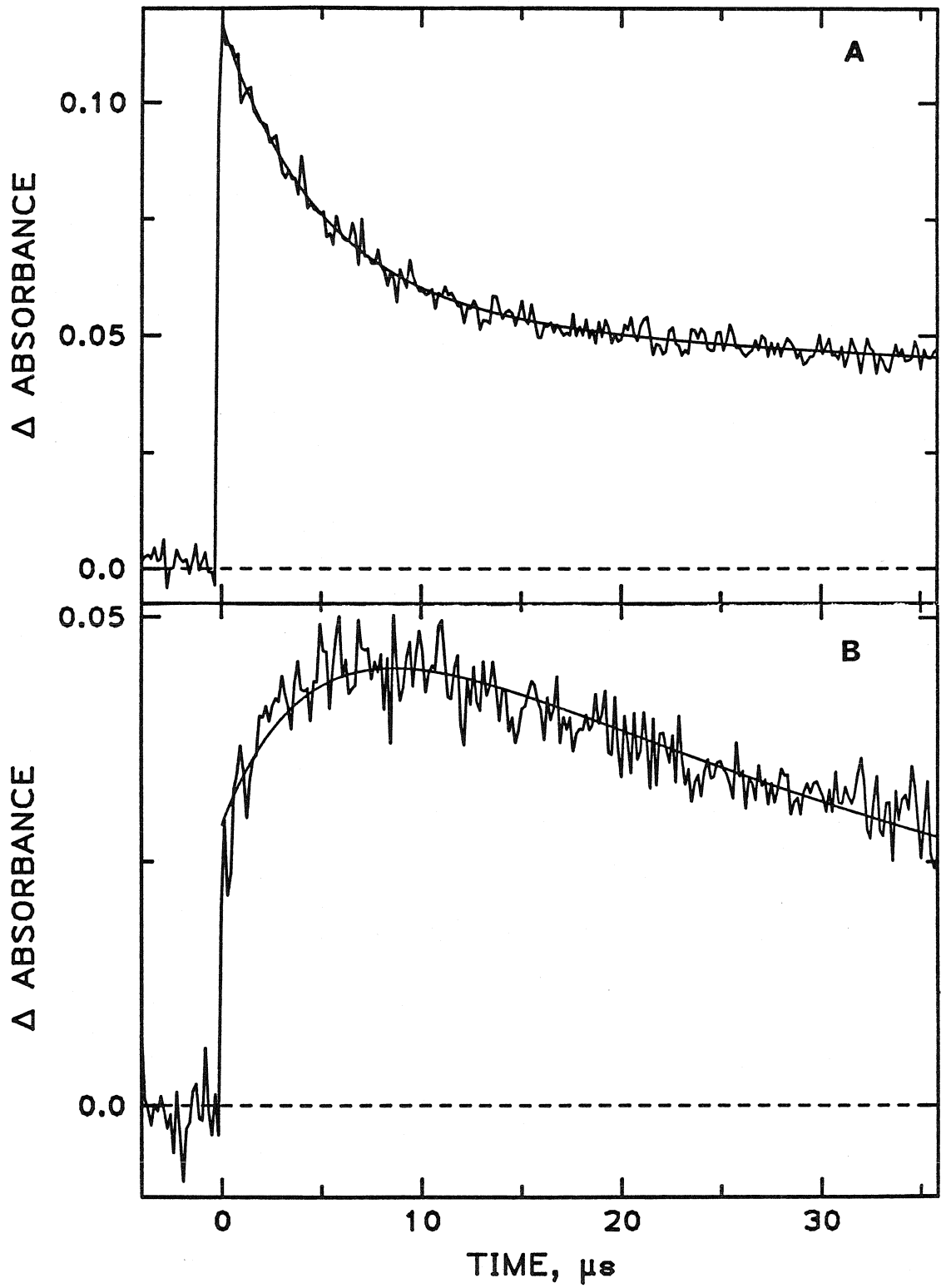
A
B
0.10
0.05
0.0
0.05
0.0
Δ ABSORBANCE
Δ ABSORBANCE
0
10
20
30
TIME, μs

yields rate constants $k_1=2.0x10^5$ and $k_2=2.1x10^4$ s^{-1}, corresponding to the forward and reverse ET processes. The curve produced from monitoring the change in absorbance at 670 nm once again shows an increase and then a decrease due to the ZnP radical cation. It can be fit with a five parameter biexponential routine (k_1 fixed at $2x10^5$) to give k_2 equal to $2.6x10^4$ s^{-1} (Figure 54b). The average values of k_f and k_b from several different experiments are equal to $2.0(5)x10^5$ and $2.0(5)x10^4$ s^{-1}.

The ET rates have also been measured for $a_4$isnRu(His-48)MbZn. From $a_4$pyRuMb to $a_4$isnRuMb, the driving force of the forward ET process increases by 80 mV. The decay curve monitored at 450 nm shows similar behavior to that of $a_4$pyRu(His-48)MbZn. A biexponential fit yielded $k_f=2.9x10^5$ and $k_b=1.4x10^4$ s^{-1} (Figure 55). It was found that the radical cation could be observed at 425 nm as well as at 670 nm. Figure 56 shows the decay curves at 425 nm.

The kinetic results and driving forces for all the Mb donor/acceptor systems are shown in Table IV. The driving force varies from almost zero (20 mV) to greater than 1 V (1.22 V) with a maximum ET rate of $3x10^5$ s^{-1}.

Reorganization Energy in Ruthenium-Labelled Myoglobin

Using the following Marcus expression for intramolecular electron transfer as described in chapter 1,[5]

7) $k_{ET} = \nu_n \kappa_e^o \exp(-\beta(d-d_o))\exp-[(G+\lambda)^2/4\lambda RT]$,

we have fit the rate and driving-force data to determine a value for the reorganization energy, λ.

Figure 55. Transient kinetics of $a_4$isnRu(His-48)MbZn monitored at 450 nm. The smooth curve is a biexponential function with rate constants of 2.9×10^5 and 1.4×10^4 s^{-1}.

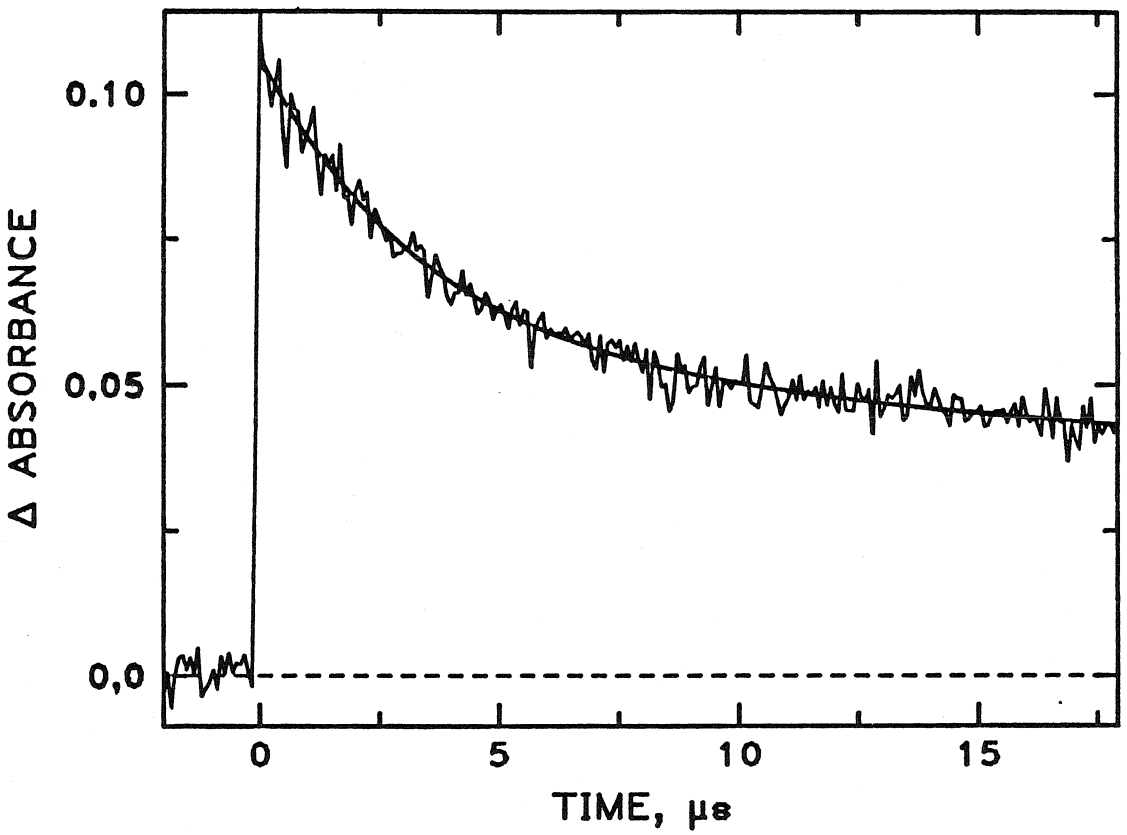
0.10
0,05
0,0
Δ ABSORBANCE
0
5
10
15
TIME, μs

Figure 56. Transient kinetics of $a_4$isnRu(His-48)MbZn monitored at 425 nm. A) Smooth curve through the data is a biexponential decay function with rate constants of $3x10^5$ and $1.4x10^4$ s^{-1}. B) Smooth curve is a biexponential function with rate constants of $2.95x10^5$ and $1.4x10^4$ s^{-1}.

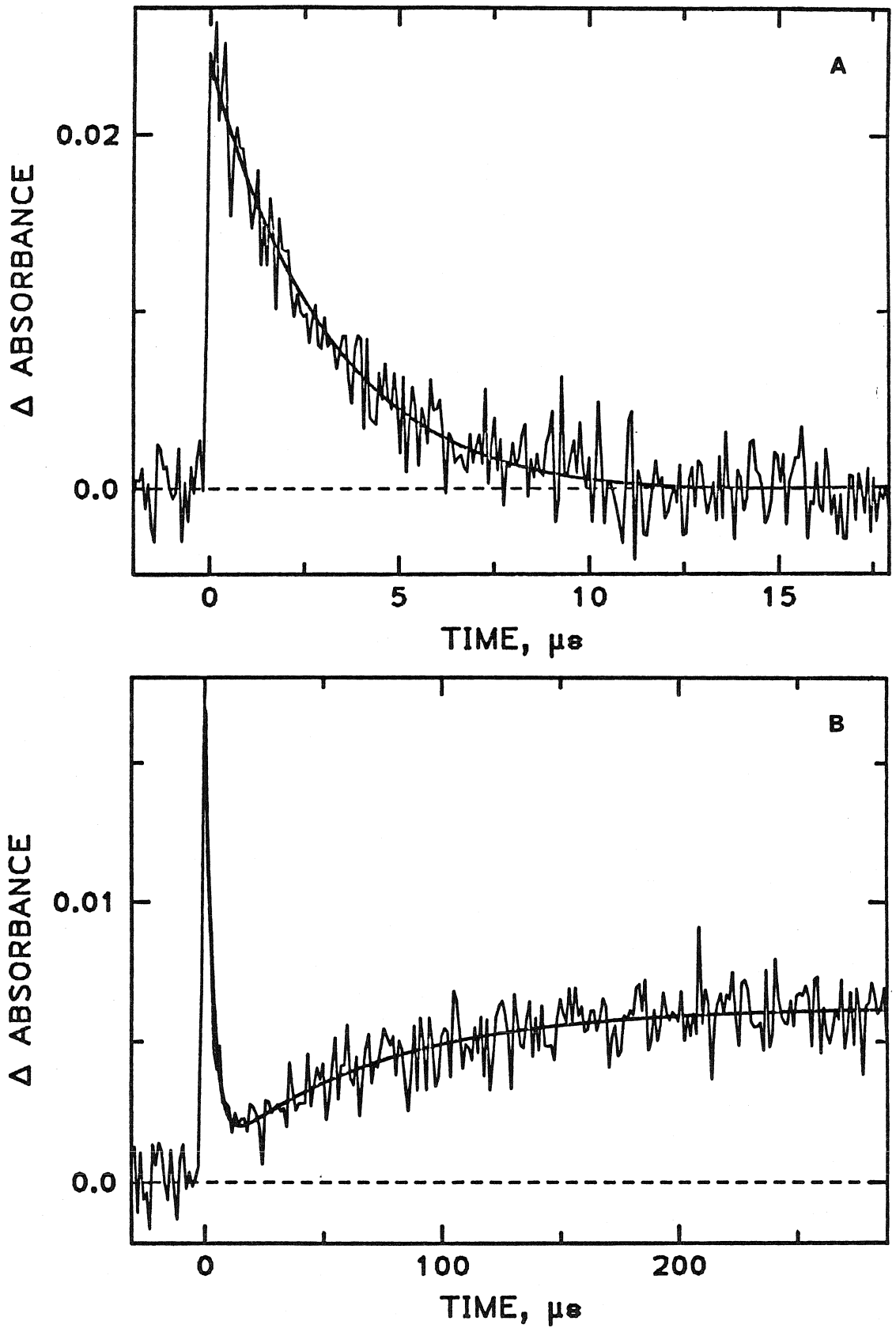
A
0.02
0.0
Δ ABSORBANCE
0
5
10
15
TIME, μs
B
0.01
0.0
Δ ABSORBANCE
0
100
200
TIME, μs

Table IV. ET rates in ruthenium-modified Mb(histidine 48).

Donor	Acceptor	ΔE^o (V)	k_{ET} (s^{-1})
$Fe^{II}P$	a_5Ru^{III}	0.020	0.040(5)
$Fe^{II}P$	a_4pyRu^{III}	0.275	2.5(5)
PdP^*	a_5Ru^{III}	0.725	$9.1(5)\times10^3$
PdP^*	a_4pyRu^{III}	0.98	$9.0(5)\times10^4$
ZnP^*	a_5Ru^{III}	0.88	$7.0(5)\times10^4$
ZnP^*	a_4pyRu^{III}	1.14	$2.0(5)\times10^5$
ZnP^*	a_4isnRu^{III}	1.22	$2.9(5)\times10^5$
a_5Ru^{II}	ZnP+	0.90	$1.5(5)\times10^5$
a_4pyRu^{II}	ZnP+	0.64	$2.0(5)\times10^4$
a_4isnRu^{II}	ZnP+	0.56	$1.4(5)\times10^4$

The distance decay factor, β, has been determined previously for Mb to be 0.9 $Å^{-1}$. The donor-acceptor distance, d, in Ru(His-48)Mb has also been determined using computer modeling studies to be 13 Å.[35] The distance at which adiabatic electron transfer is normally expected to occur, d_o, is generally taken to be 3 Å (in this case, κ_e^o=1). The nuclear frequency factor ν_n is usually assumed to be 10^{13}. Using these standard parameters, free energy curves ($\ln k_{ET}$ vs $-\Delta G^o$) have been calculated and drawn for λ=0.5, 1.5 and 2.5 eV, Figure 57. As expected from equation 7, the curves rise as the free-energy change increases, reach a maximum when $-\Delta G^o = \lambda$, and then decrease. The rate data are fit best with the Marcus curve in which λ=2.5 eV. The rates are too slow to be fit with a λ=0.5 or 1.5 eV curve. However, the rates appear to start leveling off around 1 eV, and the highest three points lie below the λ=2.5 curve.

If the electronic factor, κ_e^o, is allowed to vary, a better fit to the data is obtained. Although κ_e^o is usually assumed to be 1 (i.e., adiabatic reaction at $d=d_o$) a value less than one may be appropriate for RuMb systems. A value of κ_e^o that is less than one suggests that at $d=d_o$ the reaction is not adiabatic.

Using a two-parameter nonlinear regression program allowing λ and $\nu_n\kappa_e^o$ to vary, and keeping the other variables constant as described above, the rate data can be fit to equation 7 to yield λ=1.75 eV and $\nu_n\kappa_e^o=3\times10^{10}$ s^{-1}, Figure 58. This figure consists of a plot of $\ln k_{ET}$ vs. reaction free energy for the rate data from Table IV and the calculated Marcus curve. This value for $\nu_n\kappa_e^o$ is considerably smaller than the value commonly assumed. The data in Figure 58 fit

Figure 57. Plot of lnk_{ET} vs. $-\Delta G^{o}$ for the Ru-Mb ET reactions. (●) Fe^{II} to Ru^{III} ET. (◆) PdP^{*} to Ru^{III} ET. (■) ZnP^{*} to Ru^{III} ET. (□) Ru^{II} to ZnP^{+} ET. Included in the figure are theoretical Marcus curves (equation 7) with d=13 Å, β=0.9 $Å^{-1}$, $\nu_n=10^{13}$ s^{-1}, κ_e^{o}=1 and A) λ=0.5 eV B) λ=1.5 eV C) λ=2.5 eV.

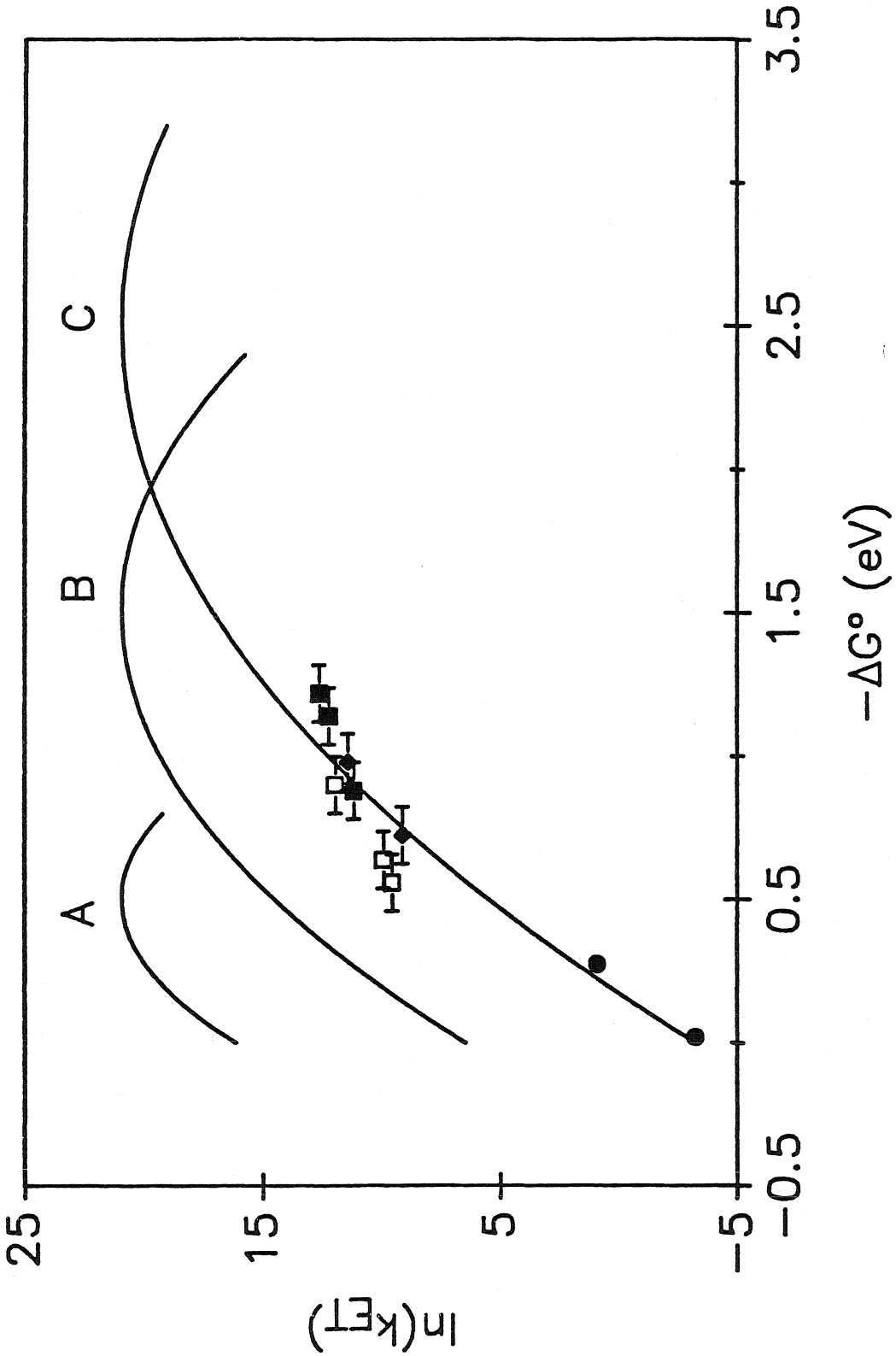
A
B
C
25
15
5
−5
ln(kET)
−0.5
0.5
1.5
2.5
3.5
−ΔG° (eV)

Figure 58. Plot of $\ln k_{ET}$ vs. $-\Delta G^{o}$ for the Ru-Mb ET reactions. Symbols for this and all subsequent plots are the same as in Figure 57. d and β are fixed at 13 Å and 0.9 $Å^{-1}$, respectively, for all plots. The solid line is the best fit to equation 7, λ=1.75 eV and $\nu_n \kappa_e^{o}=3\times10^{10}$ s^{-1}.

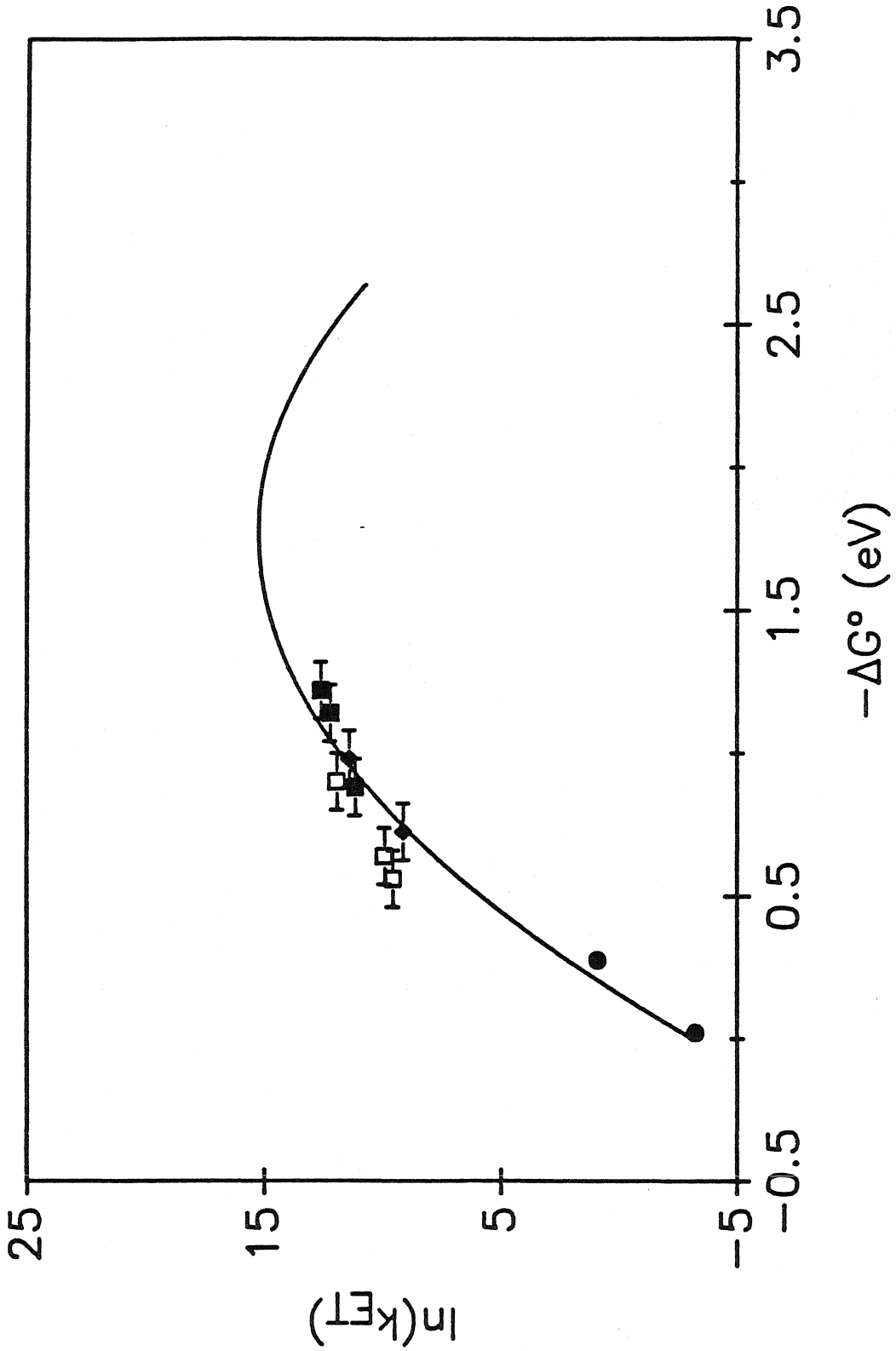
ln(k_ET)
25
15
5
−5
−0.5
0.5
1.5
2.5
3.5
−ΔG° (eV)

fairly well to the curve; however, there are some distinctive deviations. The three ET rates for the reverse process ($Ru^{II} \rightarrow ZnP^+$) lie above the calculated curve, indicating that there may be something systematically different about this process. It is possible that the electronic coupling between the Ru^{II}-donor and the ZnP^+-acceptor is stronger than the coupling between the ZnP^*-donor and Ru^{III}-acceptor. Several theories suggest that β depends on the absolute redox energy of the transferring electron.[87] The stronger coupling, manifested in a lower value for β, would give a faster rate than expected at a given ΔG^o and distance. Faster rates for the reverse ET reaction (ZnP^+ charge recombination) have been reported for other systems including Ru-cyt c-Zn,[75] cyt c/cyt b_5,[29] ZnHb/cyt b_5,[30] Zn(ccp)/ cyt c,[88] and ccp/Zn cyt c.[89] The Mb rate data have been fit without including the back rates (Figure 59) and the resulting λ is larger; λ=2 eV with $\nu_n \kappa_e^o = 1 \times 10^{11} s^{-1}$.

As can be observed from the two Marcus plots in Figures 58 and 59 the two ground state ($Fe^{II} \rightarrow Ru^{III}$) points also deviate in a systematic fashion from the calculated curve. The two low driving force points are below the curve, i.e., the ET rates in the RuMbFe systems are slower than those predicted (from these curves). Once again, the electronic coupling may be different. The orbitals of the donor (or A) molecules in the RuMbFe vs. the RuMbZn (or RuMbPd) systems may be different. It is known that the orbitals of the photoactive porphyrins (both MP^* and MP^+) are more delocalized than the orbitals of the iron porphyrin, and therefore the electronic coupling between the FeP and the surface Ru acceptor will be less

Figure 59. Plot of $\ln k_{ET}$ vs. $-\Delta G^{o}$ for the Ru-Mb ET reactions. The solid line is the best fit to equation 7, using all ET rates except for the Ru^{II} to ZnP^{+} rates; λ=2.0 eV and $\nu_n \kappa_e^{o}=1\times10^{11}$ s^{-1}.

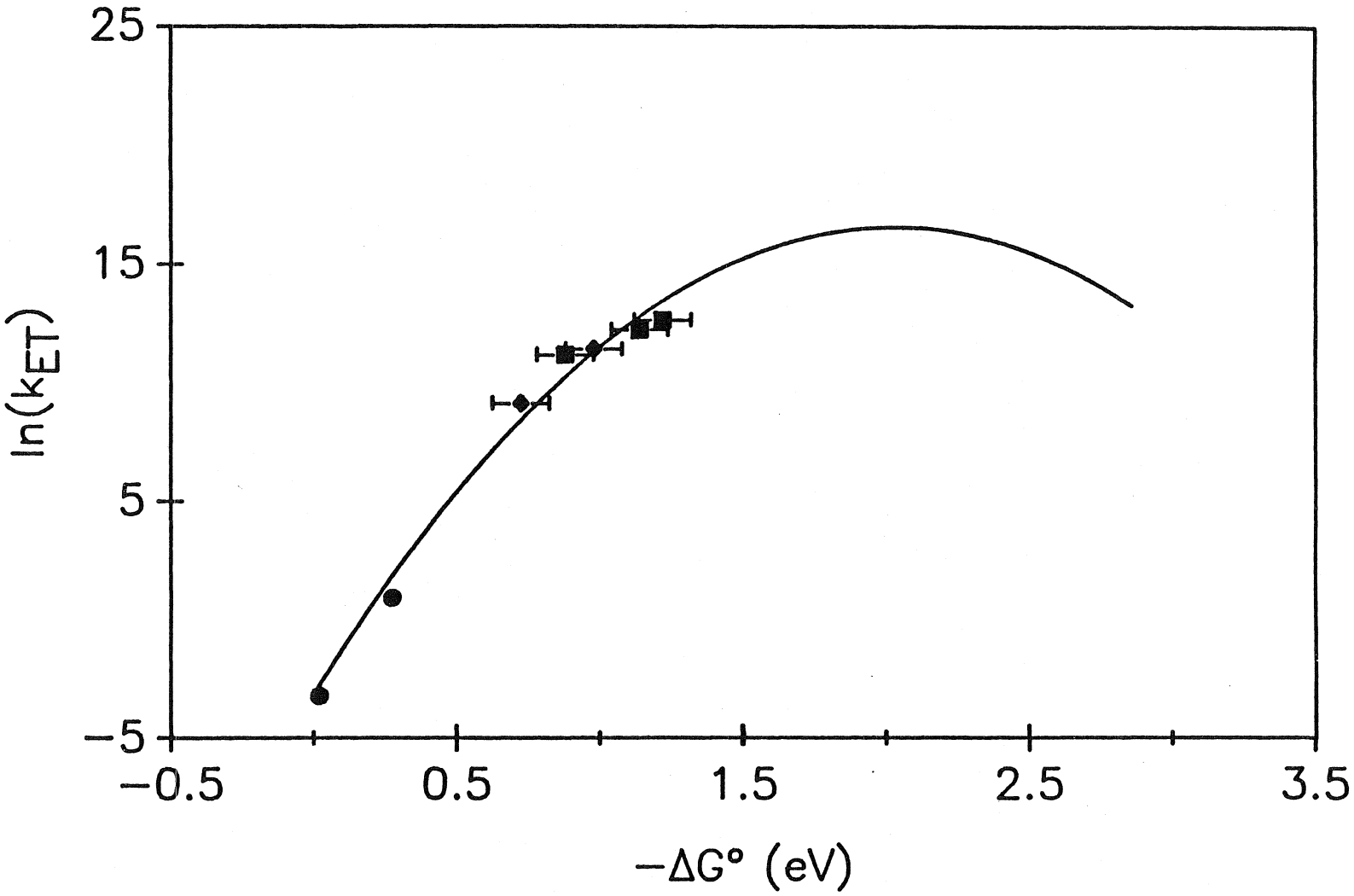
25
15
5
−5
ln(k_ET)
−0.5
0.5
1.5
2.5
3.5
−ΔG° (eV)

than the coupling between the photoactive porphyrins and the surface Ru. This difference can be expressed by a variation in the parameter d, the distance between the donor and acceptor. The distance is generally measured from the edge of the donor to the edge of the acceptor. If it is assumed that the correct distance in RuMbFe is somewhere between an edge-to-edge and a metal-to-metal measurement then d will be at least 1 to 2 Å longer than in RuMbZn systems. An ET rate has been calculated that corrects for a one Å difference in d; for $Fe^{II} \rightarrow Ru^{III}$ ET in a_5Ru- and $a_4$pyRuMb, the corrected rates are 0.099 and 6.2 s^{-1}, respectively.

Using the corrected RuMbFe rates and all the remaining rates from Table IV, the best fit for λ is calculated to be 1.6 eV and $\nu_n \kappa_e^o = 1 \times 10^{10}$ s^{-1}, Figure 60. When using the corrected rates and only the excited-state rates ($MP^* \rightarrow Ru^{III}$), the calculated λ is equal to 1.8 eV with $\nu_n \kappa_e^o = 2 \times 10^{10}$ s^{-1} (Figure 61). The corresponding calculations that utilize the corrected RuMbFe rates yield values of λ that are lower than previous calculations (Figures 60 and 61) by 0.15 to 0.2 eV.

Since it is possible that the Zn and PdMb derivatives are not analogous to the FeMb systems, Marcus curves were calculated using only the higher driving force points (Figures 62 and 63). The λ calculated using all eight rates (ΔE^o=0.48-1.22) is 1.25 eV; $\nu_n \kappa_e^o = 2 \times 10^9$ s^{-1}. If only the excited-state points are used ($MP^* \rightarrow Ru^{III}$), the best fit curve gives λ=1.45 eV and $\nu_n \kappa_e^o = 4 \times 10^9$ s^{-1}.

Figure 60. Plot of $\ln k_{ET}$ vs. $-\Delta G^{o}$ for the Ru-Mb ET reactions. The FeMbRu rates have been corrected for a 1 Å difference in distance. The solid line is the best fit to equation 7, λ=1.60 eV and $\nu_n \kappa_e^{o}=1x10^{10}$ s^{-1}.

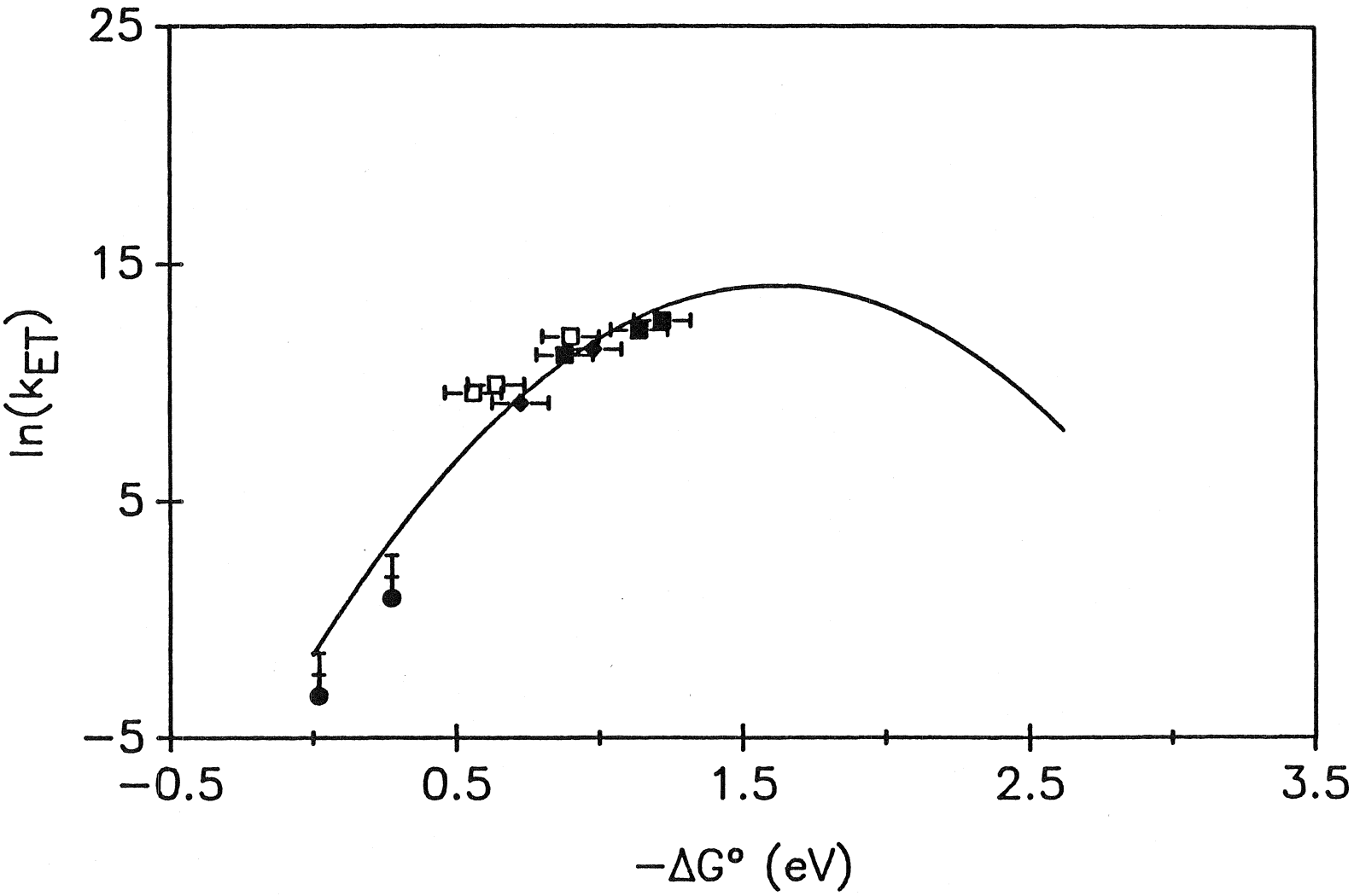
25
15
5
−5
ln(kET)
−0.5
0.5
1.5
2.5
3.5
−ΔG° (eV)

Figure 61. Plot of $\ln k_{ET}$ vs. $-\Delta G^{o}$ for the Ru-Mb ET reactions. The solid line is the best fit to equation 7, using the corrected RuMbFe rates and the MP^{*} to Ru^{III} rates ; λ=1.8 eV and $\nu_n \kappa_e{}^{o}=2x10^{10}$ s^{-1}.

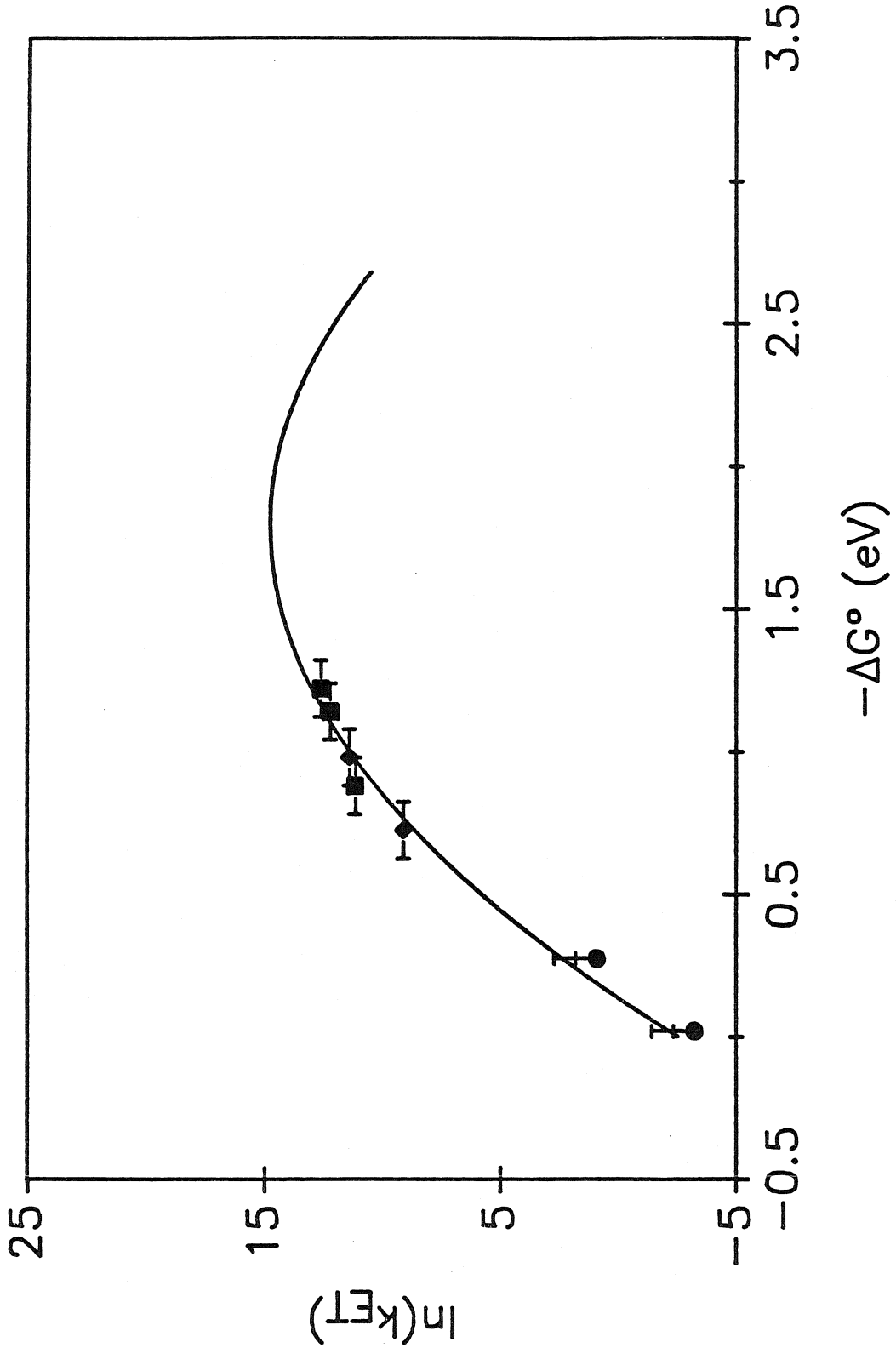
ln(kET)
25
15
5
−5
−0.5
0.5
1.5
2.5
3.5
−ΔG° (eV)

Figure 62. Plot of $\ln k_{ET}$ vs. $-\Delta G^{o}$ for the Ru-Mb ET reactions. The solid line is the best fit to equation 7, using all ET rates except for the Fe^{II} to Ru^{III} rates; λ=1.2 eV and $\nu_n \kappa_e^{o}=2\times10^{9}$ s^{-1}.

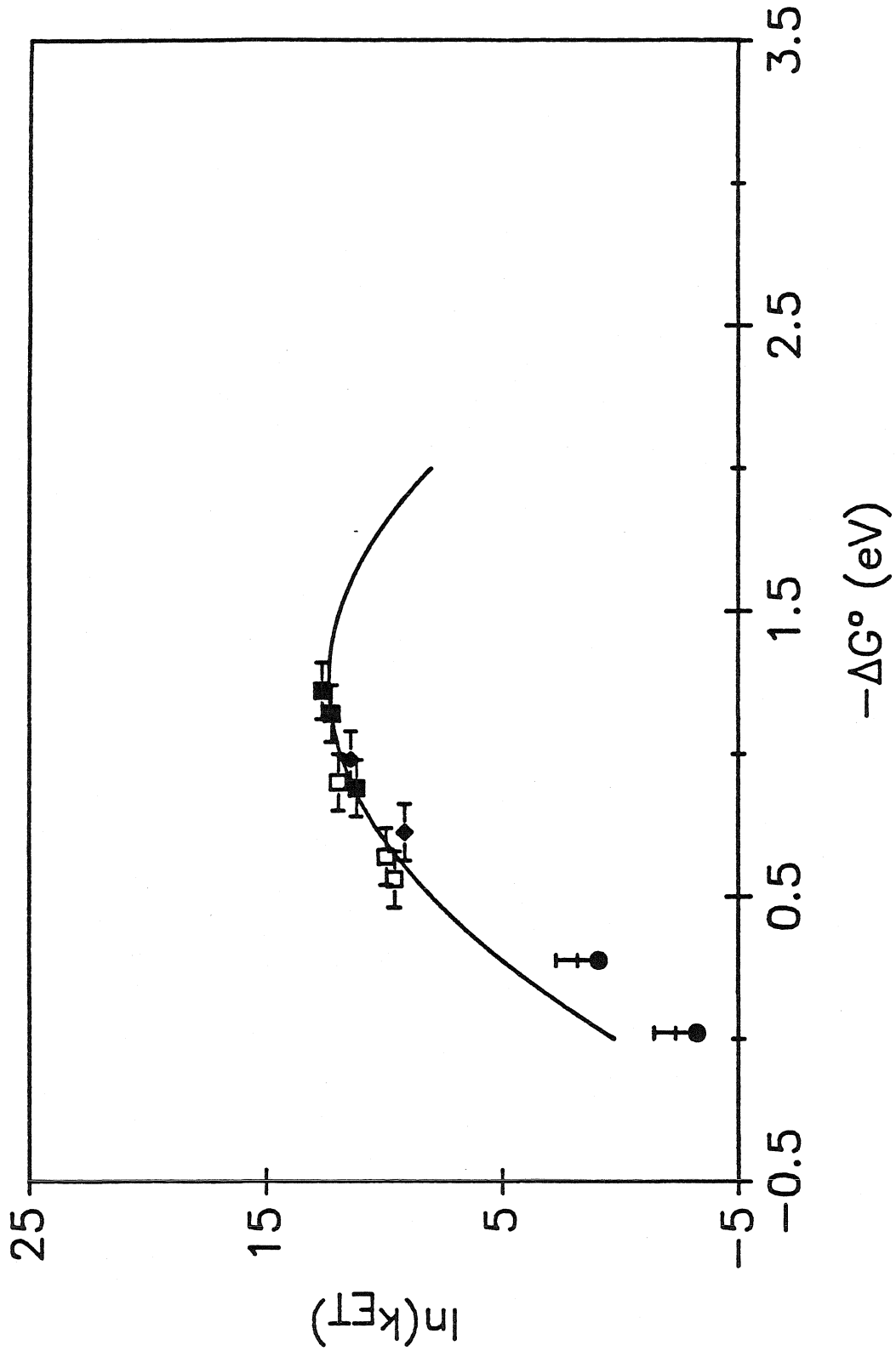
ln(kET)
25
15
5
−5
−0.5
0.5
1.5
2.5
3.5
−ΔG° (eV)

Figure 63. Plot of $\ln k_{ET}$ vs. $-\Delta G^{o}$ for the Ru-Mb ET reactions. The solid line is the best fit to equation 7 using only the MP^{*} to Ru^{III} ET rates, λ=1.45 eV and $\nu_n \kappa_e{}^{o}=4x10^{9}$ s^{-1}.

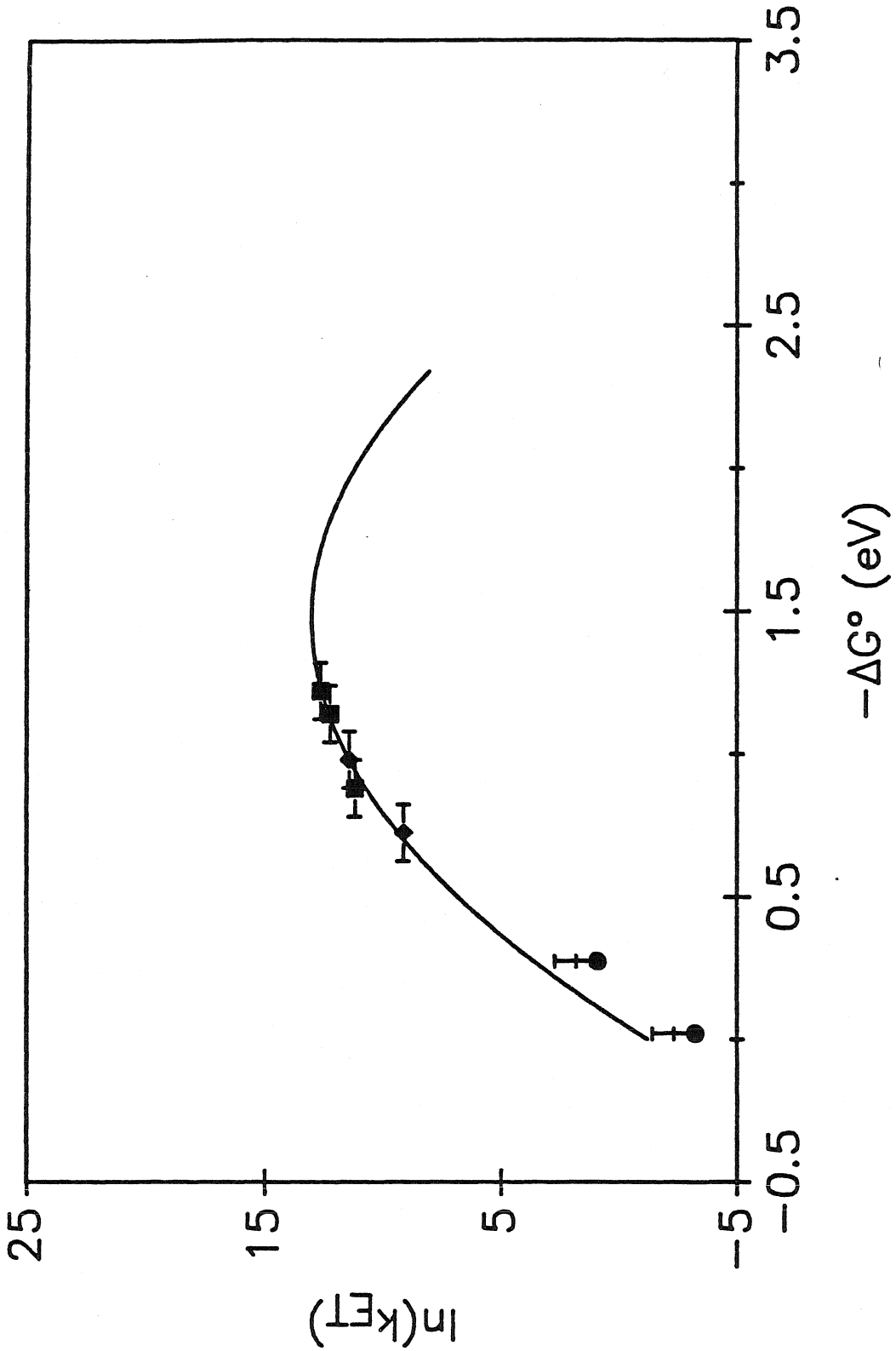
ln(kET)
25
15
5
−5
−0.5
0.5
1.5
2.5
3.5
−ΔG° (eV)

The λ values calculated from the ET rates in RuMb range from 1.25 to 2.0 eV. The best fit to the data (least scatter) utilizes only the forward rates of the photoactive porphyrins (k_f; $MP^* \rightarrow Ru^{III}$) and yields a λ of 1.45 eV, (Figure 63). The maximum rate for this system (at $-\Delta G = \lambda$) is predicted to be $4.4 \times 10^5\ s^{-1}$. It is evident that λ is greater than 1.22 eV since the ET rate is still increasing at this driving force. However, λ is probably not a great deal larger than 1.2 eV since the rates appear to be leveling off. This relatively large value of λ for Mb is similar to values reported by others for various protein systems, Table V.

McLendon et al. have studied the driving force dependence using porphyrin metal substitution in both the cyt c/cyt b_5[29] and the cyt c/ccp[31] protein-protein complexes. The λ values determined were 0.8 and 1.5 eV, respectively. One possible problem with the method used to vary the driving force in the cyt c/cyt b_5 couple is that the nature of the donor molecule changes. In the cyt c/cyt b_5 series the ET reactions that are compared have several types of donor molecules, including: a free base porphyrin radical anion, a ground state porphyrin and porphyrin excited states. It is likely that the reorganization energy and the electronic coupling will vary in this series of systems. Hoffman has used a variable temperature approach to determine λ=2.0 eV in Fe,Zn hemoglobin derivatives.[32] The major disadvantage in this experiment is that only a single donor/acceptor system is used.

The nuclear reorganization energy is made up of two parts; λ_i is due to the inner sphere coordination changes that accompany

Table V. Reorganization energies in protein donor/acceptor systems.

ET system	λ (eV)	Reference
cyt c/cyt b_5	0.8	29
cyt c/ccp	1.5	31
Zn-sub, Ru-cyt c	1.2-1.6	75
Zn, Fe-Hb	2.0	32
Zn,Pd,-RuMb	1.45	this work

electron transfer, and λ_o is due to solvation and/or protein structure changes that occur upon electron transfer. The λ_i for the attached ruthenium complex is known to be fairly small because the bond lengths are relatively unchanged in ruthenium-ammine complexes when going from the oxidized (Ru^{III}) to the reduced (Ru^{II}) state. The λ_i has been determined for ruthenium-ammine model complexes. For $Ru(NH_3)_6^{3+/2+}$ and $Ru(NH_3)_5py^{3+/2+}$, λ_i is approximately equal to 0.1 eV.[64] The differences in the inner coordination sphere between ZnP, ZnP^* and ZnP^+ have also been shown to be fairly small, and the upper limit for λ_i (of ZnP in protein) was estimated at 0.15 eV.[75] In the ruthenium-labelled Zn- and PdMb systems the inner-sphere reorganization is not likely to be more than 0.25-0.3 eV. This is a fairly small fraction of the total reorganization energy (1.45 eV).

The λ_i for the heme center in a_4LRu(His-48)Mb is expected to be larger than the λ_i for the ZnP (or PdP) because of the ligation change at the Fe that accompanies reduction of myoglobin. Crystallographic studies of metmyoglobin (Fe^{III}) and deoxymyoglobin (Fe^{II}) indicate that the axial water dissociates from the heme upon reduction.[48] The ZnP and PdP groups in Mb are not likely to coordinate to a water molecule in either oxidation state. From the temperature dependence of the ET rate in a_5Ru(His-48)MbFe, the reorganization enthalpy, ΔH^*, has previously been estimated to be ~20 kcal mol^{-1}.[36] This large value was attributed to ligation changes at the heme site. Other evidence for a larger λ_i in the Fe systems is that the ET rates for the a_5Ru and $a_4$pyRu(His-48)MbFe are slower than rates predicted for a system in which $\lambda=1.45 \pm 0.2$

eV (Figures 58-64). The slower rates are probably due to both a reduced electronic coupling and a higher reorganization energy in the MbFe derivatives.

The outer-sphere reorganization energy, λ_o, can be estimated from electron exchange rates for $(NH_3)_5pyRu^{3+/2+}$.[64] From the temperature dependence of the exchange rate, the outer-sphere activation energy (ΔG^*_o) was calculated to be 0.3 eV. Since ΔG^o is zero for the exchange reaction, Marcus theory states that $\Delta G^* = \lambda/4$. Therefore, the outer-sphere contribution to λ for one Ru center is ~0.6 eV. The a_5Rupy may not be the best model for a_4LRu attached to the imidazole of a protein. A protein is a much larger, hydrophobic group than the pyridine in a_5Rupy, and solvent reorganization upon oxidation and reduction around the model complex is likely to be different than solvation changes at a ruthenium-ammine attached to a large protein ligand. Reasonable limits placed on λ_o(Ru) are 0.5-0.7 eV.

The reorganization energy in Ru-labelled Mb probably has a large contribution due to solvent rearrangement at the redox sites, since the attached Ru moiety points directly into the aqueous medium. The heme pocket is also accessible to solvent, but an estimate of λ_o for the porphyrin centers has not been made. The contribution to λ from protein structure changes is also unknown.

Dielectric continuum theory predicts that λ_o is dependent on the nature of the solvent surrounding the redox sites.[5] Closs et al. have demonstrated for their organic model ET systems that λ

decreases as the polarity of the solvent decreases. They performed driving force studies of the ET rate in various solvents and found that in methyltetrahydrofuran the total reorganization energy for these systems is 1.20 eV and that it decreases to 0.6 eV in isooctane.[13] To investigate the role of the aqueous medium in RuMb systems, ET rates were measured in D_2O and 2:1 acetonitrile/NaPi buffer for a_5Ru(His-48)MbZn and a_5Ru(His-48)MbPd, respectively. No differences in ET rates were observed compared to the same systems in aqueous NaPi buffer.

The similarity in ET rate upon the addition of 33% acetonitrile indicates that the water molecules may interact in a specific fashion with the attached Ru complex. Since the Ru-ammine species is hydrophilic, it is likely that it will be preferentially surrounded by water molecules rather than acetonitrile. Selective solvation has also been observed for ET in the mixed-valence dimer $[(NH_3)_5Ru^{II}$-4,4'-bpy-$Ru^{III}(NH_3)_5]^{5+}$.[90] Probably the only way to effect a change in ET rate (λ) is to exclude all the water and surround the protein with something less polar. Unfortunately, the protein is not stable in greater than 33% acetonitrile or other organic solvents. A change in solvent from H_2O to D_2O had no effect on the observed ET rate in a_5Ru(His-48)MbZn. This is not surprising since there is not a large change in polarity, (solvent dielectric) in substituting D_2O for H_2O. To investigate the importance of H_2O (to λ) it will probably be necessary to use a Ru complex attached to the surface that is hydrophobic and can exclude water from the outer coordination

sphere. For example, a ruthenium capped macrocyclic complex could provide the necessary hydrophobicity.

ET Reactions at Longer Distances

The forward ($ZnP^* \rightarrow Ru^{III}$) ET rates in the three longer distance (~20 Å) a_5RuMbZn systems have been measured previously.[35] The edge-to-edge distances in these systems (a_5Ru attached at histidine 81, 116 and 12) are 19.3, 20.1 and 22.0 Å, respectively. The forward rates are all about 100 s^{-1}. To investigate the free energy dependence at a longer distance the ET rate was measured in the $a_4$pyRu(His-12)MbZn.

The ZnP triplet decay was measured by transient absorption (Scheme III), monitoring at 450 nm as described previously. The observed decay was second order with rate constants k_1=300 s^{-1} and k_2 equal to the native decay, 40 s^{-1} (Figure 64). To obtain the forward ET rate, the intrinsic decay (k_D=40 s^{-1}) must be subtracted from k_1. k_f was determined to be 260 s^{-1} and was independent of protein concentration between 1 and 5 μM. From this limited set of data (two points!) at the longer distance, it appears that the ET rate is dependent on free energy in a similar fashion to that reported for Ru(His-48)Mb at a distance of 13 Å. The reorganization energy is probably not drastically different from that at 13 Å; however, further ET measurements are needed at the longer distance to resolve this issue. The distance dependence of the ET rate for $a_4$pyRu(His-48) and $a_4$pyRu(His-12) is consistent with the previously obtained value of β (0.9 $Å^{-1}$).

Figure 64. Transient kinetics of $a_4$pyRu(His-12)MbZn monitored at 450 nm. The smooth curve is a biexponential function with rate constants of 300 and 40 s^{-1}.

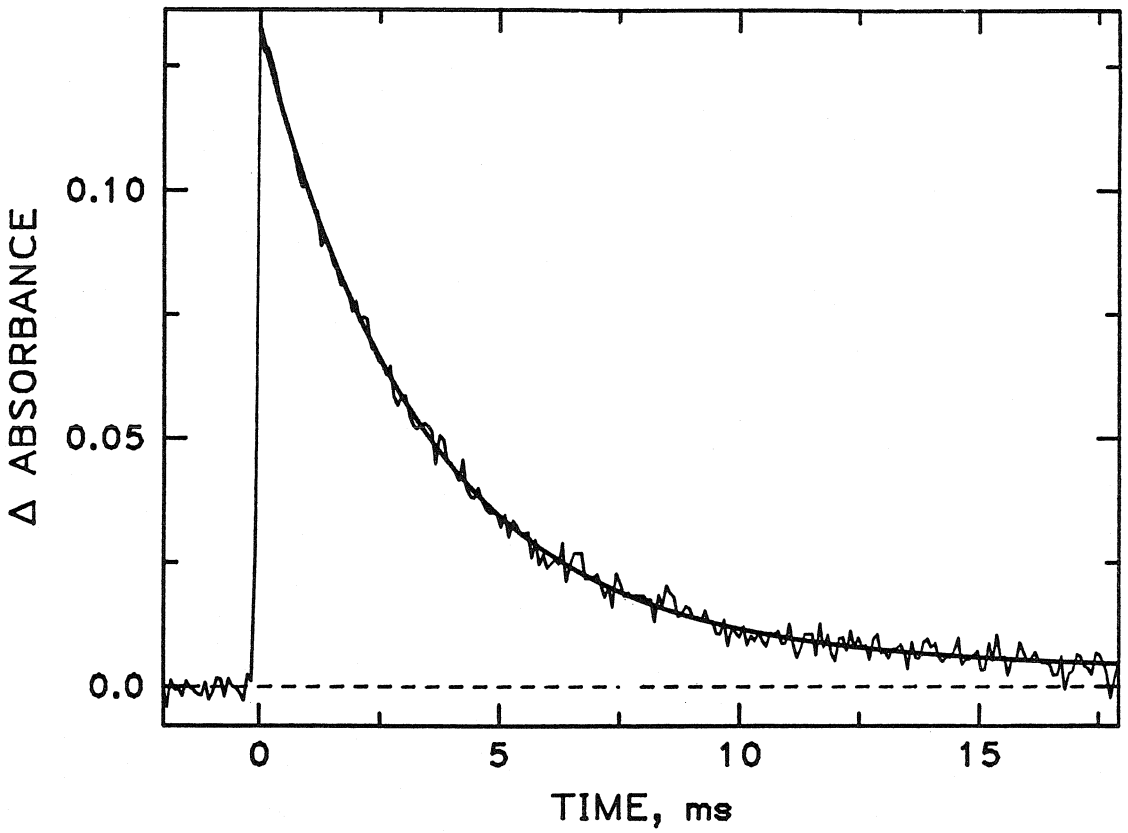
Δ ABSORBANCE
0.10
0.05
0.0
0
5
10
15
TIME, ms

Conclusions

There are several conclusions to be drawn from this work. The first important result is that electron transfer is reversible in Mb. We have shown that the ET rate in Ru-labelled Mb is not directional and that it is dependent on reaction free energy. The second major result is the determination of the reorganization energy. The reorganization energy in Ru-labelled Mb systems is rather large, ~1.5 eV. This value of λ is in reasonable agreement with other values of λ reported for protein and organic-spacer ET systems. The ET data indicate that the electronic coupling at $d=d_o$ (κ_e^o) may be smaller for protein systems than previously assumed. The ET results also indicate that the electronic coupling in the reverse ET reactions ($Ru^{II} \rightarrow ZnP^+$) may be slightly different than the coupling in the forward reactions. Further studies to measure the distance dependence of the back reaction are in progress.

Since the electron-transfer rate is strongly dependent on the magnitude of λ (Equation 7), it is possible that long-range ET reactions may be controlled through variations in the reorganization energy. There are large variations expected in k_{ET} by varying λ at constant d, ΔG^o and β. These results indicate that specificity could be achieved through changes in reorganization energy. Changes in λ could be made by reducing the number of water molecules in the first coordination sphere of the donor and acceptor by some conformational transition (Figure 65). Since rearrangements of solvent water molecules are usually associated with large

Figure 65. Schematic depicting a water-eliminating conformational transition.

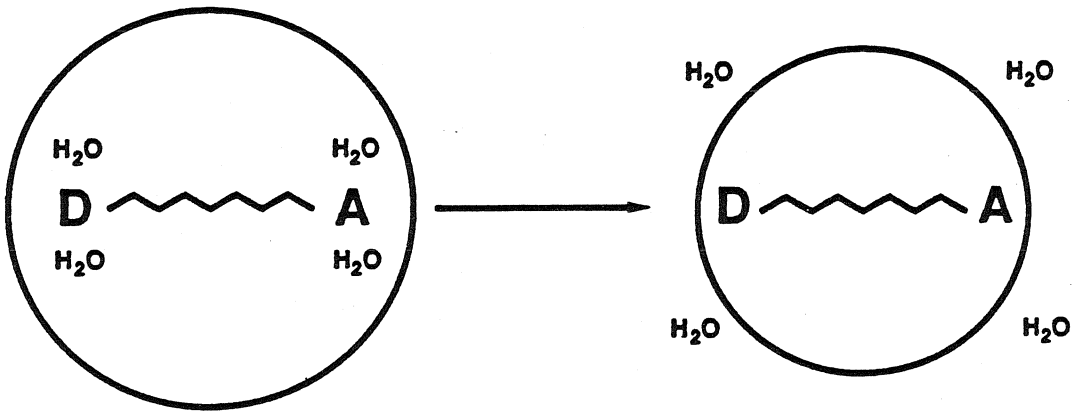
H2O
H2O
D
A
H2O
H2O
H2O
H2O
D
A
H2O
H2O

reorganization energies, the exclusion of water would be expected to lower λ.

Future Work

We are continuing to explore the reorganization energy in Mb through the synthesis of systems in which the redox-active metal complex has a substantially lower λ than the ruthenium complexes used in this study. Another area that is being pursued is the distance dependence of the reorganization energy. The free energy dependence of ET in a_5Ru(His-12)Mb will yield a value for λ at an ET distance of 20 Å. The electronic coupling for the reverse ET process ($Ru^{II} \rightarrow ZnP^+$) is also under investigation. From measurements of reverse ET rates at several distances, a value of β for the reverse process should be obtained.

References

1. Hatefi, Y. *Annu. Rev. Biochem.* **1985**, *54*, 1015.

2. Dixit, B. P. S. N.; Vanderkooi, J. M. *Curr. Top. Bioenerg.* **1984**, *13*, 159.

3. Budil, D. E.; Gast, P.; Chang, C-H.; Schiffer, M.; Norris, J. R. *Annu. Rev. Phys. Chem.* **1987**, *38*, 561.

4. Michel-Beyerle, M. E., Ed., *Antennas and Reaction Centers of Photosynthetic Bacteria* Springer-Verlag, Berlin, **1985**.

5. Marcus, R. A.; Sutin, N. *Biochim. Biophys. Acta* **1985**, *811,* 265.

6. DeVault, D. *Quantum-Mechanical Tunneling in Biological Systems, 2nd Ed.,* Cambridge University Press **1984.**

7. McLendon, G.; *Acc. Chem. Res.* **1988**, *21*, 160.

8. Peterson-Kennedy, S. E.; McGourty, J. L.; Ho, P. S.; Sutoris, C. J.; Liang, N.; Zemel, H.; Blough, N. V.; Margoliash, E.; Hoffman, B. M. *Coord. Chem. Rev.* **1985**, *64*, 125.

9. Isied, S. S. *Prog. Inorg. Chem.* **1984**, *32*, 443.

10. Mayo, S. L.; Ellis, W. R., Jr.; Crutchley, R. J.; Gray, H. B. *Science*, **1986**, *233*, 948.

11. Lieber, C. M.; Karas, J. L.; Mayo, S. L.; Albin, M.; Gray, H. B. *Welch Symposium*; **1987**.

12. Scott, R. A.; Mauk, A. G.; Gray, H. B. *J. Chem. Ed.* **1985**, *62*, 932.

13. Closs, G. L.; Miller, J. R. *Science* **1988**, *240*, 440.

14. Chance, B.; Mueller, P.; DeVault, D; Powers, L. *Physics Today* **1980**, *33*, 32.

15. Deisenhofer, J.; Epp, O.; Miki, K.; Huber, R.; Michel, H. *J. Mol. Biol.* **1984**, *180*, 385.

16. Allen, J. P.; Feher, G. *Proc. Natl. Acad. Sci. USA* **1987**, *81*, 4795.

17. Fleming, G. R.; Martin, J. L.; Breton, J. *Nature* **1988**, *333*, 190.

18. Marcus, R. A. *Chem. Phys. Lett.* **1987**, *133*, 471.

19. Bixon, M.; Jortner, J.; Michel-Beyerle, M. E.; Ogrodnik, A.; Lersch, W. *Chem. Phys. Lett.* **1987**, *140*, 626.

20. Sutin, N. *Prog. Inorg. Chem.* **1983**, *30*, 441.

21. Ulstrup, J.; Jortner, J. *J. Chem. Phys.* **1975**, *63*, 4358.

22. Brunschwig, B. S.; Ehrenson, S.; Sutin, N. *J. Phys. Chem.* **1986**, *90*, 3657.

23. Marcus, R. A. *Annu. Rev. Phys. Chem.* **1964**, *15*, 155.

24. Closs, G. L.; Calcaterra, L. T.; Green, N. J.; Penfield, K. W.; Miller, J. R. *J. Phys. Chem.* **1986**, *90*, 3673.

25. Wasielewski, M. R.; Niemczyk, M. P.; Svec, W. A.; Pewitt, E. B. *J. Am. Chem. Soc.* **1985**, *107*, 1080.

26. Joran, A. D.; Leland, B. A.; Felker, P. M.; Zewail, A. H.; Hopfield, J. J.; Dervan, P. B. *Nature* **1987**, *327*, 508.

27. Oevering, H.; Paddon-Row, M. N.; Heppener, M.; Oliver, A. M.; Cotsaris, E.; Verhoeven, J. W.; Hush, N. S. *J. Am. Chem. Soc.* **1987**, *109*, 3258.

28. Heitele, H.; Michel-Beyerle, M. E. *J. Am. Chem. Soc.* **1985**, *107*, 8286.

29. McLendon, G.; Miller, J. R. *J. Am. Chem. Soc.* **1985**, *107*, 7811.

30. Simolo, K. R.; McLendon, G. L.; Mauk, M. R.; Mauk, A. G. *J. Am. Chem. Soc.* **1984**, *106*, 5012.

31. Conklin, K. T.; McLendon, G. *J. Am. Chem. Soc.* **1988**, *110*, 3345.

32. Peterson-Kennedy, S. E.; McGourty, J. L.; Kalweit, J. A.; Hoffman, B. M. *J. Am. Chem. Soc.* **1986**, *108*, 1739.

33. Karas, J. L.; Lieber, C. M.; Gray, H. B. *J. Am. Chem. Soc.* **1988**, *110*, 599.

34. Lieber, C. M.; Karas, J. L.; Gray, H. B. *J. Am. Chem. Soc.* **1987**, *109,* 3778.

35. Axup, A. W.; Albin, M.; Mayo, S. L.; Crutchley, R. J.; Gray, H. B. *J. Am. Chem. Soc.* **1988**, *110*, 435.

36. Crutchley, R. J.; Ellis, W. R., Jr.; Gray, H. B. *J. Am. Chem. Soc.* **1986**, *107,* 5002.

37. Crutchley, R. J.; Ellis, W. R., Jr.; Gray, H. B. *Frontiers in Bioinorganic Chemistry,* Xavier, A. V., ed., VCH Verlagsgesellschaft, Weinham, FRG, **1986**, 679.

38. Yocom, K. M.; Shelton, J. B.; Shelton, J. R.; Schroeder, W. A.; Worosila, G.; Isied, S. S.; Bordignon, E.; Gray, H. B. *Proc. Natl. Acad. Sci. USA* **1982**, *79,* 7052.

39. Nocera, D. G.; Winkler, J. R.; Yocom, K. M.; Bordignon, E.; Gray, H. B. *J. Am. Chem. Soc.* **1984**, *106,* 5145.

40. Isied, S. S.; Kuehn, C.; Worosila, G. *J. Am. Chem. Soc.* **1984**, *106*, 1722.

41. Elias, H.; Chou, M.H.; Winkler, J. R. *J. Am. Chem. Soc.* **1988**, *110,* 429.

42. Kostic, N. M.; Margalit, R.; Che, C.-M.; Gray, H. B. *J. Am. Chem. Soc.* **1983**, *105*, 7765.

43. Margalit, R.; Kostic, N. M.; Che, C.-M.; Blair, D. F.; Chiang, H.-J.; Pecht, I.; Shelton, J. B.; Shelton, J. R.; Schroeder, W. A.; Gray, H. B. *Proc. Natl. Acad. Sci. USA* **1984**, *81,* 6554.

44. Leland, B. A.; Joran, A. D.; Felker, P. M.; Hopfield, J. J.; Zewail, A. H.; Dervan, P. B. *J. Phys. Chem.* **1985**, *89*, 5571.

45. The data were fit with a single vibrational mode, hν, according to the following equation:[13] $k = (\pi/\hbar^2\lambda_S k_B T)^{1/2}|V|^2 \sum_{w=0}^{\infty} (e^{-S}S^w/w!) \times \exp\{-[(\lambda_S + \Delta G^0 + wh\nu)^2/4\lambda_S k_B T]\}$

$S = \lambda_v/h\nu$

46. The data were fit with the equation from reference 45.

47. McLendon, G.; Pardue, K.; Bak, P. *J. Am. Chem. Soc.* **1987**, *109*, 7540.

48. (a) Takano, T. *J. Mol. Biol.* **1977**, *110*, 537. (b) Takano, T. *J. Mol. Biol.* **1977**, *110*, 537.

49. Mottonen, J.; Ringe, D.; Petsko, G. unpublished results.

50. Matsubara, T.; Ford, P. C. *Inorg. Chem.* **1976**, *15*, 1107.

51. Sutton, J. E. Ph.D. Thesis, Stanford University **1979**.

52. Gaunder, R. G.; Taube, H. *Inorg. Chem.* **1970**, *9*, 2627.

53. Lim, H. S.; Barclay, D. J.; Anson, F. C. *Inorg. Chem.* **1972**, *11*, 1460.

54. Axup, A. W. Ph.D. Thesis, California Institute of Technology, **1987**.

55. Schlit, A. A.; Taylor, R. C. *Russ. J. Inorg. Chem. (Engl. Transl.)* **1959**, *9*, 211.

56. Adler, A. D.; Longo, F. R.; Kampas, F.; Kim, J. *J. Nucl. Chem,.* **1970**, *32*, 2443.

57. Vogt, L. H., Jr.; Katz, J. L.; Wiberley, S. E. *Inorg. Chem.* **1965**, *4*, 1157.

58. Curtis, J. C.; Sullivan, B. P.; Meyer, T. J. *Inorg. Chem.* **1983**, *22*, 224.

59. Marchant, J. A.; Matsubara, T.; Ford, P. C. *Inorg. Chem.* **1977**, *16*, 2160.

60. von Kameke, A.; Tom, G. M.; Taube, H. *Inorg. Chem.* **1978**, *17*, 1790.

61. Baumann, J. A.; Meyer, T. J. *Inorg. Chem.* **1980**, *19*, 345.

62. Teale, F. W. J. *Biochim. Biophys. Acta* **1959**, *35*, 543.

63. Yonetoni, T. *J. Biol. Chem.* **1967**, *242*, 5008.

64. Brown, G. M.; Sutin, N. *J. Am. Chem. Soc.* **1979**, *101*, 883.

65. Sheperd, R. E.; Taube, H. *Inorg. Chem.* **1973**, *12*, 1392.

66. Isied, S. Taube, H. *Inorg. Chem.* **1974**, *13*, 1545.

67. Freiser, B. S.; Woodin, R. L.; Beauchamp, J. L. *J. Am. Chem. Soc.* **1979**, *101*, 883.

68. Hoffman, B. M. *The Porphyrins*; Vol. VII, Dolphin, D. Ed.; Academic Press, New York 1978, p. 403.

69. Markley, J. L. *Acc. Chem. Res.* **1975**, *8*, 70.

70. Botelho, L. H.; Gurd, F. R. N. *Biochemistry* **1978**, *17*, 5188.

71. King, G.; Wright, P. E. *Biochem. Biophys. Res. Comm.* **1982**, *106*, 559.

72. Toi, H.; LaMar, G. N.; Margalit, R.; Che, C-M.; Gray, H. B. *J. Am. Chem. Soc.* **1984**, *106*, 6213.

73. Carver, J. A.; Bradbury, J. H. *Biochemistry* **1984**, *23*, 4890.

74. Dalvit, C.; Wright, P. E. *J. Mol. Biol.* **1987**, *194*, 313.

75. Meade, T. J.; Gray, H. B.; Winkler, J. R. *J. Am. Chem. Soc.* submitted for publication.

76. Cowan, J. A.; Upmacis, R. K.; Beratan, D. N.; Onuchic, J. N.; Gray, H. B. submitted for publication.

77. Felton, R. H. *The Porphyrins*; Dolphin, D. Ed.; Academic Press, New York 1978.

78. Rillema, D. P.; Endicott, J. F.; Papaconstantinou, E. *Inorg. Chem.* **1971**, *10*, 1739.

79. (a) Hanania, G. I. H.; Yeghiayan, A.; Cameron, B. F. *Biochem. J.* **1966**, *98*, 189. (b) Bowen, W. J. *J. Biol. Chem.* **1949**, *179*, 235.

80. Milder, S. J.; Goldbeck, R. A.; Kliger, D. S.; Gray, H. B. *J. Am. Chem. Soc.* **1980**, *102,* 6761.

81. Winkler, J. R.; Nocera, D. G.; Netzel, T. L. *J. Am. Chem. Soc.* **1986**, *108,* 4451.

82. Becker, J. Y.; Kerr, J. B.; Pletcher, D.; Rosas, R. *J. Electronanal. Chem.* **1981**, *117*, 87.

83. Ram, M. S.; Bakac, A.; Espenson, J. H. *Inorg. Chem.* **1986**, *25*, 3267.

84. Bechtold, R.; Kuehn, C.; Lepre, C.; Isied, S. S. *Nature* **1986**, *322*, 286.

85. Kalyanasundaaraam, K. unpublished results.

86. Frost, A. A.; Pearson, R. G. *Kinetics and Mechanism 2nd ed.*; Wiley, New York, 1961, p. 166-169.

87. Miller, J. R.; Beitz, J. V. *J. Chem. Phys.* **1981**, *74*, 6746.

88. Liang, N.; Pielak, G.; Mauk, A. G.; Smith, M.; Hoffman, B. *Proc. Natl. Acad. Sci. USA* **1987**, *84,* 1249.

89. Pardue, K.; McLendon, G.; Bak, P. *J. Am. Chem. Soc.* **1987**, *109,* 7540.

90. Blackbourn, R. L.; Hupp, J. T. *J. Phys. Chem.* **1988**, *92*, 2817.

91. Bands I, II, III and IV correspond to the elution order off the cation-exchange column during the separation of the singly-labelled a_5RuMb derivatives.

92. Sundberg, R. J.; Gupta, G. *Bioinorg. Chem.* **1973**, *3*, 39.

Appendix

This appendix contains the results of peptide mapping for the $(NH_3)_5Ru$(His-X)myoglobin (a_5RuMb) derivatives. The work was performed by R. J. Crutchley, W. R. Ellis Jr., J. B. Shelton, J. R. Shelton, W. A. Schroeder and H. B. Gray.

The preparation of a_5RuMb yields four singly-labelled derivatives.[35,37] Computer graphics modeling has shown that four histidines are accessible to reaction with Ru complexes. These are histidines 12, 48, 81 and 116. The labelling site of the Ru moiety in the singly-labelled derivatives has been verified by peptide mapping experiments.

The native and Ru-labelled protein were digested with trypsin using procedures that were identical to those reported previously.[38] Peptides T1 through T23 were obtained (Figure 66). Histidines 12, 48, 81 and 116 are contained in separate tryptic peptides; T1, T7, T14 and T17, respectively.

<u>a_5Ru(His-48)Mb</u> The tryptic peptides of a_5Ru(Band IV)Mb[91] and native Mb were separated by reverse-phase HPLC and the eluate was monitored at 300 nm (Figure 67). Only the peaks corresponding to the T1 and T1,2 (tryptophan-containing) peptides and heme are present in the chromatogram of the native Mb tryptic peptides. (The two peaks between T1 and T1,2 are artifacts.) A new peak at an elution volume of 15 mL appears in the chromatogram of the Ru-labelled protein; it was identified by amino acid analysis[38] as the T6,7 peptide. The attachment of $Ru^{III}(NH_3)_5$ to a histidine in the

Figure 66. Tryptic peptides of sperm whale myoglobin.

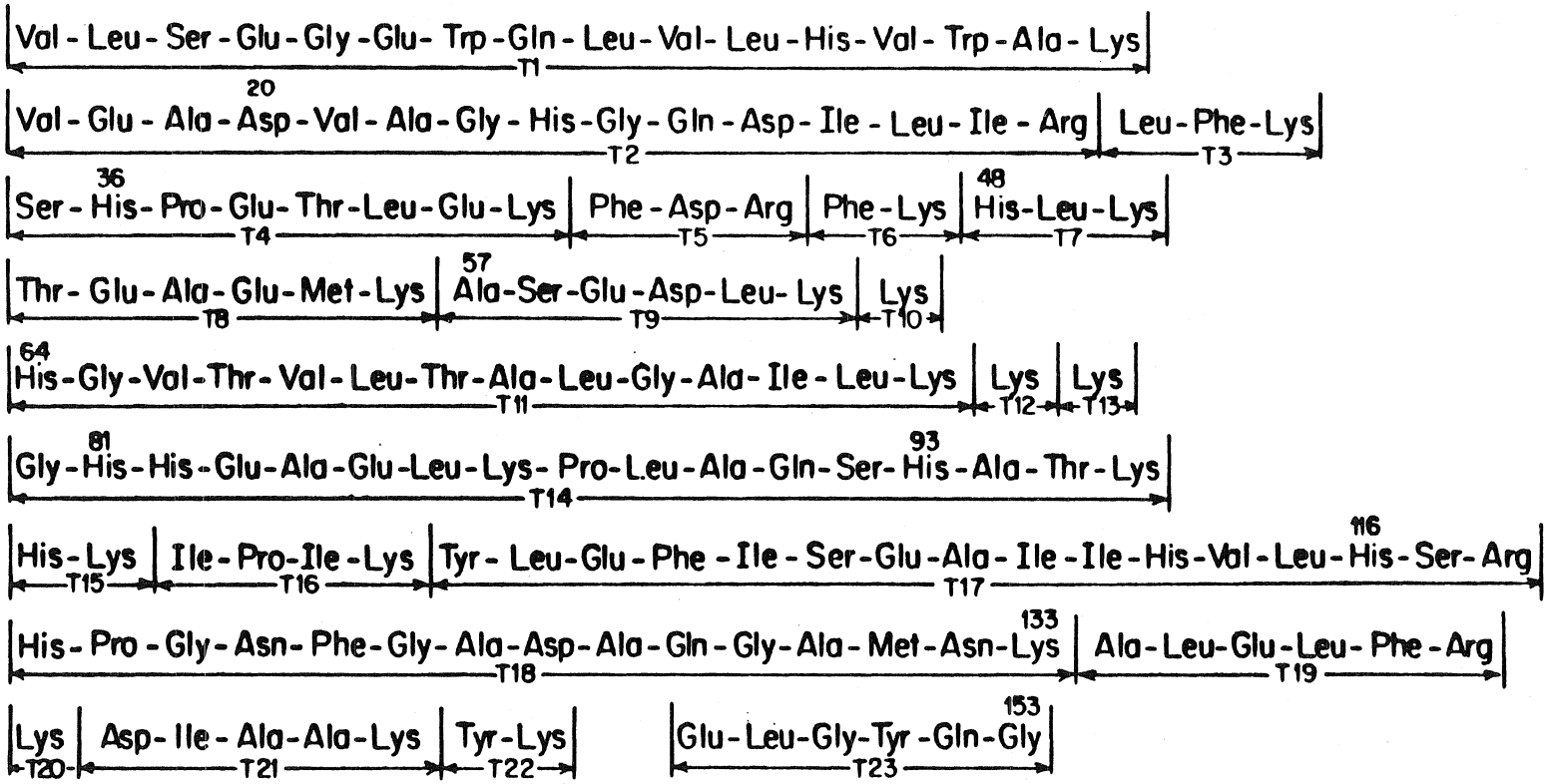
Val - Leu - Ser - Glu - Gly - Glu - Trp - Gln - Leu - Val - Leu - His - Val - Trp - Ala - Lys
T1
20
Val - Glu - Ala - Asp - Val - Ala - Gly - His - Gly - Gln - Asp - Ile - Leu - Ile - Arg
T2
Leu - Phe - Lys
T3
36
Ser - His - Pro - Glu - Thr - Leu - Glu - Lys
T4
Phe - Asp - Arg
T5
Phe - Lys
T6
48
His - Leu - Lys
T7
Thr - Glu - Ala - Glu - Met - Lys
T8
57
Ala - Ser - Glu - Asp - Leu - Lys
T9
Lys
T10
64
His - Gly - Val - Thr - Val - Leu - Thr - Ala - Leu - Gly - Ala - Ile - Leu - Lys
T11
Lys
T12
Lys
T13
81
Gly - His - His - Glu - Ala - Glu - Leu - Lys - Pro - Leu - Ala - Gln - Ser - His - Ala - Thr - Lys
93
T14
His - Lys
T15
Ile - Pro - Ile - Lys
T16
Tyr - Leu - Glu - Phe - Ile - Ser - Glu - Ala - Ile - Ile - His - Val - Leu - His - Ser - Arg
116
T17
His - Pro - Gly - Asn - Phe - Gly - Ala - Asp - Ala - Gln - Gly - Ala - Met - Asn - Lys
133
T18
Ala - Leu - Glu - Leu - Phe - Arg
T19
Lys
T20
Asp - Ile - Ala - Ala - Lys
T21
Tyr - Lys
T22
Glu - Leu - Gly - Tyr - Gln - Gly
153
T23

Figure 67. Reverse-phase HPLC of tryptic digests of native Mb and $Ru(NH_3)_5$(His-48)Mb at 300 nm. A 2 mg sample of hydrolyzed protein was chromatographed (flow rate 2mL/min) with a linear gradient between 0% and 55% CH_3CN in which both the initial aqueous developer and the CH_3CN contained 0.1% CF_3COOH.

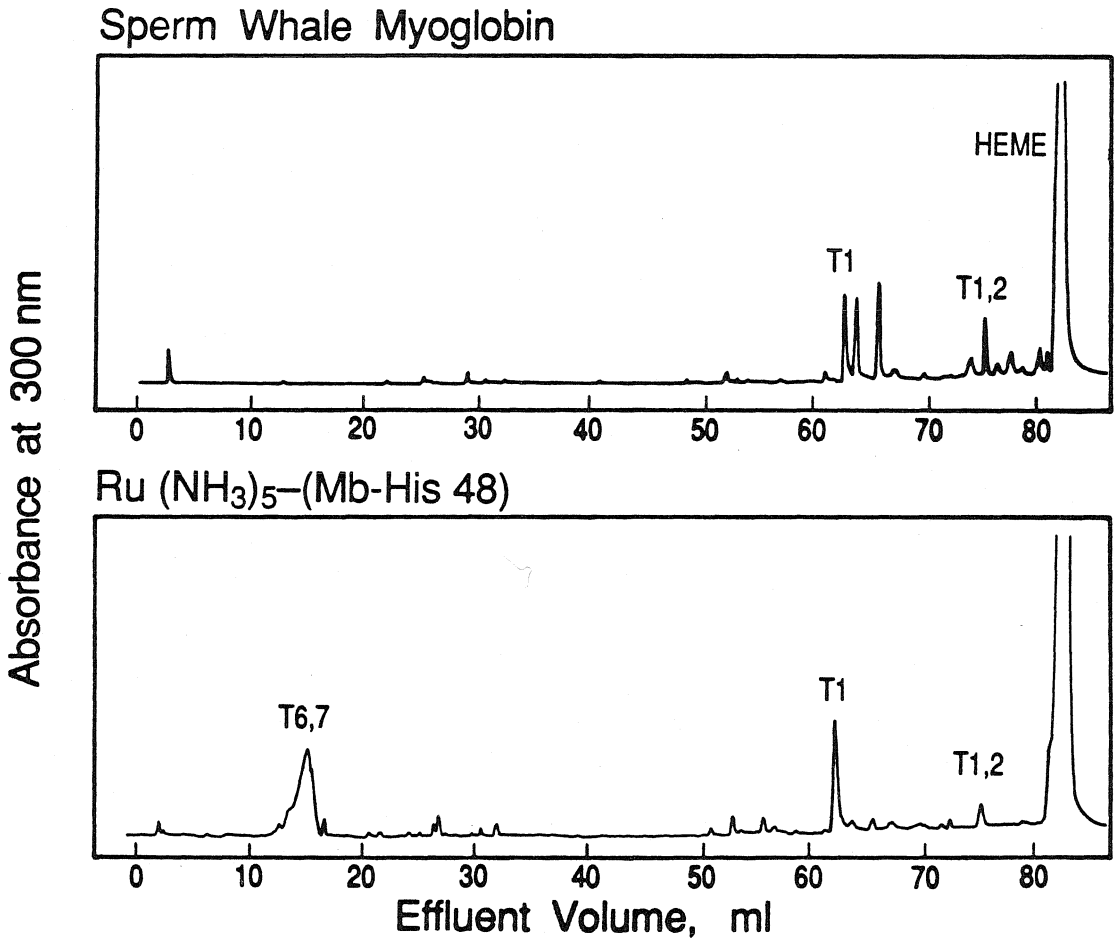
Sperm Whale Myoglobin
HEME
T1
T1,2
0
10
20
30
40
50
60
70
80
Ru (NH3)5–(Mb-His 48)
T6,7
T1
T1,2
0
10
20
30
40
50
60
70
80
Absorbance at 300 nm
Effluent Volume, ml

peptide generates a chromophore that makes it possible to detect T6,7 at 300 nm. The spectrum of the $Ru^{III}(NH_3)_5$histidine complex exhibits a maximum at 300 nm (ε=2100 M^{-1} cm^{-1}).[92]

a_5Ru(His-12)Mb In the HPLC chromatogram of the Band I a_5RuMb, the only peaks present are the T1 and T1,2 peptides (Figure 68). These tryptic peptides contain the histidine 12.

a_5Ru(His-81)Mb In the HPLC chromatogram of the Band III a_5RuMb new peaks appear at 35 mL and 58 mL (Figure 69). They were identified by amino acid analysis to be peptides T14, and T9,10,11,12,13,14, respectively. These peptides contain histidine 81.

a_5Ru(His-116)Mb The HPLC chromatogram from the tryptic digestion of Band II a_5RuMb shows peaks at 68, 69 and 72 mL (Figure 70). They were identified by amino acid analysis to be peptides T15,16,17,18, T17 and T15,16,17, respectively. The T17 peptide contains both histidines 113 and 116. The ruthenium-labelled peptides were further cleaved by thermolysin (Figure 71). The ruthenium-labelled thermolytic peptide at 42 mL (HPLC band 2) had an amino acid sequence corresponding to amino acid residues 115 to 124 of Mb. This region contains only one binding site, histidine 116.

Figure 68. Reverse-phase HPLC of tryptic digests of native Mb and $Ru(NH_3)_5$(His-12)Mb at 300 nm. A 2 mg sample of hydrolyzed protein was chromatographed (flow rate 2mL/min) with a linear gradient between 0% and 55% CH_3CN in which both the initial aqueous developer and the CH_3CN contained 0.1% CF_3COOH.

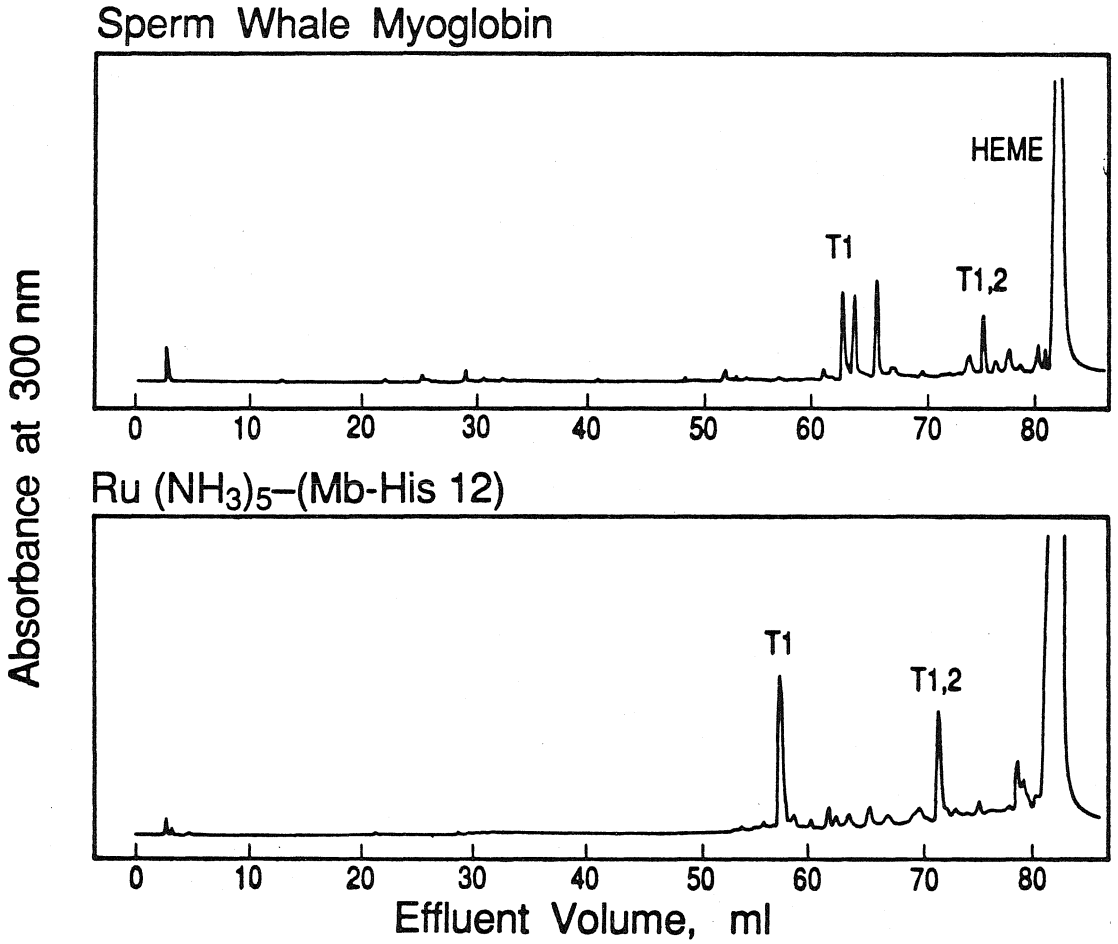
Sperm Whale Myoglobin
HEME
T1
T1,2
Ru (NH3)5–(Mb-His 12)
T1
T1,2
Absorbance at 300 nm
0
10
20
30
40
50
60
70
80
Effluent Volume, ml

Figure 69. Reverse-phase HPLC of tryptic digests of native Mb and $Ru(NH_3)_5$(His-81)Mb at 300 nm. A 2 mg sample of hydrolyzed protein was chromatographed (flow rate 2mL/min) with a linear gradient between 0% and 55% CH_3CN in which both the initial aqueous developer and the CH_3CN contained 0.1% CF_3COOH.

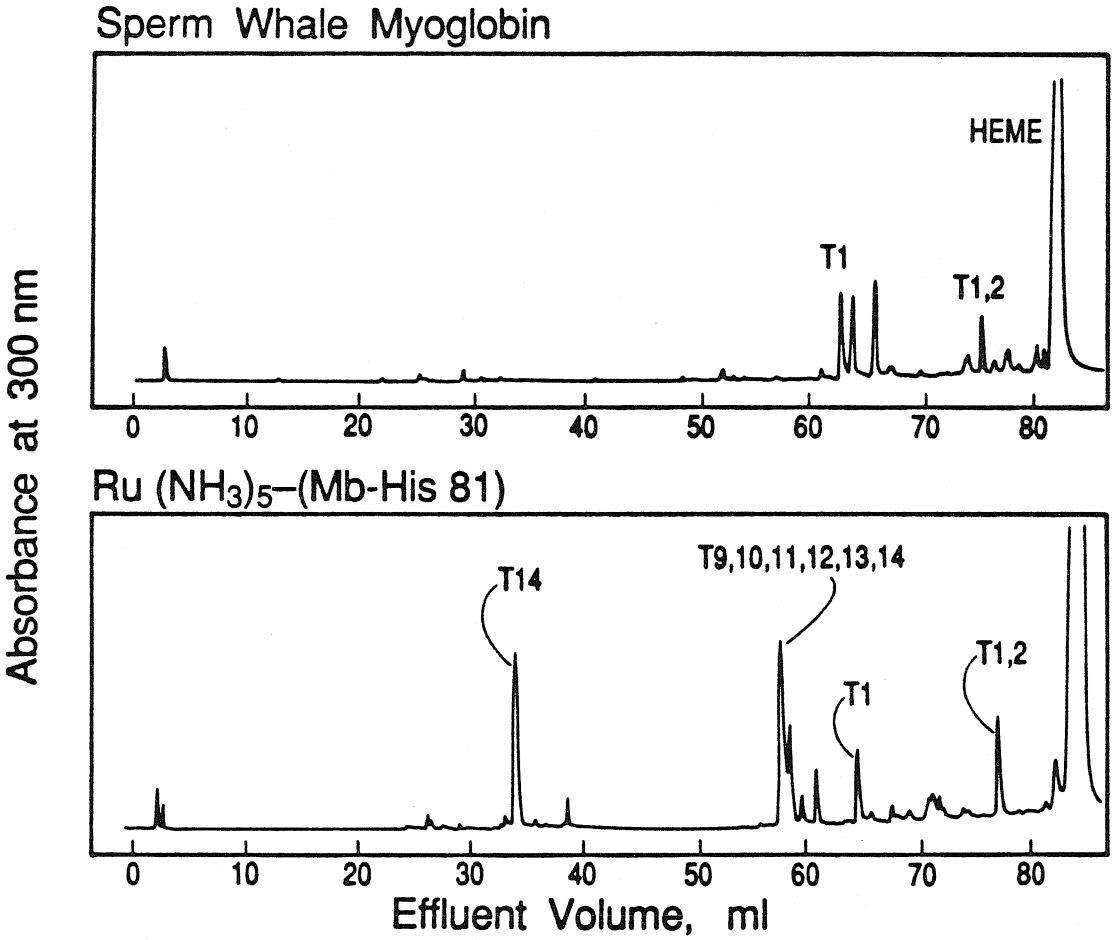
Sperm Whale Myoglobin
HEME
T1
T1,2
0
10
20
30
40
50
60
70
80
Ru $(NH_3)_5$–(Mb-His 81)
T14
T9,10,11,12,13,14
T1,2
T1
0
10
20
30
40
50
60
70
80
Absorbance at 300 nm
Effluent Volume, ml

Figure 70. Reverse-phase HPLC of tryptic digests of native Mb and $Ru(NH_3)_5$(His-116)Mb at 300 nm. A 2 mg sample of hydrolyzed protein was chromatographed (flow rate 2mL/min) with a linear gradient between 0% and 55% CH_3CN in which both the initial aqueous developer and the CH_3CN contained 0.1% CF_3COOH.

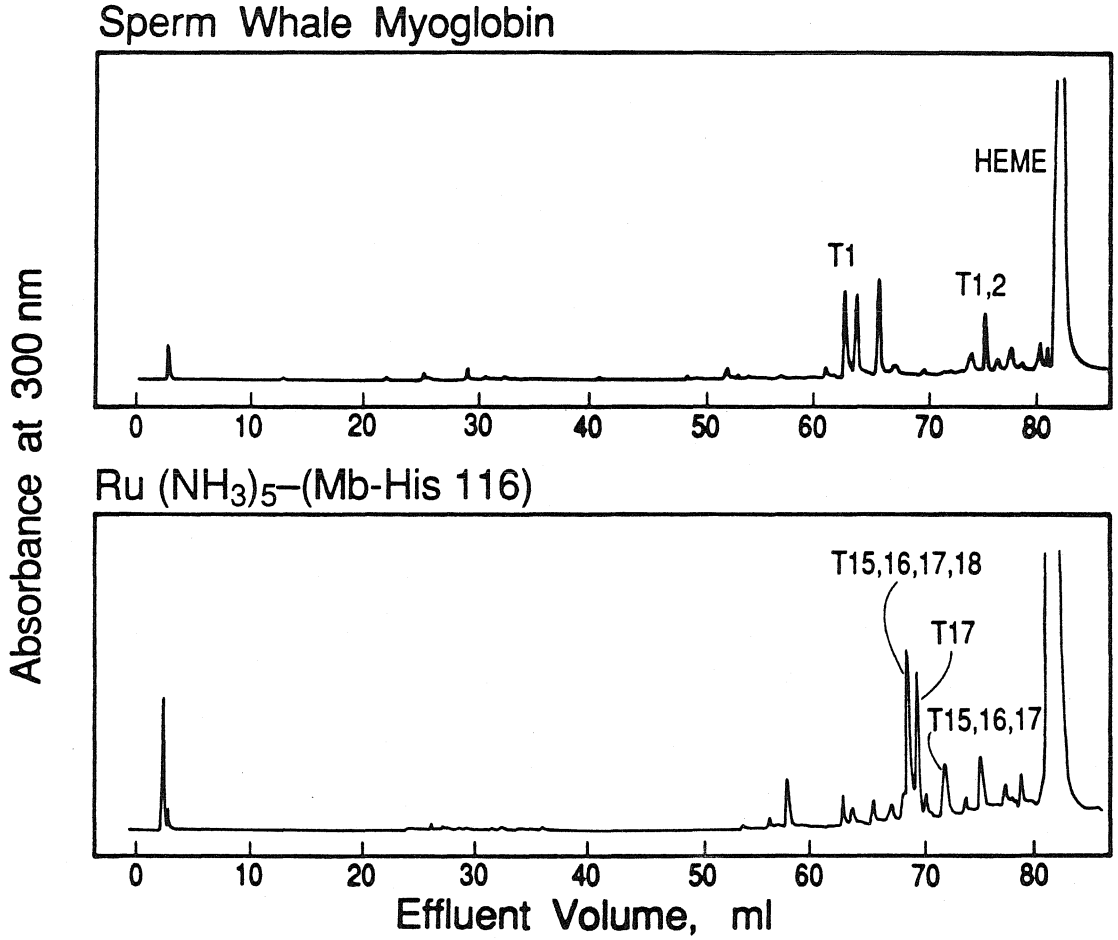
Sperm Whale Myoglobin
HEME
T1
T1,2
0
10
20
30
40
50
60
70
80
Ru (NH3)5–(Mb-His 116)
T15,16,17,18
T17
T15,16,17
0
10
20
30
40
50
60
70
80
Absorbance at 300 nm
Effluent Volume, ml

Figure 71. Reverse-phase HPLC of thermolytic digest of the Ru-labelled peptide from tryptic digestion of a_5Ru(Band II)Mb (Figure 70). A 2 mg sample of hydrolyzed protein was chromatographed (flow rate 2mL/min) with a linear gradient between 0% and 55% CH_3CN in which both the initial aqueous developer and the CH_3CN contained 0.1% CF_3COOH.

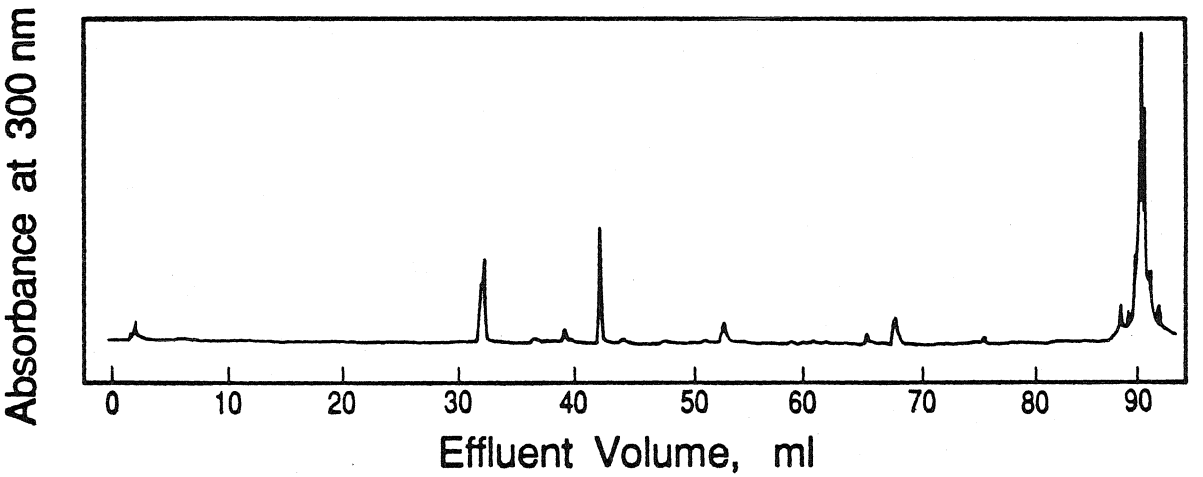
Absorbance at 300 nm
0
10
20
30
40
50
60
70
80
90
Effluent Volume, ml